

Numerical modelling study of rock support system for deep  
mine haulage drift

by

Wei Wei, B.Eng.

A thesis submitted to McGill University  
in partial fulfilment of the requirements  
for the Degree of Master of Engineering

Department of Mining and Materials Engineering

McGill University

Montreal, Quebec, Canada

April, 2010

©Wei Wei, 2010

## Abstract

Haulage drifts are used for the transportation of blasted ore from the draw point to nearby ore pass or dumping point in sublevel mining systems. During production, haulage drifts are occupied by mine operators and haulage equipment. Therefore the stability of haulage drifts is important to the safe and uninterrupted production of a mining operation. It would be advantageous to know a priori how drift stability is influenced by mining activities in the proximity of the drift. This thesis presents the results of a study to examine drift stability and rock support system performance of a haulage drift, based on a case study of Garson mine from Vale Inco, Sudbury, Canada.

The Mohr-Coulomb and Hoek-Brown models are the most widely used constitutive laws to describe the elastoplastic behaviour of rock materials under load. They are available in many numerical modeling codes including *Phase2* and *FLAC*, which were selected to perform the numerical modeling analyses in this thesis. Consequently, the Mohr-Coulomb and Hoek-Brown constitutive models are reviewed in the first place. The finite element method is selected, together with Hoek-Brown model, to study the influencing factors of stability of haulage drift; finite difference method is chosen, along with Mohr-Coulomb model, to examine the performance of rock support system design.

Much information is gathered from the mine site to help understand the entire mining environment. Parameters like rock mass character, mining plan and stress environment need to be known ahead of time in preparation for building the numerical model. Consequently, a geomechanical database named “*Data Integrator for Mine Analysis and Design (DIMAND)*”, including the most important features related to mining activities, has been developed.

Numerical modeling results reveal that there is a dominant trend of low stress regime (postpeak) in the drift back, which results from the stoping activities in both cases of low and high horizontal to vertical in situ stress ratios. There is a gradual spread of yielding around the haulage drift with mining activity. However, it is not until the nearest two stopes are mined and backfilled that the haulage drift is affected severely with yielding

extending from the drift toward the orebody. Significantly higher wall convergence ratio of the haulage drift is noticed when the nearest stope to the haulage drift is mined.

The *FLAC* modeling study on rock support performance reveals that primary support alone is not sufficient to take on the full duty of the haulage drift during the life of a mine plan. When the enhanced support system is installed, the total support system is capable of sustaining mining induced loads to the end of the planned mining sequence. The system performance may be further improved if the enhanced support is placed after the first stope was excavated, at lower level to the haulage drift, has been mined out and backfilled. Shotcrete plays an important role in the enhanced support system performance. The highest stress in the shotcrete layer is located at the left upper corner of the drift toward the orebody contact and occurred at the end of the mining sequences.

## Résumé

Dans les opérations de minage en vrac, le minerai est transporté des points de soutirages aux chûtes à minerai grâce aux galeries de halage. Ces galeries de halage sont utilisés par le personnel quotidiennement. Donc, la stabilité des galeries de halage est primordiale pour garantir une production constante et sécuritaire. Il serait avantageux de savoir a priori comment la galerie de halage sera affectée par l'activité minière avoisinante. Ce mémoire décrit les résultats d'une étude qui examine la stabilité et la performance du soutènement d'une galerie de halage de la mine Garson, Sudbury Ontario, Canada, propriété de Vale.

Les critères de Mohr-Coulomb et de Hoek-Brown sont les plus utilisés pour décrire le comportement du massif rocheux soumis à des contraintes. Les logiciels Phase 2 et FLAC ont été retenus pour compléter l'analyse numérique de ce travail, car les critères de Mohr-Coulomb et de Hoek-Brown y sont intégrés. Pour étudier les facteurs influençant la stabilité de la galerie de halage, un code avec éléments finis (Phase2) utilisant le critère de Hoek-Brown a été choisi. Pour évaluer la performance du soutènement, un code avec différences finis (FLAC) utilisant le critère de Mohr-Coulomb a été choisi.

Beaucoup de données ont été obtenues de la mine Garson afin de comprendre entièrement la zone étudiée. Des paramètres tel les caractéristiques du massif rocheux, les plans miniers, le régime de contrainte, etc. sont requis pour construire le modèle numérique. Donc, une base de données géomécanique intitulée 'Data Integrator for Mine Analysis and Design (Dimand)' répertoriant les caractéristiques critiques de l'activité minière a été développée.

Les résultats de l'analyse numérique montrent un état de relaxation dans le toit de la galerie créé par l'extraction des chantiers dans les deux cas de faible et de fort rapport de la contrainte horizontale sur la contrainte verticale. La zone de relaxation s'étend graduellement autour de la galerie de halage en fonction du taux d'extraction du minerai. Néanmoins, la galerie de halage est sévèrement affectée par la zone de relaxation seulement quand les deux chantiers les plus proches sont excavés. Le taux de



convergence des parements de la galerie de halage augmente significativement lorsque le chantier le plus proche de la galerie de halage est excavé.

Les résultats obtenus avec le code FLAC sur la performance du soutènement montrent que le soutènement initial ne suffit pas à maintenir la stabilité de la galerie de halage pour son entière vie. Lorsqu'un soutènement additionnel est ajouté, la combinaison des deux soutènements permet d'assurer la stabilité de la galerie de halage pour son entière vie. La performance du soutènement peut-être amélioré si le soutènement additionnel est installé après l'extraction et le remblayage du premier chantier situé au niveau inférieur. Le béton projeté joue un rôle important dans la performance du soutènement additionnel. Le point dans le béton projeté avec le maximum de contrainte est situé dans le coin supérieur gauche de la galerie de halage lorsque que tous les chantiers sont excavés.

## **Acknowledgement**

I wish to express my sincere appreciation to my supervisor, Professor Hani S. Mitri, for his endless encouragement, support and guidance throughout my studies. Also, I wish to thank Dr. Denis Thibodeau from Vale Inco for his great help and support during the entire research project. I would like to thank Dr. Xiaoyou Yun and Mr. Yaohua Zhang for their support and helpful opinions. I wish to thank Dr. Wenxue Chen for his valuable tips on development of the database.

# Table of Contents

<b>Abstract .....</b>	<b>I</b>
<b>Résumé .....</b>	<b>III</b>
<b>Acknowledgement .....</b>	<b>V</b>
<b>Table of Contents .....</b>	<b>VI</b>
<b>List of Figures .....</b>	<b>X</b>
<b>List of Tables .....</b>	<b>XVII</b>
<b>Nomenclature .....</b>	<b>XVIII</b>
<b>Chapter 1 Introduction .....</b>	<b>1</b>
1.1 General .....	1
1.2 Research Objectives .....	2
1.3 Thesis Structure .....	3
<b>Chapter 2 Mechanical Behaviour of Rock Materials .....</b>	<b>5</b>
2.1 Behaviour of Rock Material under Loading .....	5
2.1.1 Viscous Behaviour of Rock Material .....	7
2.1.2 Elastic Behaviour of Rock Material .....	8
2.1.2.1 Linear Elasticity .....	8
2.1.2.2 Nonlinear Elasticity .....	10
2.1.3 Plastic Behaviour of Rock Material .....	11
2.2 Plasticity Theory .....	11
2.2.1 Mohr-Coulomb Model .....	12
2.2.1.1 Stress Invariants .....	12
2.2.1.2 Mohr-Coulomb Yield Function .....	16
2.2.2 Hoek-Brown Model .....	17
2.2.2.1 Relationship between Mohr-Coulomb and Hoek-Brown .....	18
2.2.3 Modulus of Elasticity of The Rock Mass .....	20

<b>Chapter 3 Geomechanical Database of Garson Mine .....</b>	<b>22</b>
3.1 Concept of the Database .....	22
3.2 Structure of the Database .....	25
3.2.1 Illustration of Each Frame Element .....	25
3.2.1.1 Diamond Drillhole Data .....	25
3.2.1.2 Haulage Drift Geometry .....	30
3.2.1.3 Haulage Drift Development and Latest Stope Sequence Plan .....	32
3.2.1.4 Primary Rock Support Pattern .....	34
3.2.1.5 Distance between Haulage Drift and Stopes .....	34
3.2.1.6 Stope Construction and Blasting Details .....	35
3.2.1.7 Stope Type Category .....	38
3.2.1.8 Planned Mining Sequence .....	38
3.2.1.9 Stress Environment .....	39
3.2.1.10 Mine Backfill Properties .....	40
3.3 Flow Chart .....	41
3.4 Programming Technique in VB and Access .....	44
3.4.1 Programming Technique .....	45
3.4.2 Error Handling .....	51
3.5 Query Methodology .....	52
3.6 Features of DIMAND .....	55
3.7 Suggestions for Further Development .....	56
<b>Chapter 4 Stability of Haulage Drift During Nearby Mining Activities .....</b>	<b>57</b>
4.1 Introduction .....	57
4.2 Numerical Model .....	58
4.2.1 Finite Element Model .....	61
4.3 Drift Stability Evaluation Criteria .....	62
4.3.1 Model Parametric Study .....	63
4.3.2 Model Results .....	64
4.3.2.1 Stresses .....	64
4.3.2.2 Extent of Yield Zones .....	67

4.3.2.3 Displacements .....	69
4.3.2.4 Effect of Drift Proximity to the Orebody Contact .....	70
4.4 Conclusion and Discussions .....	72
<b>Chapter 5 Rock Supports for Mining Applications .....</b>	<b>73</b>
5.1 General Introduction of Various Rockbolts .....	73
5.2 Cable bolt Installation In The Field .....	84
5.2.1 Using a Breather Tube .....	85
5.2.2 Using a Grout Hose .....	86
5.3 Rockbolt Design .....	87
5.3.1 Analytical Design .....	88
5.3.1.1 Suspension Design .....	88
5.3.1.2 Wedge Design .....	90
5.3.1.3 Compression Arch Design .....	91
5.3.2 Empirical Design .....	92
5.4 Numerical Modeling .....	98
<b>Chapter 6 Assessment of Drift Support System Performance .....</b>	<b>110</b>
6.1 Introduction .....	110
6.2 FLAC Model .....	111
6.2.1 Rockbolt Modeling Technique .....	115
6.3 Support System Analysis .....	117
6.3.1 Primary Support .....	117
6.3.2 Enhanced Support .....	124
6.3.3 Effect of Enhanced Support Installation .....	135
6.4 Conclusion and discussion .....	137
<b>Chapter 7 Summary and Conclusions.....</b>	<b>139</b>
7.1 Summary .....	139
7.2 Conclusions .....	141
7.3 Future work .....	142

<b>References .....</b>	<b>144</b>
-------------------------	------------

## List of Figures

Figure 1-1 Influencing factors of haulage drift stability .....	2
Figure 2-1 Ideal, complete axial stress-strain curve for uniaxial compression of rock materials (Hallbauer, Wagner, & Cook, 1973) .....	6
Figure 2-2 Three stages of viscous process (Pariseau, 1992a) .....	7
Figure 2-3 Elastic Behaviour of Rock Materials (Pariseau, 1992b) .....	8
Figure 2-4 Elastic perfectly-plastic stress-strain relationship .....	12
Figure 2-5 Stress components of s and t in stress space .....	14
Figure 2-6 Lode angle and stress component t in $\pi$ plane .....	15
Figure 2-7 Mohr-Coulomb yield surface in the principal stress space (Pariseau, 1992b) .....	16
Figure 3-1 Flowchart of Data Integrator for Mine Analysis and Design (DIMAND) .....	23
Figure 3-2 Visual on Diamond drillhole location in space .....	26
Figure 3-3 RQD histogram .....	27
Figure 3-4 Q histogram .....	27
Figure 3-5 RMR histogram .....	28
Figure 3-6 Density histogram .....	28
Figure 3-7 Young's Modulus histogram .....	29
Figure 3-8 UCS histogram .....	29
Figure 3-9 4900 level mine plan .....	30

Figure 3-10 5000 level mine plan .....	31
Figure 3-11 5100 level mine plan .....	31
Figure 3-12 Haulage drift development and latest stope sequence plan of 4900 level ....	32
Figure 3-13 Haulage drift development and latest stope sequence plan of 5000 level ....	33
Figure 3-14 Haulage drift development and latest stope sequence plan of 5100 level ....	33
Figure 3-15 Stope type and distance to the haulage drift (ft) .....	35
Figure 3-16 Mining sequence .....	36
Figure 3-17 Blast hole pattern of stope 2981-3 .....	37
Figure 3-18 Stope type illustration .....	38
Figure 3-19 Planned mining sequence .....	39
Figure 3-20 Stress environment .....	39
Figure 3-21 Principal stress projected to the YZ plan .....	40
Figure 3-22 Flow chart of database .....	41
Figure 3-23 Diamond drillhole info .....	42
Figure 3-24 File content of the database .....	43
Figure 3-25 Searching engine of the database .....	43
Figure 3-26 Drawing a part in AutoCAD with VB instead of manually .....	45
Figure 3-27 Illustration of a cursor .....	47
Figure 3-28 Rock mass properties of granite-norite on 5100 level .....	49
Figure 3-29 Query drift geometry .....	50
Figure 3-30 Query Haulage drift development and latest stope sequence .....	51



Figure 3-31 Location of numerical model .....	52
Figure 3-32 DIMAND of Garson Mine .....	53
Figure 3-33 Query rock mass characterization by level .....	53
Figure 3-34 Query results of 5100 level .....	54
Figure 3-35 Real geometry of numerical model of 5100 level .....	54
Figure 3-36 Transformed numerical model from real geometry of drift and stopes on 5100 level .....	55
Figure 4-1 Layout of problem analyzed showing haulage drift in the vicinity of mining .....	58
Figure 4-2 Plan view of level 50 – Garson mine .....	59
Figure 4-3 Three-dimensional view of level 50 .....	61
Figure 4-4 Finite element mesh showing the modeled mining sequence .....	62
Figure 4-5 Major principal stress redistribution around the drift .....	65
Figure 4-6 Major principal stress redistribution for $k=1.67$ , $L=12$ m .....	66
Figure 4-7 Major principal stress redistribution for $k=1.2$ , $L=12$ m .....	66
Figure 4-8 Yield zone progression with mining sequence, $L=12$ m .....	68
Figure 4-9 Initial drift displacements .....	70
Figure 4-10 Total displacement variation with modelling stages, $L=12$ m .....	71
Figure 4-11 Total displacement variation with modelling stages, $k=1.67$ .....	71

Figure 5-1 Rock bolt with a slot and wedge anchor (After Hoek & Brown 1980).....	74
Figure 5-2 Rock bolt with an expansion shell anchor, tensioned and grouted (After Hoek & Brown 1980).....	75
Figure 5-3 Rock bolt with a deformed section used to form a grouted anchorage (After Hoek & Brown 1980).....	77
Figure 5-4 Forged Head Rebar (Mansour Group).....	78
Figure 5-5 Threaded Rebar (Mansour Group).....	78
Figure 5-6 Resin-grouted rock bolt made from threaded bar (After Hoek & Brown 1980).....	79
Figure 5-7 Split-set dowel (After Hoek & Brown 1980).....	80
Figure 5-8 Swellex dowel, Atals Copco (After Hoek & Brown 1980).....	81
Figure 5-9 Applications of swellex (Atlas Copco).....	82
Figure 5-10 Modified Cone Bolt (Mansour Group).....	83
Figure 5-11 Standard cable bolt (Mansour Group).....	83
Figure 5-12 Nut cage cable bolt (Mansour Group).....	83
Figure 5-13 Dynamic Cable Bolt (DSI).....	84
Figure 5-14 Principle of installation of a long fully grouted cable bolt .....	85
Figure 5-15 Rock bolts installation machine .....	86
Figure 5-16 Grouting a cable bolt in down hole .....	87
Figure 5-17 Rockbolt design to support the weight of a roof beam in laminated rock (After Hoek & Brown 1980).....	88

Figure 5-18 Design of a rockbolt or cable system to prevent sliding of a triangular prism (After Hoek & Brown 1980).....	90
Figure 5-19 A self-support arch occurring due to rockbolting .....	91
Figure 5-20 Q-support chart for selecting reinforcement and support, Barton 2002 .....	96
Figure 5-21 Rock support–interaction analysis (After Hoek & Brown 1980).....	97
Figure 5-22 Geometry and degrees of freedom of cable element (Mitri and Rajaie 1990) .....	99
Figure 5-23 layout of case study (Mitri and Rajaie 1990) .....	100
Figure 5-24 Finite element mesh (Mitri and Rajaie 1990) .....	101
Figure 5-25 Rock anchor element (Tang 2000) .....	102
Figure 5-26 Definition of numerical example analysed (Tang 2000) .....	103
Figure 5-27 Rockbolt and surrounding rockmass (Tannant et al. 1995) .....	104
Figure 5-28 comparison between numerical and measured results (Tannant et al. 1995) .....	105
Figure 5-29 Four-node bolt element and connection with FE mesh (Marence and Swobodac 1995) .....	106
Figure 5-30 Bolt crossing joint element and connection with finite element mesh (Marence et al.) .....	108
Figure 5-31 Axial force in bolts for final loading step (Marence and Swobodac 1995) .....	109
Figure 6-1 Layout of numerical modeling problem .....	111
Figure 6-2 Drift primary support pattern .....	112

Figure 6-3 Enhanced support pattern .....	113
Figure 6-4 Plan view of 5000 level - Garson mine .....	114
Figure 6-5 FLAC model of section A-A (see Figure 6-4) .....	114
Figure 6-6 Basic model of a rockbolt element .....	116
Figure 6-7 Degree of freedom of a rockbolt element .....	116
Figure 6-8 Fixed boundary condition of rockbolts .....	117
Figure 6-9 Principal stress distribution around haulage drift .....	119
Figure 6-10 Initial deformations around haulage drift .....	120
Figure 6-11 Rock mass yielding around haulage drift .....	120
Figure 6-12 Axial loads in rebars after drift excavation .....	122
Figure 6-13 Axial loads of rebars after stope 6 is mined out .....	123
Figure 6-14 Deformed drift profile after stope 1 is mined out - primary support system .....	124
Figure 6-15 Deformed drift profile after stope 1 is mined out - primary and enhanced support systems .....	125
Figure 6-16 Maximum total displacements at drift back with respect to mining sequence .....	126
Figure 6-17 Maximum total displacements at left wall with respect to mining sequence .....	126
Figure 6-18 Maximum total displacements at right wall with respect to mining sequence .....	127
Figure 6-19 Wall convergence ratio (WCR) .....	128
Figure 6-20 Variation of wall convergence ratio (WCR) with mining sequence .....	129

Figure 6-21-a Axial stress in shotcrete after stope 1 is mined out .....	130
Figure 6-21-b Shear stress of shotcrete after stope 1 is mined out .....	130
Figure 6-22-a Axial stress of shotcrete after stope 6 is mined out .....	131
Figure 6-22-b Shear stress of shotcrete after stope 6 is mined out .....	131
Figure 6-23 Location of potential failure of shotcrete layer .....	132
Figure 6-24 Simulation results of MCBs after stope 6 is mined out .....	134
Figure 6-25 Axial loads of rebars after stope 6 is mined out .....	135
Figure 6-26 Axial loads of rebars after stope 1 is mined out .....	136
Figure 6-27 Presentation of yielding rebars in FLAC .....	136
Figure 6-28 Axial loads in MCBs when installed after stope 1 is mined out .....	137
 Figure 7-1 Procedure for haulage drift stability assessment .....	 140

## **List of Tables**

Table 4-1 Mechanical properties of materials as obtained from the Garson Mine database .....	61
Table 4-2 Numerical models analyzed .....	63
Table 6-1 Mechanical properties of geomaterials used in FLAC models .....	115
Table 6-2 Model input parameters .....	118
Table 6-3 Axial and shear stresses location of shotcrete layer .....	133

## Nomenclature

$\sigma$	stress
$\sigma_{ij}$	stress on plane i in the direction of j if $i=j$ , $\sigma_{ii}$ is normal stress, and $\sigma_{xx}=\sigma_x$ , $\sigma_{yy}=\sigma_y$ , $\sigma_{zz}=\sigma_z$ if $i \neq j$ , $\sigma_{ij}$ is shear stress, and $\sigma_{ij}=\tau_{ij}$
$\tau_{ij}$	shear stress
$\sigma_1, \sigma_2, \sigma_3$	major, intermediate, and minor principal stress, respectively
$\sigma_m$	mean stress or hydrostatic stress $\sigma_m = \frac{1}{3} J_1$
$s_{ij}$	deviatoric stress at plane i in the direction of j $s_{ij} = \sigma_{ij} - \sigma_m$
$\bar{\sigma}$	deviatoric stress in triaxial test
$\theta$	Lode angle in Mohr-Coulomb model
$\sigma_Y$	yield strength
$\sigma_c$	uniaxial compressive strength of intact rock (UCS)
$\sigma_{bc}$	uniaxial compressive strength of rock mass
$\sigma^0$	initial stress
$\sigma_t$	tensile strength
$\varepsilon$	strain
$\varepsilon_{ij}$	strain at plane i in the direction of j if $i=j$ , $\varepsilon_{xx}=\varepsilon_x$ , $\varepsilon_{yy}=\varepsilon_y$ , $\varepsilon_{zz}=\varepsilon_z$ if $i \neq j$ , $\varepsilon_{ij}=\frac{1}{2}\gamma_{ij}$
$\gamma_{ij}$	engineering shear strain
$\varepsilon_1, \varepsilon_2, \varepsilon_3$	major, intermediate, and minor principal strain, respectively
$\varepsilon^0$	initial strain
$\varepsilon_v$	volumetric strain $\varepsilon_v = \varepsilon_x + \varepsilon_y + \varepsilon_z$
$\varepsilon^e$	elastic strain

$\varepsilon^p$	plastic strain
$d\varepsilon$	strain increment
$d\varepsilon^e$	elastic strain increment
$d\varepsilon^p$	plastic strain increment
$d\varepsilon_v$	volumetric strain increment
$\dot{\varepsilon}$	strain rate
$\Delta\varepsilon^{vp}$	accumulated viscoplastic strain
$\varepsilon_m$	mean strain
$e_{ij}$	deviatoric strain
	$e_{ij} = \varepsilon_{ij} - \varepsilon_m$
E	Young's modulus
$E_i$	Young's modulus for intact rock
$E_{rm}$	Young's modulus for rock mass
$\nu$	Poisson's ratio
$\gamma$	material specific gravity
$\rho$	material density
G	shear modulus
	$G = \frac{E}{2(1 + \nu)}$
K	bulk modulus
	$K = \frac{E}{3(1 - 2\nu)}$
$\Lambda$	Lame's constant
	$\Lambda = \nu E / (1 + \nu)(1 - 2\nu)$
$\phi$	angle of internal friction
c	cohesion
$m, s, a$	material constants of Hoek-Brown failure criterion
$m_i$	intact rock material constant of Hoek-Brown failure criterion
$m_b, m_{rm}$	broken rock material constant of Hoek-Brown failure criterion



RMR	Rock Mass Rating
RQD	Rock Quality Designation
GSI	Geological Strength Index
Q	Q System
$D$	disturbance factor of Hoek-Brown failure criterion
F	yield function
$\lambda$	hardening/softening parameter or plastic multiplier

$\sigma_v$  vertical in situ stress

$\sigma_h$  horizontal in situ stress (average)

$\sigma_{H \max}$  maximum horizontal in situ stress

$\sigma_{H \min}$  minimum horizontal in situ stress

W stope width

$k$  the ratio of horizontal stress to vertical stress

$$k = \sigma_h / \sigma_v$$

WCR wall convergence ratio

# Chapter 1

## Introduction

### 1.1 General

Sublevel stoping is a popular mining method that is adopted by most Canadian metal mines for the extraction of orebody. In such a system, haulage drifts are used for the transportation of blasted ore from the draw point to a nearby ore pass or dumping point. During production, haulage drifts are occupied by mine operators and mining equipment. Therefore the stability of haulage drifts is important to the safe and uninterrupted production of a mining operation. It would be advantageous to know how stability is influenced by mining activities in the proximity of the drift.

A case study, using finite element and finite difference numerical analysis techniques, was launched at Garson mine, Vale Inco, to help examine the performance of haulage drift during nearby mining activity in a sublevel stopping environment.

A geomechanical database of Garson mine was programmed using *Visual Basic (VB)* to be a data management system, as well as a mine design tool. As such, it included: mining plan view function, three dimensional visualization of rock mass characterization, rock mass property query and mining related information query such as blasting parameters, distance from drift to orebody contact etc.

Numerical modeling results are helpful in revealing several key factors that influence haulage drift stability with respect to adjacent mining activities, and to examine the performance of rock support systems that are in current use.

This thesis introduces a general methodology of studying a specific problem in a specific mine.

## 1.2 Research Objectives

There are three major tasks in the research of stability of haulage drift:

- Build a geomechanical database to manage a large quantity of data information gathered from the mine site and use it efficiently, not only for mine design purposes, but also for numerical modeling input.
- Build a finite element model to analyze stability-influencing factors, such as in situ stress, drift dimension, mining sequence, and distance between haulage drift and orebody contact, as illustrated in Figure 1-1.

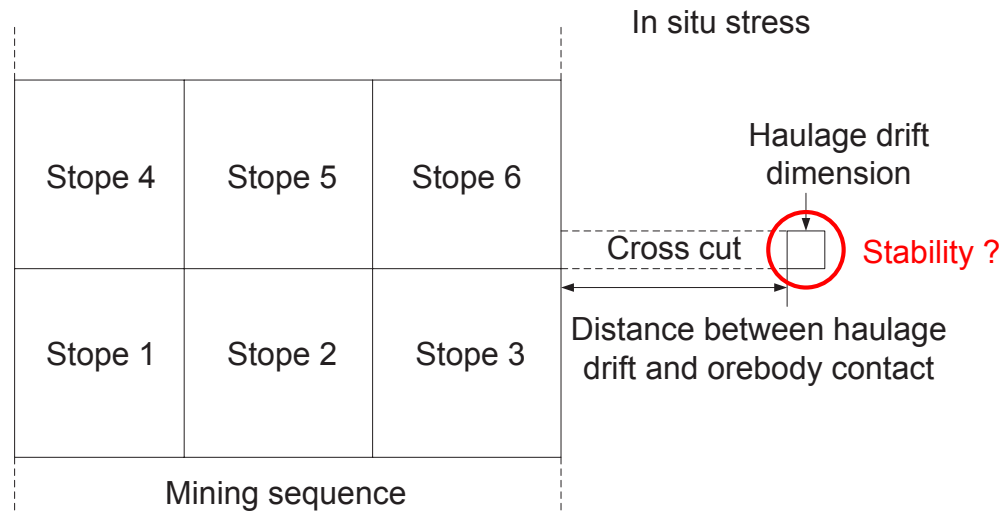


Figure 1-1 Influencing factors of haulage drift stability

- Build a finite difference model to examine the status of support systems, including rebars, modified cone bolts (MCB) and shotcrete layer, with respect to mining sequence.

### 1.3 Thesis Structure

Chapter 1 is a general introduction of the research problem definition, methodology and objectives.

Chapter 2 documents an intensive literature review of plasticity theory, nonlinear behavior of rock material and constitutive model widely used in rock mechanics.

Chapter 3 explains the importance of data management and techniques of building a geomechanical database using *Visual Basic*. A demonstration of the database is also given.

Chapter 4 reviews the basics of the finite element numerical modeling technique, thus laying a foundation for the research presented in Chapter 5, based on which a research foundation for Chapter 5 has been set up.

Chapter 5 presents a case study at Garson mine, Sudbury, of stability of haulage drift in a dynamic mine environment. A finite element nonlinear numerical model is developed in *Phase2* to study all influential factors influencing to the stability of haulage drift.

Chapter 6 introduces widely used rockbolts as rock supports that are currently in daily use in mines.

Chapter 7 examines the performance of rock support systems, with respect to mining sequence. A finite difference nonlinear numerical model is built in *FLAC* to study the

performance, with respect to mining sequence, of primary support systems, as well as the enhanced support system, including rebars, modified cone bolts (MCB) and shotcrete.

Chapter 8 summarizes the key points of the research project, as well as making recommendations for future research.

## Chapter 2

### Mechanical Behaviour of Rock Materials

In this chapter, the constitutive laws commonly used for rock masses are reviewed as well as their linear elastic behaviour. The Mohr-Coulomb and Hoek-Brown models are the most widely used constitutive laws to describe the behaviour of rock materials under a certain loading condition. Specifically, they constitute the foundation of many numerical modeling softwares, including *Phase2* and *FLAC*, which were selected to launch the numerical modeling analysis in this thesis. Consequently, the Mohr-Coulomb and Hoek-Brown constitutive models will be presented in detail in this chapter.

#### 2.1 Behaviour of Rock Material under Loading

There are three main successive stages describing the behaviour of rock material under loading conditions, namely viscous behaviour, elastic behaviour and plastic behaviour; they can be interpreted in terms of the stress-strain relation. Coulomb, 1776; Drucker and Prager, 1952; Hoek and Brown, 1980; Kaiser et al, 2000; Hajiabdolmajid and Kaiser, 2003 had developed a number of constitutive models to represent the true behaviour of rock materials.

Carnavas, 2000, divided the response of rock materials into 6 parts as shown in Figure 2-

1. Parts 1 to 6 can be illustrated as follows:

- (1) Closure of pre-existing cracks; presentation of acceleration of the tangent at the end of stress-strain curve.

- (2) Linear elastic stress-strain relation.
- (3) Crack growth and sliding on existing crack interfaces, with a new micro-structure forming.
- (4) Approaching the material's ultimate strength.
- (5) Material failure is attributed to the increase of micro-structure.
- (6) Failure of material.

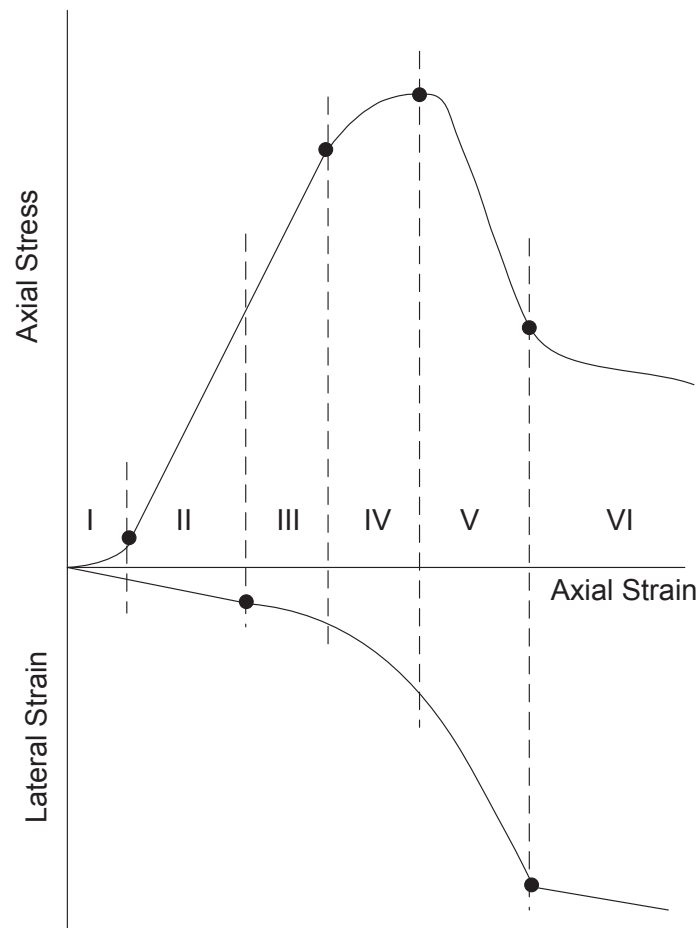


Figure 2-1 Ideal, complete axial stress-strain curve for uniaxial compression of rock materials (Hallbauer, Wagner, & Cook, 1973)

### 2.1.1 Viscous Behaviour of Rock Material

The viscoplastic behaviour of rock material can be subdivided into three phases, Figure 2-2.

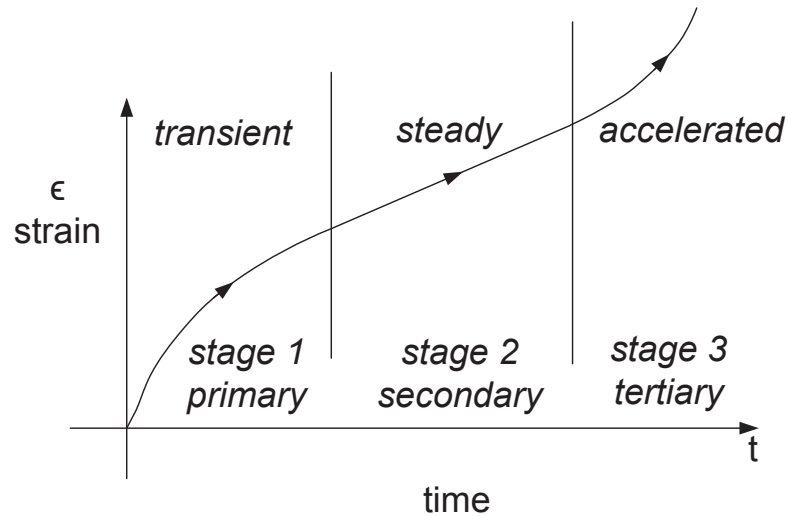


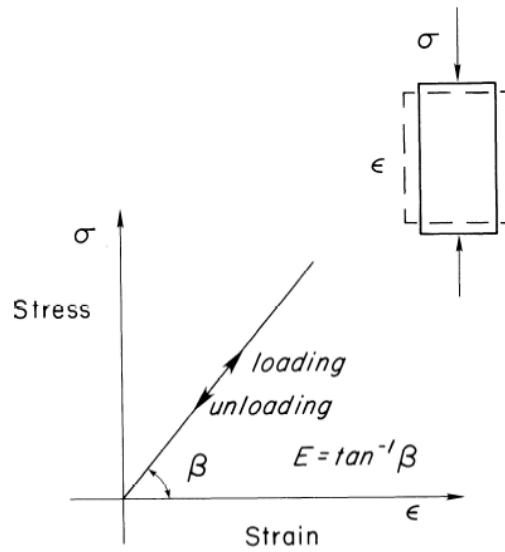
Figure 2-2 Three stages of viscous process (Pariseau, 1992a)

Viscous behaviour, known as creep behaviour, describes the time-dependent behaviour of rock materials; e.g., soils and weak rocks, such as sedimentary and metamorphic rocks.

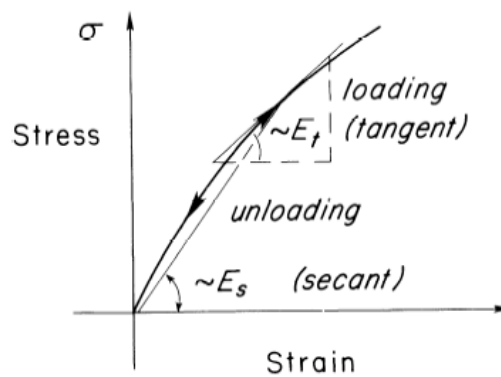
### 2.1.2 Elastic Behaviour of Rock Material

For stage II and III of Figure 2-2, an elastic model is employed to describe the rock material behaviour, where Hooke's law stands for linear elastic behaviour, and the generalized Hooke's law governs nonlinear elastic behaviour.





(a) Linear Elasticity



(b) Non-linear Elasticity

Figure 2-3 Elastic Behaviour of Rock Materials (Pariseau, 1992b)

### 2.1.2.1 Linear Elasticity

The linear elastic behaviour of rock material under uniaxial loading is controlled by Hooke's law as illustrated in Figure 2-3 (a). The constitutive law is:

$$\sigma = E\epsilon \quad (2.1)$$

where  $\sigma$  = stress,  $\epsilon$  = strain, and  $E$  = Young's modulus, respectively.

Also, the generalized Hooke's law can be applied to three-dimensional rock mass; it is expressed as:

$$\sigma_{ij} = E_{ijkl} \varepsilon_{kl} \quad (2.2)$$

where  $E_{ijkl}$  is the 4<sup>th</sup>-order material stiffness tensor.

If the material satisfies isotropic behaviour, equation (2.2) becomes:

$$\sigma_{ij} = \frac{1}{3} \Lambda \varepsilon_v \delta_{ij} + 2G \varepsilon_{ij} \quad (2.3)$$

where  $\Lambda$  is the Lamé's constant,  $G$  the shear modulus, and  $\varepsilon_v$  the volumetric strain, respectively.

$$\varepsilon_v = \varepsilon_{ii} = \varepsilon_x + \varepsilon_y + \varepsilon_z \quad (2.4)$$

For programming convenience, the constitutive law is transformed into matrixes:

$$\{\sigma\} = [D] \{\varepsilon\} \quad (2.5)$$

$$\{\sigma\} = \{\sigma_x, \sigma_y, \sigma_z, \tau_{xy}, \tau_{yx}, \tau_{zx}\} \quad (2.6)$$

$$\{\varepsilon\} = \{\varepsilon_x, \varepsilon_y, \varepsilon_z, \gamma_{xy}, \gamma_{yz}, \gamma_{zx}\} \quad (2.7)$$

where  $[D]$  is the stiffness matrix,  $\tau_{ij}$  are shear stresses, and  $\gamma_{ij}$  are shear strains, respectively.

The complete form of  $[D]$  is:

$$[D] = \frac{E}{(1+\nu)(1-2\nu)} \begin{vmatrix} 1-\nu & \nu & \nu & 0 & 0 & 0 \\ \nu & 1-\nu & \nu & 0 & 0 & 0 \\ \nu & \nu & 1-\nu & 0 & 0 & 0 \\ 0 & 0 & 0 & \frac{1}{2}(1-2\nu) & 0 & 0 \\ 0 & 0 & 0 & 0 & \frac{1}{2}(1-2\nu) & 0 \\ 0 & 0 & 0 & 0 & 0 & \frac{1}{2}(1-2\nu) \end{vmatrix} \quad (2.8)$$

where  $\nu$  is the Poisson ratio.

The stiffness matrix  $[D]$  can be reduced to equation (2.9) for plane stress conditions, and equation (2.10) for plane strain conditions.

$$[D] = \frac{E}{1-\nu^2} \begin{vmatrix} 1 & \nu & 0 \\ \nu & 1 & 0 \\ 0 & 0 & \frac{1-\nu}{2} \end{vmatrix} \quad (2.9)$$

$$[D] = \frac{E}{(1+\nu)(1-2\nu)} \begin{vmatrix} 1-\nu & \nu & 0 \\ \nu & 1-\nu & 0 \\ 0 & 0 & \frac{1-2\nu}{2} \end{vmatrix} \quad (2.10)$$

### 2.1.2.2 Nonlinear Elasticity

For nonlinear rock material behaviour, the governing law is:

$$\sigma_{ij} = f_{ij}(\epsilon_{kl}) \quad (2.11)$$

where  $f_{ij}$  are material response functions.

### 2.1.3 Plastic Behaviour of Rock Material

Starting with stage IV in Figure 2-1, rock material under loading conditions exhibits plastic behaviour. Plastic behaviour can be divided into perfectly plastic behaviour, hardening behaviour and softening behaviour. Rock materials like basalt, granite, andesite, and rhyolite follow elastoplastic behaviour. Plasticity theory will be further discussed in the following sections.

## 2.2 Plasticity Theory

As noticed in Figure 2-1, starting from stage IV onward, the stress/strain relationship of rock material under loading is irregular and nonlinear. The incremental form of the plasticity equation (equation (2.12) below) is used to study the elastoplastic behaviour of rock material at the microscopic level.

$$d\varepsilon^p = F(F, \lambda) \quad (2.12)$$

where  $F$  is the yield function and is model-dependent, and  $\lambda$  is the hardening/softening parameter.

From equation (2.12), known as flow rule, it is noted that there are two components: the yield function and the hardening/softening law. The yield function controls the yield surfaces in the principal stress space and/or the  $\pi$  plane. The hardening/softening parameter determines the size, shape and position of the yield surface of the rock material in post-peak stage.

In general,  $F$  is given by:

$$F = F[\sigma, h(\varepsilon^p)] \quad (2.13)$$

where  $h(\varepsilon^p)$  is the hardening function. If  $h(\varepsilon^p) = 0$ , the condition is perfect plasticity. In this stress state, the yield function is only related to stress invariants, with no hardening or softening phenomena.

### 2.2.1 Mohr-Coulomb Model

The Mohr-Coulomb model is one of the most well-known and widely used models as applied to the plasticity theory of rock materials. It will be discussed next in detail.

#### 2.2.1.1 Stress Invariants

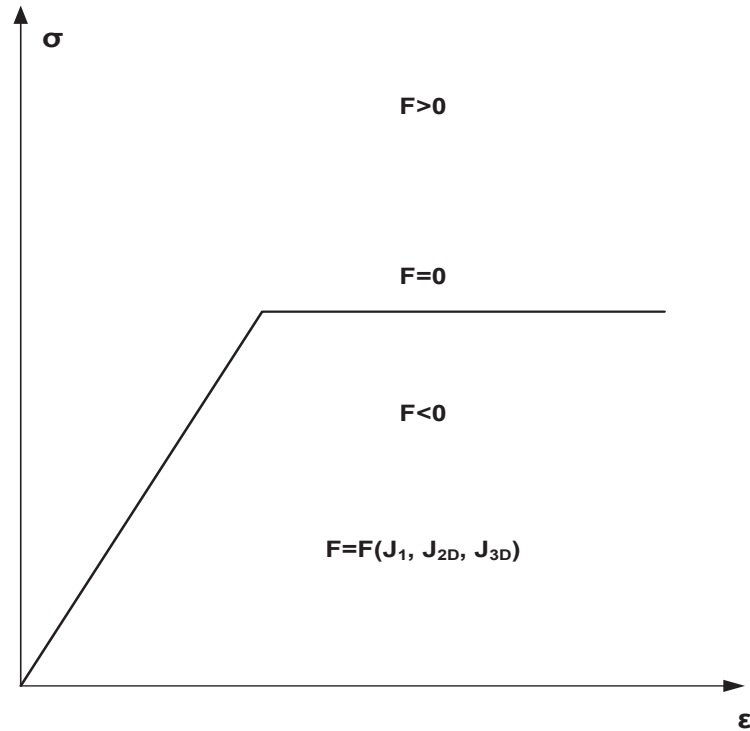


Figure 2-4 Elastic perfectly-plastic stress-strain relationship

Figure 2-4 shows the elastic/perfectly-plastic stress-strain relationship, in which  $J_1$ ,  $J_{2D}$  and  $J_{3D}$  are stress invariants.

The mean stress is given by:

$$\sigma_m = \frac{1}{3}(\sigma_x + \sigma_y + \sigma_z) = \frac{1}{\sqrt{3}}s \quad (2.14)$$

where

$$s = \frac{1}{\sqrt{3}}(\sigma_x + \sigma_y + \sigma_z) \quad (2.15)$$

The deviatoric stress is defined as:

$$\bar{\sigma} = \sqrt{\frac{3}{2}}t \quad (2.16)$$

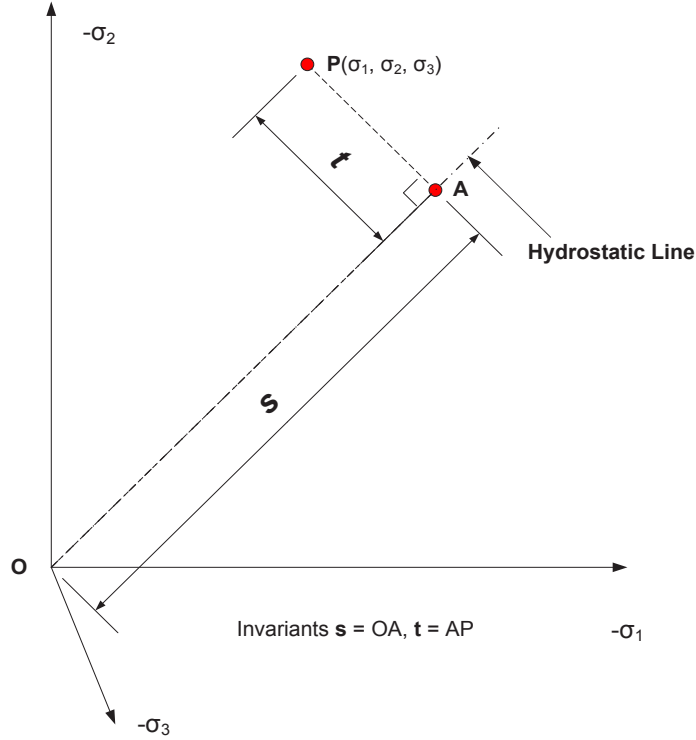
or

$$\bar{\sigma} = \sqrt{3}\sqrt{J_{2D}} \quad (2.17)$$

$$J_{2D} = \frac{1}{6}[(\sigma_x - \sigma_y)^2 + (\sigma_y - \sigma_z)^2 + (\sigma_z - \sigma_x)^2] + \tau_{xy}^2 + \tau_{yz}^2 + \tau_{zx}^2 \quad (2.18)$$

$$t = \frac{1}{\sqrt{3}}[(\sigma_x - \sigma_y)^2 + (\sigma_y - \sigma_z)^2 + (\sigma_z - \sigma_x)^2 + 6\tau_{xy}^2 + 6\tau_{yz}^2 + 6\tau_{zx}^2]^{\frac{1}{2}} \quad (2.19)$$

where  $J_{2D}$  is the second invariant of the deviatoric stress tensor, and  $t$  is the stress component to the hydrostatic line, as illustrated in Figure 2-5.


 Figure 2-5 Stress components of  $s$  and  $t$  in stress space

$P$  is a random point in stress space,  $s$  is the stress component along the hydrostatic line and  $t$  is the stress component normal to the hydrostatic line.

The Lode angle  $\theta$ , in Figure 2-6, is the angle from bisection to the stress component  $t$ , expressed as:

$$\theta = \frac{1}{3} \arcsin\left(\frac{-3\sqrt{6}J_{3D}}{t^3}\right) = \frac{1}{3} \arcsin\left(\frac{-3\sqrt{3}J_{3D}}{2J_{2D}^{\frac{3}{2}}}\right) \quad (2.20)$$

where  $-\pi/6 \leq \theta \leq \pi/6$ , and  $J_{3D}$  is the third invariant of the deviatoric stress tensor.

$$J_{3D} = s_x s_y s_z - s_x \tau_{yz}^2 - s_y \tau_{zx}^2 - s_z \tau_{xy}^2 + 2\tau_{xy} \tau_{yz} \tau_{zx} \quad (2.21)$$

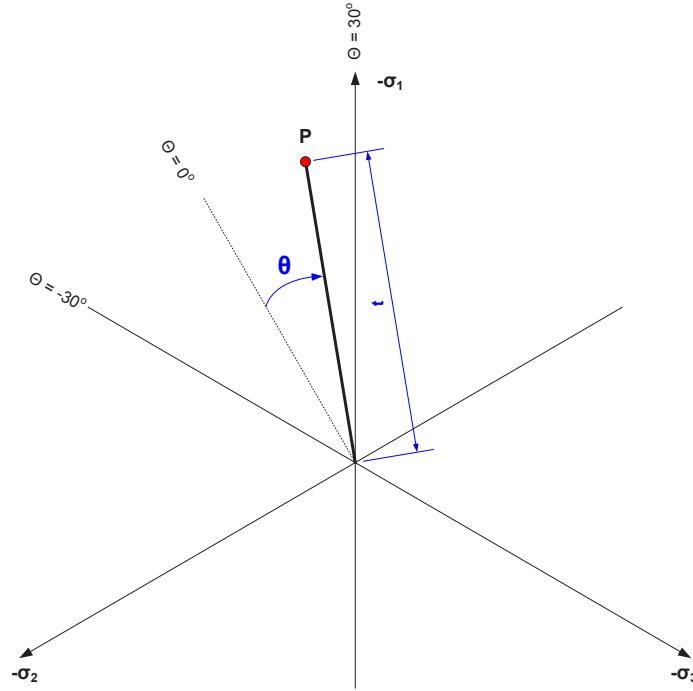


Figure 2-6 Lode angle and stress component  $t$  in  $\pi$  plane

$\theta$  is positive if stress point P is between the bisector and the principal stress axis.

The relationship between principal stresses and stress invariants can be expressed as follows:

$$\begin{aligned}\sigma_1 &= \sigma_m + \frac{2}{3} \bar{\sigma} \sin\left(\theta - \frac{2\pi}{3}\right) \\ \sigma_2 &= \sigma_m + \frac{2}{3} \bar{\sigma} \sin \theta \\ \sigma_3 &= \sigma_m + \frac{2}{3} \bar{\sigma} \sin\left(\theta + \frac{2\pi}{3}\right)\end{aligned}\quad (2.22)$$

where the range of  $\theta$  is:  $-\pi/6 \leq \theta \leq \pi/6$ .



### 2.2.1.2 Mohr-Coulomb Yield Function

The Mohr-Coulomb yield function,  $F$ , as a component in the flow rule, controls the stress surface, Figure 2-7, and can be written as:

$$F = \sigma_m \sin \phi + \bar{\sigma} \left( \frac{\cos \theta}{\sqrt{3}} - \frac{\sin \theta \sin \phi}{3} \right) - c \cos \phi \quad (2.23)$$

where  $\phi$  and  $c$  are the material friction angle and the cohesion respectively.

If  $F < 0$ , the stress state is inside the yield surface—elastic;

If  $F = 0$ , the stress state is on the yield surface—yielding;

If  $F > 0$ , the stress state is outside the yield surface—yielding (and/or hardening) and the stresses must be redistributed and drop to the yield surface, Figure 2-4.

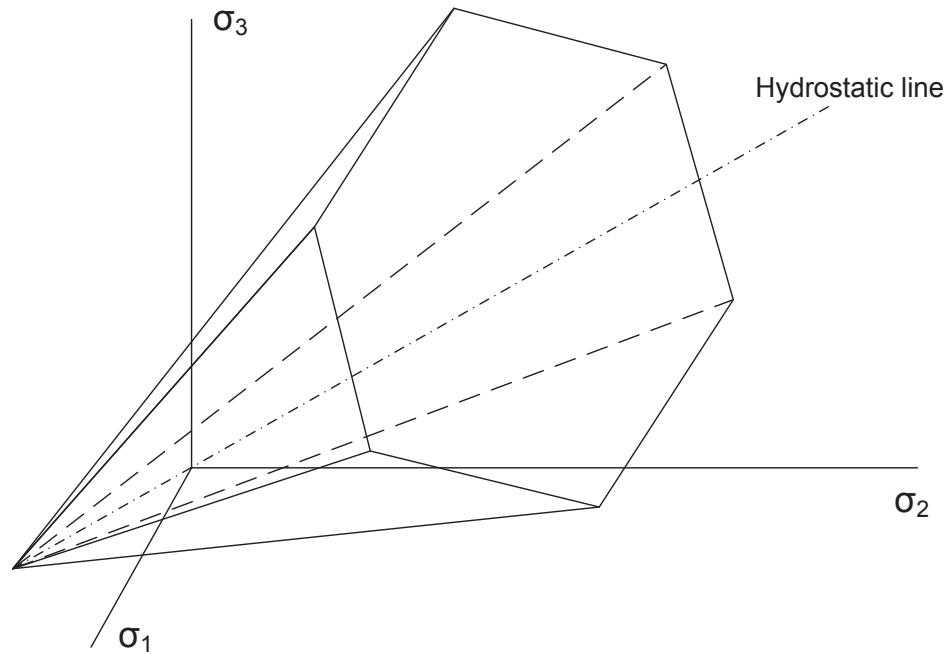


Figure 2-7 Mohr-Coulomb yield surface in the principal stress space (Pariseau, 1992b)

### 2.2.2 Hoek-Brown Model

Unlike Mohr-Coulomb, the Hoek-Brown model is an empirical failure criterion which has been developed and improved in several versions. Bieniawski's Rock Mass Rating (RMR) (Bieniawski, 1973) and the Geological Strength Index (GSI) are combined into the Hoek-Brown model for experienced mining engineers to quickly quantify the rock mass quality.

The original Hoek-Brown empirical failure criterion (Hoek & Brown, 1980a, 1980b) is

$$\sigma_1 = \sigma_3 + (m\sigma_3\sigma_c + s\sigma_c^2)^{\frac{1}{2}} \quad (2.24)$$

where  $m$  and  $s$  are the rock mass constants, and  $\sigma_c$  is the uniaxial compressive strength of intact rock material.

Hoek and Brown, 1988 have updated the expressions for  $m$  and  $s$  as follows:

For disturbed rock masses:

$$m_b = m_i \exp\left(\frac{RMR - 100}{14}\right) \quad (2.25)$$

$$s = \exp\left(\frac{RMR - 100}{6}\right) \quad (2.26)$$

and for undisturbed rock masses:

$$m_b = m_i \exp\left(\frac{RMR - 100}{28}\right) \quad (2.27)$$

$$s = \exp\left(\frac{RMR - 100}{9}\right) \quad (2.28)$$

$$E = 10 \exp\left(\frac{RMR - 10}{40}\right) \quad (2.29)$$

where  $m_b$  is for broken rock and  $m_i$  is for intact rock.

For intact rock,  $m = 0$ ,  $s = 1$  (Hoek, Wood, & Shah, 1992).

For broken rock,  $m = 0$ ,  $s = 0.11$  (Martin, Kaiser, & Creath, 1999).

The Hoek-Brown model has been updated and generalized by Hoek, Carranza-Torres and Corkum, 2002 as follows:

$$\sigma_1 = \sigma_3 + \sigma_c \left\{ m_b \frac{\sigma_3}{\sigma_c} + s \right\}^a \quad (2.30)$$

where

$$m_b = m_i \exp\left(\frac{GSI - 100}{28 - 14D}\right) \quad (2.31)$$

$$s = \exp\left(\frac{GSI - 100}{9 - 3D}\right) \quad (2.32)$$

$$a = \frac{1}{2} + \frac{1}{6} \left( e^{\frac{-GSI}{15}} - e^{\frac{-20}{3}} \right) \quad (2.33)$$

where  $D$  is a factor determined by the degree of disturbance of rock masses, varying from 0 for undisturbed rock masses, to 1 for very disturbed rock masses.

### 2.2.2.1 Relationship between Mohr-Coulomb and Hoek-Brown

Most of the numerical analyses used for evaluating the stability of underground excavations are based on the Mohr-Coulomb failure criterion. Consequently, a frequently asked question is, how to calculate the equivalent cohesion and friction angle values for Mohr-Coulomb inputs, from Hoek-Brown equations, with all the parameters known.

Hoek (1990) has published a technical note estimating the Mohr-Coulomb friction and cohesion values from the Hoek-Brown failure criterion, as follows:

If  $m$ ,  $s$  and the normal stress  $\sigma_n$  are known, then  $c$  and  $\phi$  can be calculated from the following sequence:

$$h = 1 + \frac{16(m\sigma_n + s\sigma_c)}{3m^2\sigma_c} \quad (2.34)$$

$$\theta = \frac{1}{3} \left( 90 + \arctan \frac{1}{\sqrt{h^3 - 1}} \right) \quad (2.35)$$

$$\phi_i = \arctan \frac{1}{\sqrt{4h \cos^2 \theta - 1}} \quad (2.36)$$

$$\tau = (\cot \phi_i - \cos \phi_i) \frac{m\sigma_c}{8} \quad (2.37)$$

$$c_i = \tau - \sigma_n \tan \phi_i \quad (2.38)$$

where  $c_i$  and  $\phi_i$  are the cohesion and friction angle for intact rock, respectively.

Two situations arise

- (a) If the in situ stress environment is the same for both the Mohr-Coulomb and the Hoek-Brown failure criteria, and  $m$ ,  $s$ ,  $\sigma_1$  (the major principal stress) and  $\sigma_3$  (the minor principal stress) are known, then  $\phi$  can be calculated from the following sequence:

$$\sigma_n = \sigma_3 + \frac{(\sigma_1 - \sigma_3)^2}{2(\sigma_1 - \sigma_3) + \frac{1}{2}m\sigma_c} \quad (2.39)$$

$$\tau = (\sigma_n - \sigma_3) \sqrt{1 + \frac{m\sigma_c}{2(\sigma_1 - \sigma_3)}} \quad (2.40)$$

$$\phi_i = 90 - \arcsin\left(\frac{2\tau}{\sigma_1 - \sigma_3}\right) \quad (2.41)$$

where  $\sigma_c$  is the uniaxial compressive strength of intact rock, and the cohesive strength  $c_i$  can be calculated from equation (2.38).

(b) If the uniaxial compressive strength of the rock mass is the same for both the Mohr-Coulomb and Hoek-Brown failure criteria, and  $m$  and  $s$  are known,  $\phi$  can be calculated by the following sequence:

$$\sigma_n = \frac{2s\sigma_c}{4\sqrt{s} + m} \quad (2.42)$$

$$\tau = \sigma_n \sqrt{1 + \frac{m}{2\sqrt{s}}} \quad (2.43)$$

$$\phi_i = 90 - \arcsin\left(\frac{2\tau}{\sigma_c \sqrt{s}}\right) \quad (2.43)$$

The cohesive strength  $c_i$  could be calculated from equation (2.38).

### 2.2.3 Modulus of Elasticity of The Rock Mass

For purposes of modeling, it is not correct to assume that the entire rock mass is made up of intact rock. Several researchers have proposed empirical relationships for estimating the rock mass modulus.

Mitri et al, 1995 proposed an empirical equation expressed as below:

$$E_{rm} = 0.5E_i \left( 1 - \cos \left( \frac{\pi RMR}{100} \right) \right) \quad (2.39)$$

where  $E_i$  and  $E_{rm}$  are for intact rock and rock mass, respectively.

On the other hand, Hoek, Carranza-Torres and Corkum (Hoek, Carranza-Torres and Corkum, (2002) have proposed a set of two equations, depending on the compressive strength of the rock mass. These are:

For uniaxial compressive strength less than 100 MPa:

$$E_{rm} = \left( 1 - \frac{D}{2} \right) \sqrt{\frac{\sigma_c}{100}} 10^{\frac{GSI-10}{40}} \quad (2.40)$$

Or, for uniaxial compressive strength higher than 100 MPa:

$$E_{rm} = \left( 1 - \frac{D}{2} \right) 10^{\frac{GSI-10}{40}} \quad (2.41)$$

Finally, the generalized Hoek and Diederichs equation (Hoek & Diederichs, 2006) is:

$$E_{rm} = E_i \left( 0.02 + \frac{1 - \frac{D}{2}}{1 + e^{\frac{60+15D-GSI}{11}}} \right) \quad (2.41)$$

where  $E_i$  and  $E_{rm}$  are for intact rock and rock mass, respectively.

## **Chapter 3**

### **Geomechanical Database of Garson Mine**

At present, many engineers are using numerical modeling for examining the overall stability of haulage drifts. As a starting point, parameters like rock mass properties, mining plan and stress environment need to be known ahead of time as preparation for setting up the numerical model. Included within each of the three groups of parameters, there are many subgroups, which include a large amount of data, CAD plans, charts, etc., and these have to be dealt with in an efficient and precise way. A haulage drift risk assessment research project between McGill and Vale Inco was launched. As a part of this project, a geomechanical database named “Data Integrator for Mine Analysis and Design (DIMAND)”, including the most important features related to mining activities, has been built.

With the help of sufficient geomechanical data and a well developed database, not only the geologists, but also the mining engineers, can obtain a further awareness of the underground environment, such as geological structures, rock types and strength, rock density, etc. Mine plan details also play an important role in analyzing the stability of haulage drifts. Efficiently combining geological information and in situ stress redistribution patterns becomes the first priority before running a numerical model for haulage drift stability evaluation.

#### **3.1 Concept of the Database**

The database is a multifunctional query system, Figure 3-1.

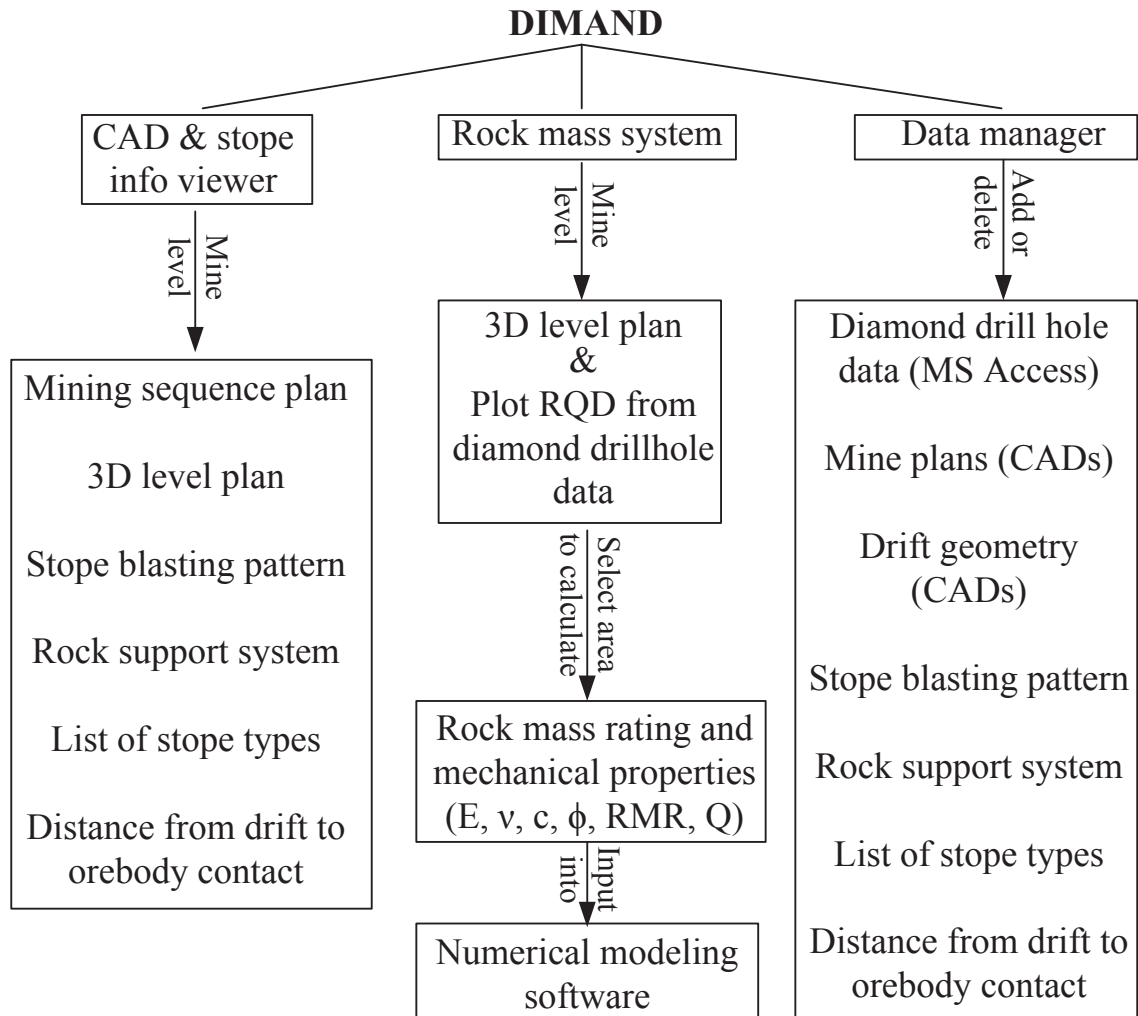


Figure 3-1 Flowchart of Data Integrator for Mine Analysis and Design (DIMAND)

Referring to underground structure stability analysis, a model was set up incorporating various factors like stope size, dip of hanging-wall and footwall, drift orientation with respect to principal stress, rock mass quality, mining depth, drift proximity to the orebody and stress regime; the model allows for introducing different settings of these parameters, as well as using various combinations of parameters. It was convenient to incorporate all the combinations in a single instrument.

In order for engineers to make use of the data, the DIMAND was set up to sort out a unique query among a mass of data and plans, by inputting one or more keywords. As a



practical example, a stope will be excavated soon, and the effect on the haulage drift serving the 5100 level needs to be determined. In the numerical model, rock mass characterization and in situ stress can be calculated automatically through the database, by querying a certain area, constrained by certain coordinates.

The DIMAND was set up, using *Microsoft Access* as the repository of data, and *Microsoft Visual Basic 6* as both a user-friendly interface as well as the query engine. Its purpose was to manage and query all the information of the mine relevant to the evaluation of the stability of haulage drifts. All information was sorted into three groups, relating respectively to the 4900 level, 5000 level and 5100 level of the mine. For each group there was a set of diamond drillhole data, haulage drift geometry, haulage drift development and latest stope sequence plan, primary rock support pattern, distance between haulage drift and stopes, stope construction and blasting details, stope type category, planned stope sequencing, geology structures, stress environment and mine backfill details.

Diamond drillhole data, distance between haulage drift and stopes, stope type category were saved in *Access*. Haulage drift geometry and planned stope sequencing for all the three levels in plain view are the three dimensional *AutoCAD* workspace. Primary rock support pattern was a text file recording Inco's primary support standard. Haulage drift development and latest stope sequence plan, stope construction and blasting details were in portable document format (PDF).

## **3.2 Structure of the Database**

As mentioned above, the Garson mine database included the following elements: diamond drillhole data, haulage drift geometry, haulage drift development and latest stope sequence plan, primary rock support pattern, distance between haulage drift and stopes, stope construction and blasting details, stope type category, planned stope sequencing, geological structures, stress environment and mine backfill details.

### **3.2.1 Illustration of Each Frame Element**

It is essential to take into consideration every item of the mine plan detailed below for purposes of decision making and for evaluating the stability of haulage drifts.

#### **3.2.1.1 Diamond Drillhole Data**

Diamond drillhole data like RQD, RMR, UCS, etc. are real reflections of underground rock mass properties. For example, Figure 3-2 presents a visual concept of RQD values in space, from which engineers can obtain general information about nearby rock mass properties.

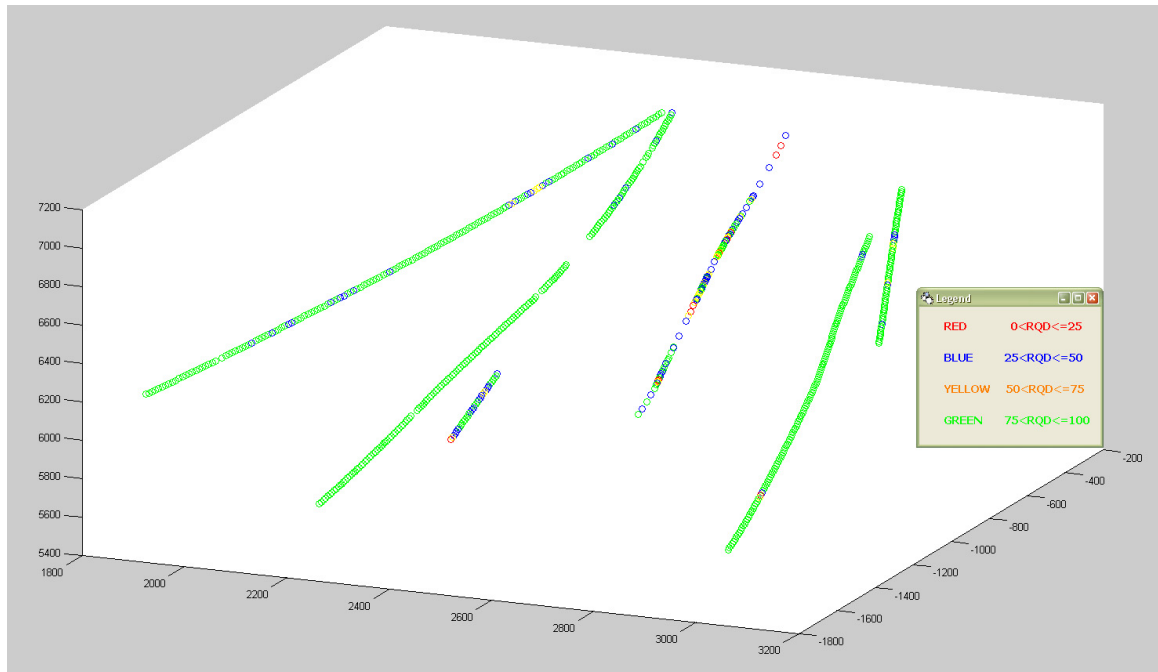


Figure 3-2 Visual on Diamond drillhole location in space

In a 1250ft × 1444ft × 1572ft volume of rock mass, RQD, Q, RMR, density, E, UCS and rock types are employed to identify rock properties. RQD has a statistical distribution shown in Figure 3-3; Q in Figure 3-4; RMR in Figure 3-5; density in Figure 3-6; E in Figure 3-7; UCS in Figure 3-8.

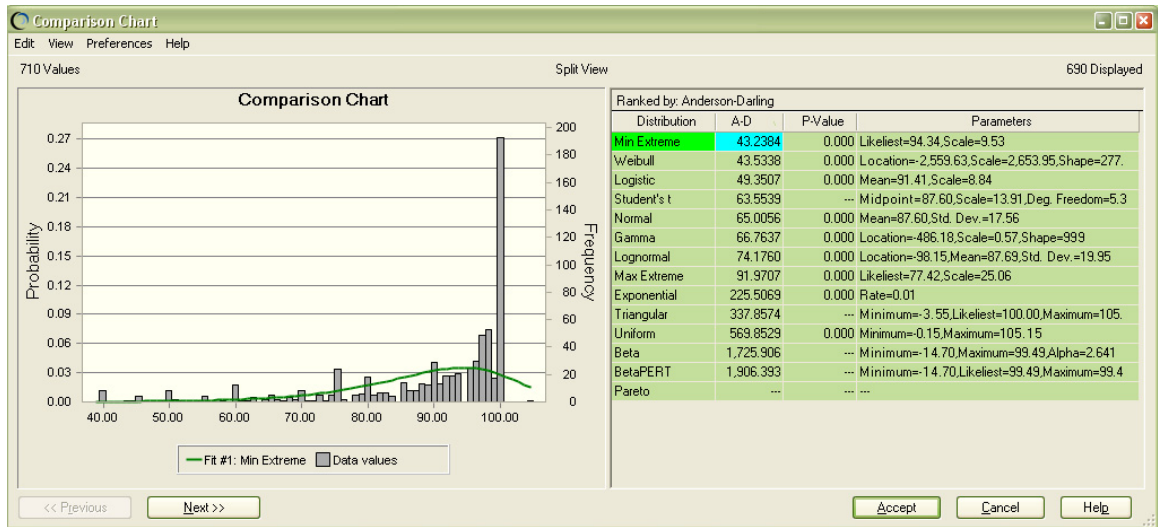


Figure 3-3 RQD histogram

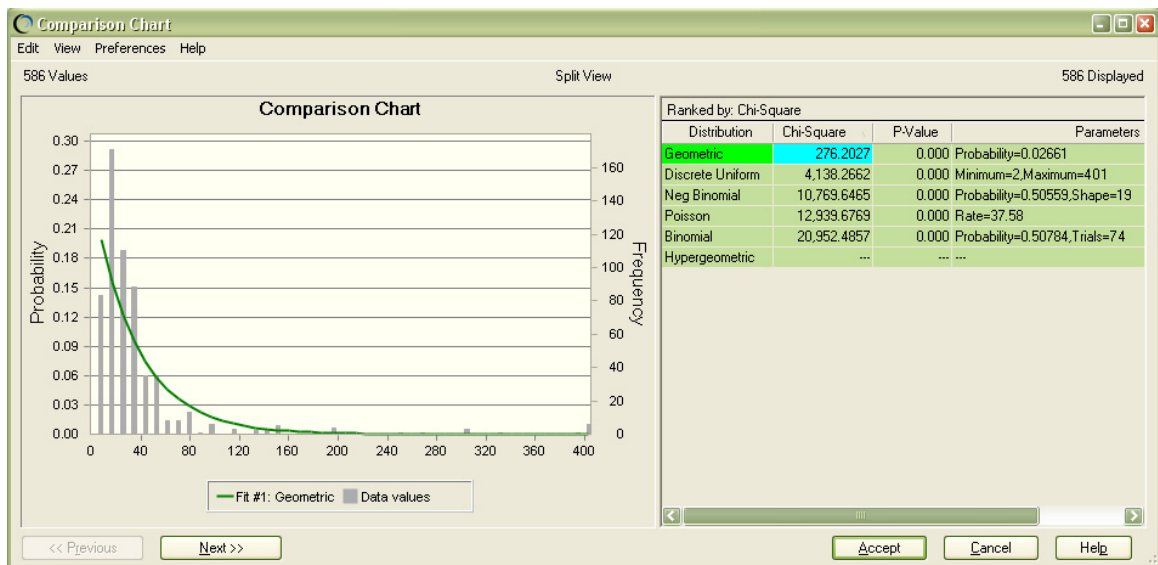


Figure 3-4 Q histogram

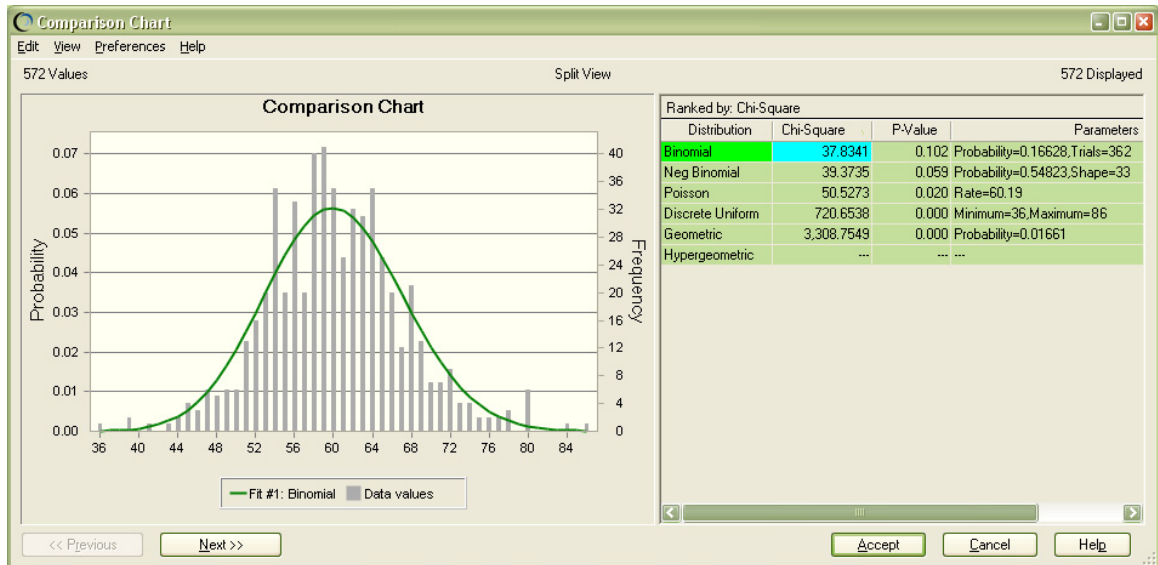


Figure 3-5 RMR histogram

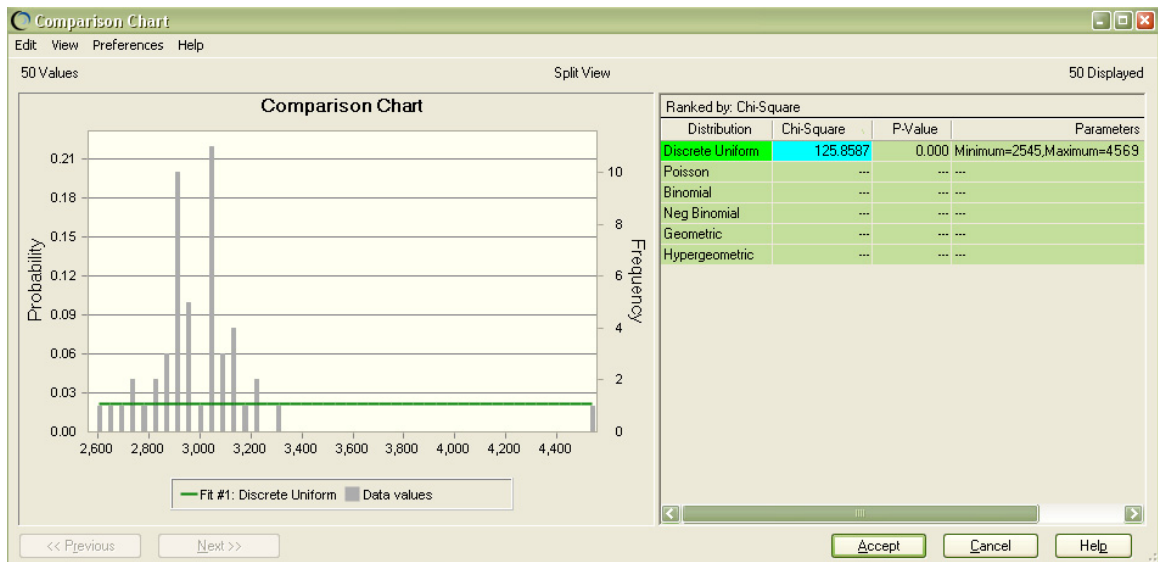


Figure 3-6 Density histogram

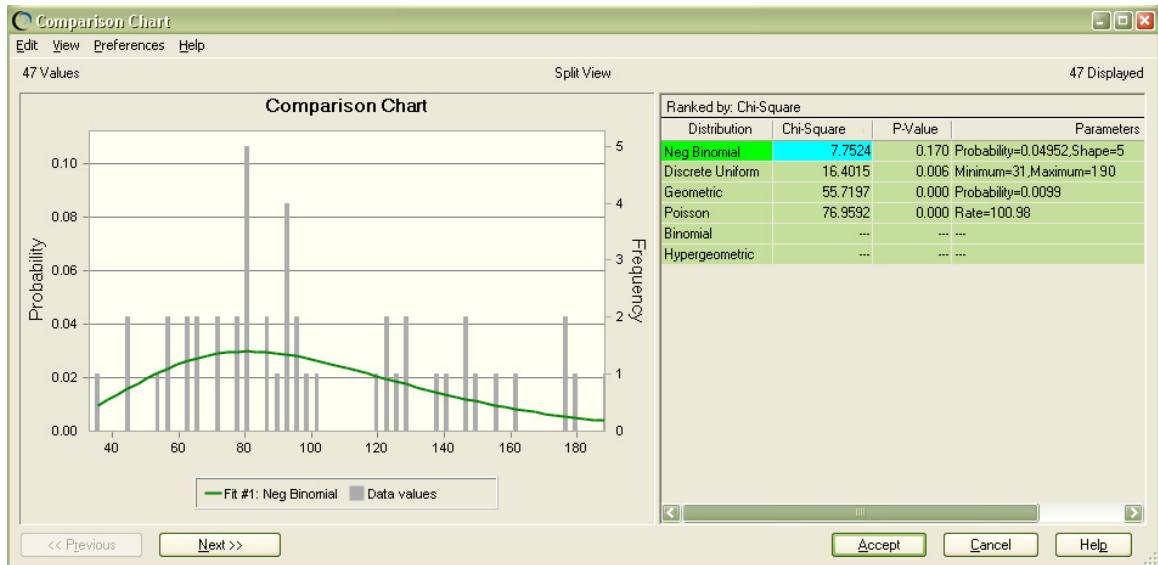


Figure 3-7 Young's Modulus histogram

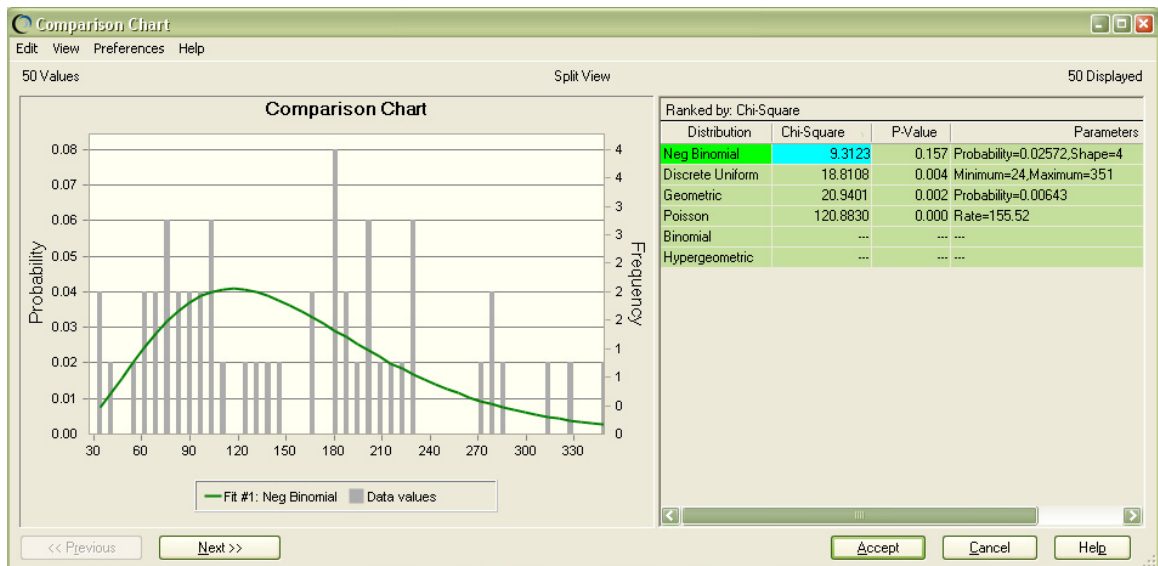


Figure 3-8 UCS histogram

When evaluating haulage drift stability, engineers use these point rock mass properties to further their understanding of the geomechanical environment of a haulage drift, by plotting the drillhole features on a level plan.

### 3.2.1.2 Haulage Drift Geometry

A three dimensional wire mesh of haulage drift geometry has been created for each level, illustrating drift height and span, as shown in Figure 3-9 to Figure 3-11.

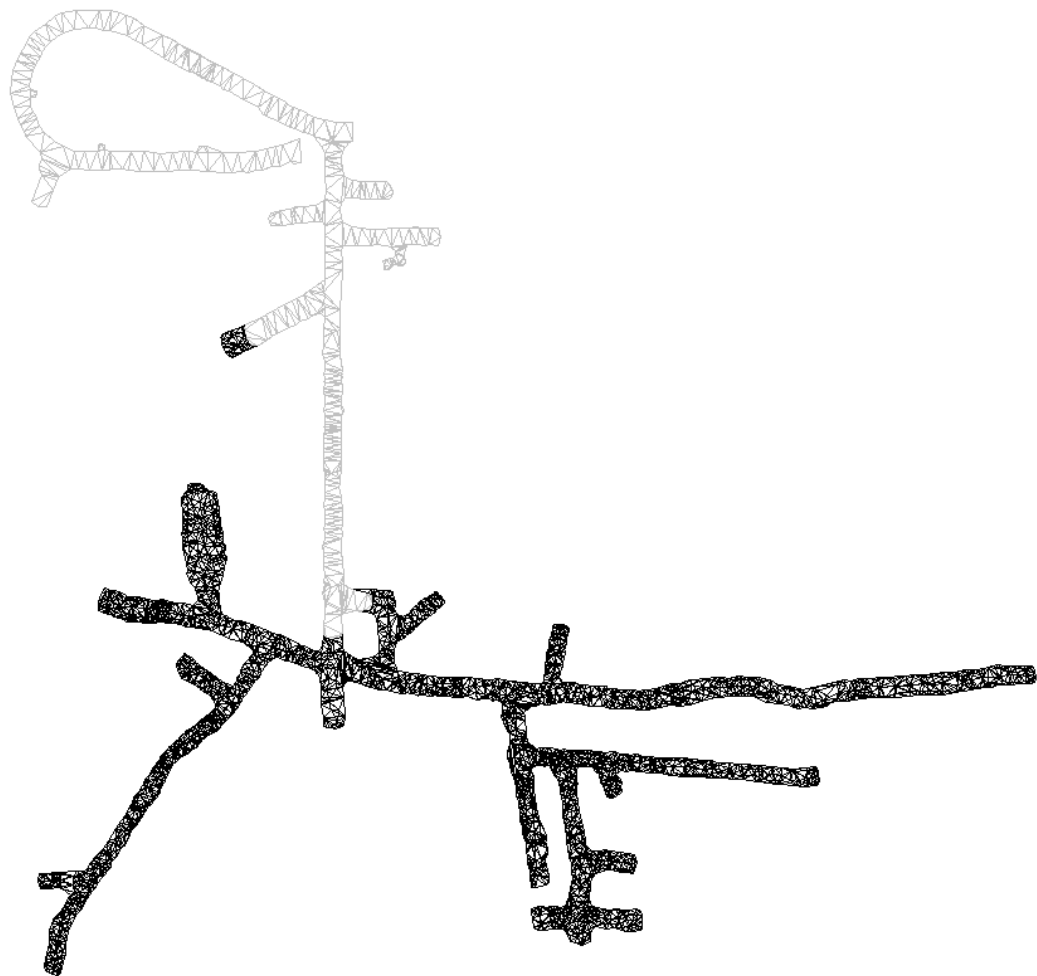


Figure 3-9 4900 level mine plan



Figure 3-10 5000 level mine plan

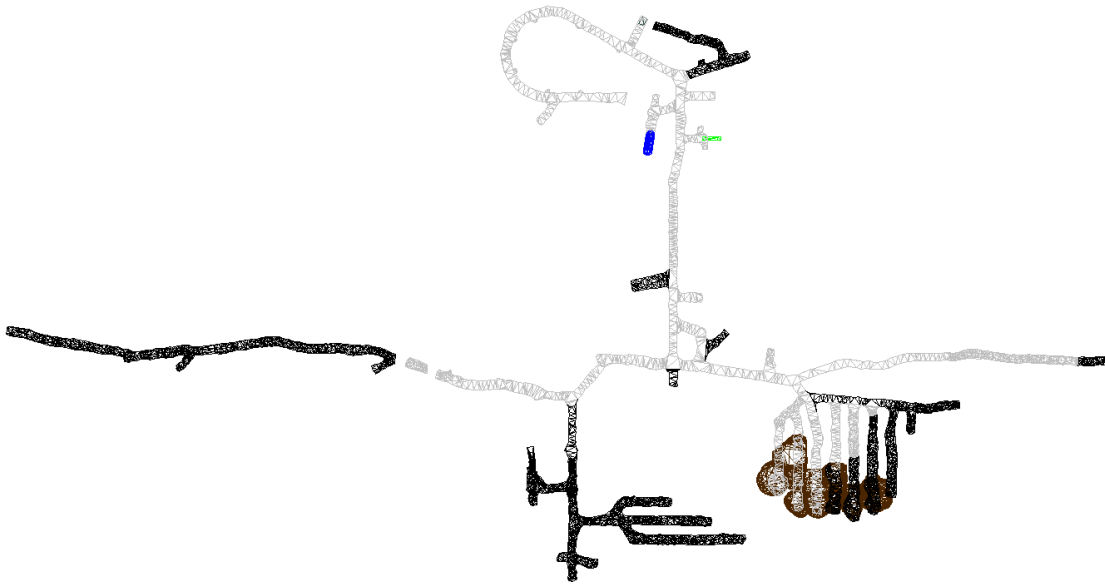


Figure 3-11 5100 level mine plan



### 3.2.1.3 Haulage Drift Development and Latest Stope Sequence Plan

A plan view of each level, with haulage drift development, and latest stope sequence plan, has been created for evaluating drift stability, Figure 3-12 to Figure 3-14. In these Figures, green lines are drifts under development.

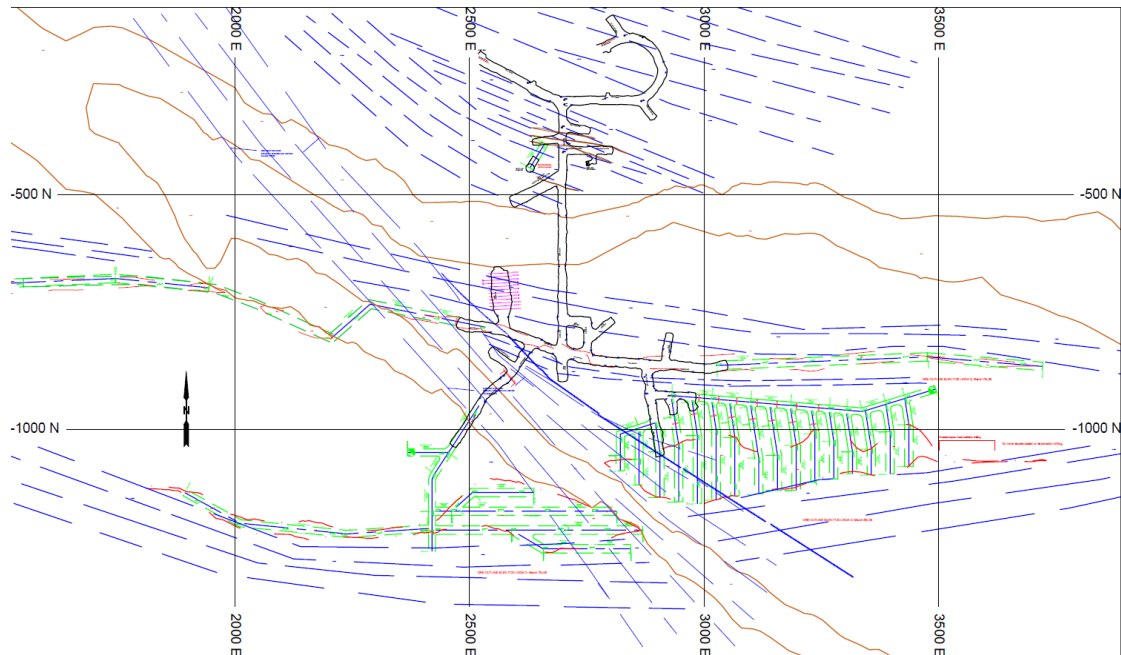


Figure 3-12 Haulage drift development and latest stope sequence plan of 4900 level

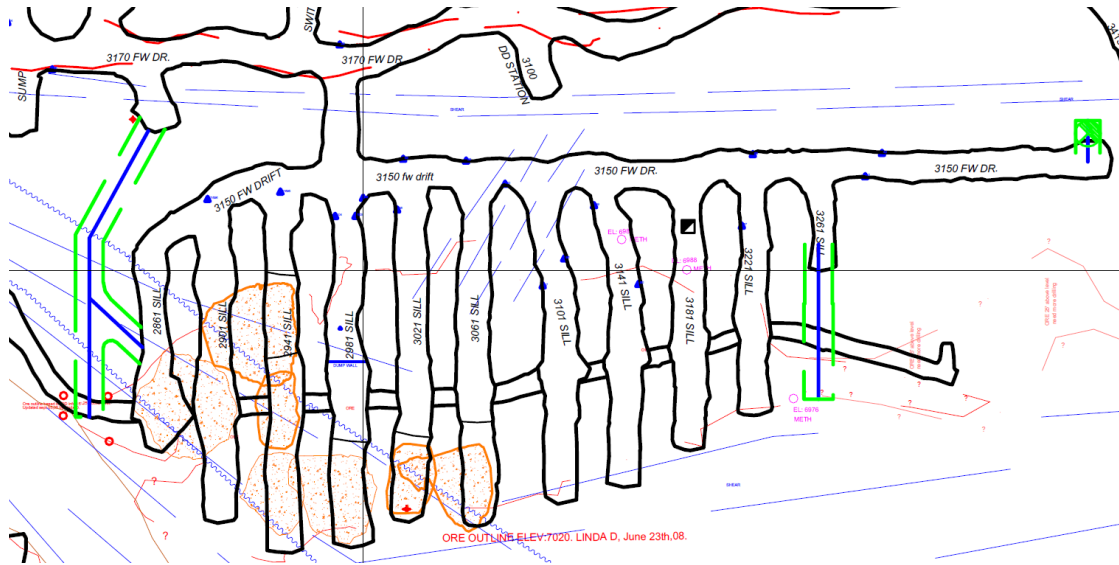


Figure 3-13 Haulage drift development and latest stope sequence plan of 5000 level

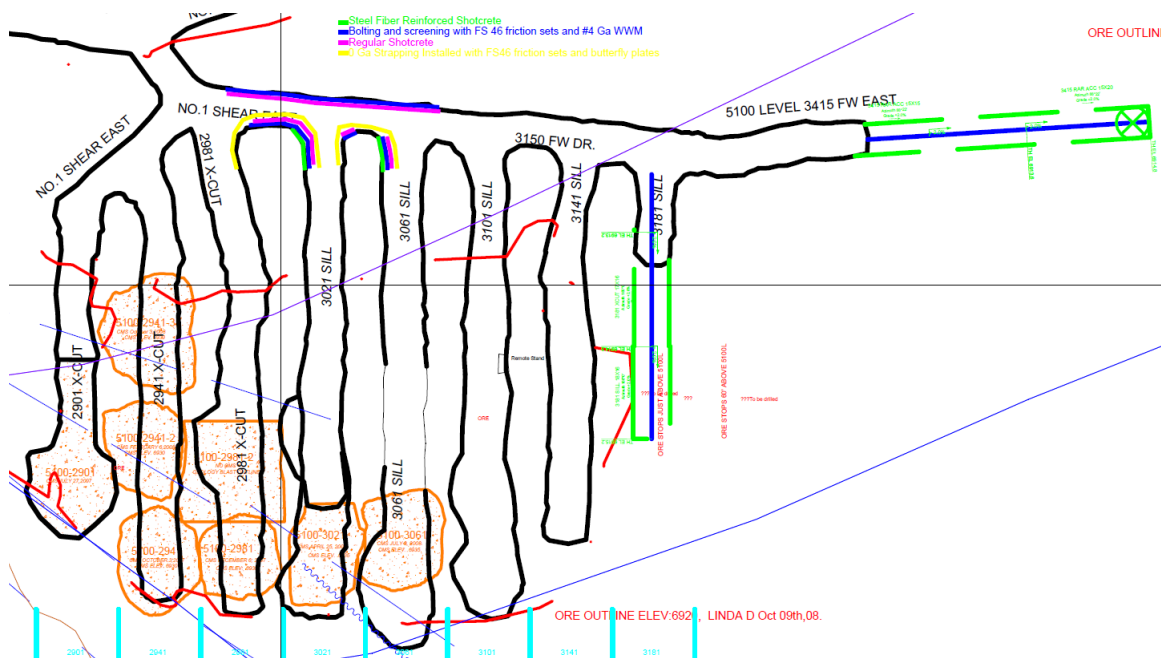


Figure 3-14 Haulage drift development and latest stope sequence plan of 5100 level

#### **3.2.1.4 Primary Rock Support Pattern**

At Inco, the primary rock support pattern consists of:

- Steel fibre reinforced shotcrete
- No.6 WWM
- Bolting to B.R with 8 ft long rebars in the back and shoulders, and 6 ft long rebars in the upper walls (i.e. below the shoulders but above B.R)
- 5.5 ft long FS39 Friction Set Stabilizers in the lower walls

#### **3.2.1.5 Distance between Haulage Drift and Stopes**

The relationship between mining sequence and drift stability has been researched by Zhang and Mitri, 2006 and has been proven to be important for drift stability evaluation. The distance between each stope and the haulage drift on each level has been measured, and is shown in Figure 3-15.

ID	Stope number	type	distance
1	5000-2861	P0	60
2	5000-2901	P0	84
3	5000-2901-2	P1	48
4	5000-2941	P0	161
5	5000-2941-2	P1	115
6	5000-2941-3	P2	58
7	5000-2981	P0	158
8	5000-3021	P0	156
9	5000-3061	P0	156
10	5100-2901	P0	74
11	5100-2941	P0	157
12	5100-2941-2	P1	107
13	5100-2941-3	P2	43
14	5100-2981	P0	188
15	5100-2981-2	P1	143
16	5100-3021	P0	181
17	5100-3061	P0	169

Figure 3-15 Stope type and distance to the haulage drift (ft)

### 3.2.1.6 Stope Construction and Blasting Details

Stope sizes affect drift stability as well. In general, the height between two consecutive stope levels is 100 ft. In each level, the stope is thirty feet high, and the mining sequence is illustrated below in Figure 3-16.

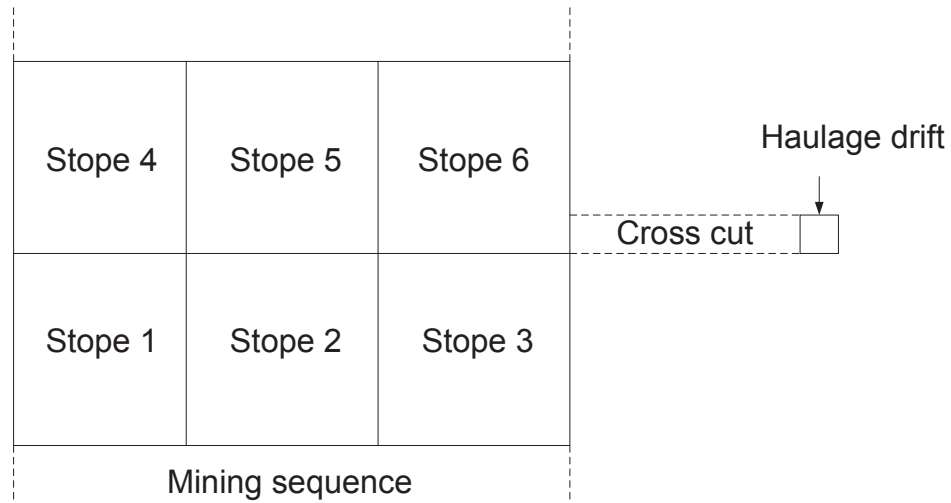


Figure 3-16 Mining sequence

Figure 3-17 shows a blasting pattern of a stope. The red square is to be blasted out at first, in order to form an empty space, into which adjacent rock will fall when blasting the yellow holes.

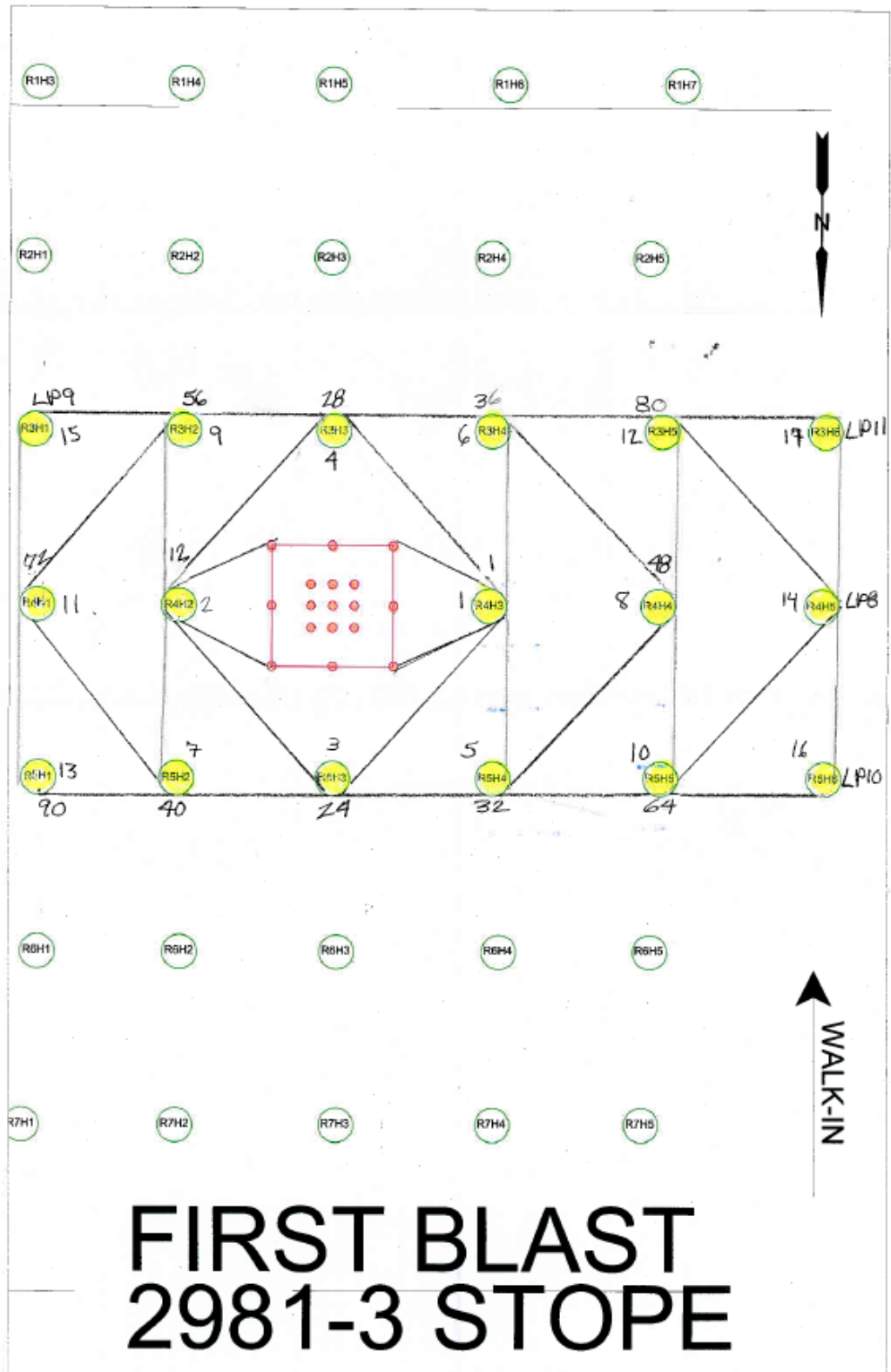


Figure 3-17 Blasthole pattern of stope 2981-3

### 3.2.1.7 Stope Type Category

All stopes have been separated into several types following the name pattern P0, P1, P2 etc., where P stands for “Primary” as shown in Figure 3-18

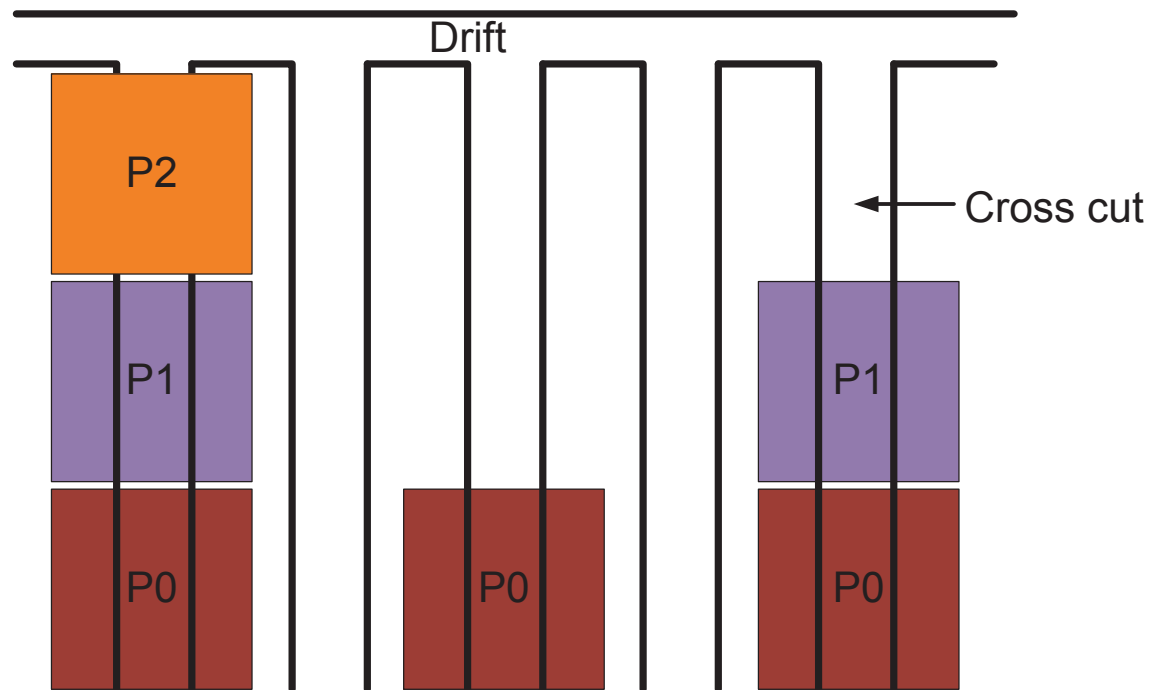


Figure 3-18 Stope type illustration

### 3.2.1.8 Planned Mining Sequence

Before any mining activity is initiated, a well designed mining sequence must be prepared, (Figure 3-19). With respect to production progress, this mining sequence will be modified depending on newly acquired rock mass properties.

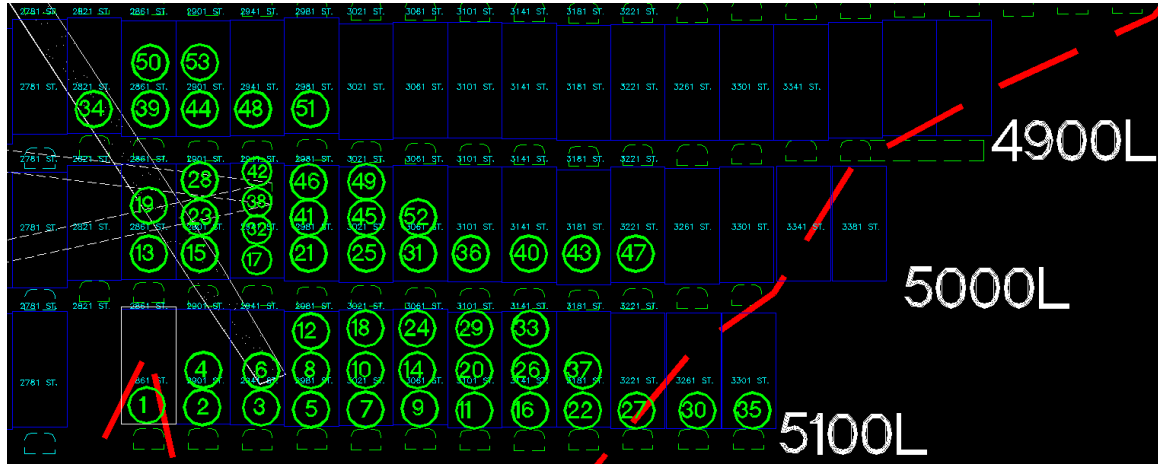


Figure 3-19 Planned mining sequence

### 3.2.1.9 Stress Environment

According to a geotechnical report by MIRARCO, the principal stress environment is as follows:

ID	Mine	Stress	Orientation	Plunge	Value with depth in ft
1	Garson	Major	70		2 1575+1.8*Z
2	Garson	Intermediate	162		44 1260+1.06*Z
3	Garson	Minor	157	-46	1.18*Z

Figure 3-20 Stress environment

As a two dimensional numerical model will be initially set up, principal stresses are projected into the YZ plan, and are decomposed into the Y and Z directions, as illustrated in Figure 3-21, where

$$\sum Z = (1575 + 1.8z) \sin(2^\circ) + (1260 + 1.06z) \sin(44^\circ) - 1.18z \sin(46^\circ)$$

$$\sum Y = (1575 + 1.8z) \cos(2^\circ) \sin(70^\circ) + (1260 + 1.06z) \cos(44^\circ) \sin(162^\circ) + 1.18z \cos(46^\circ) \sin(157^\circ)$$



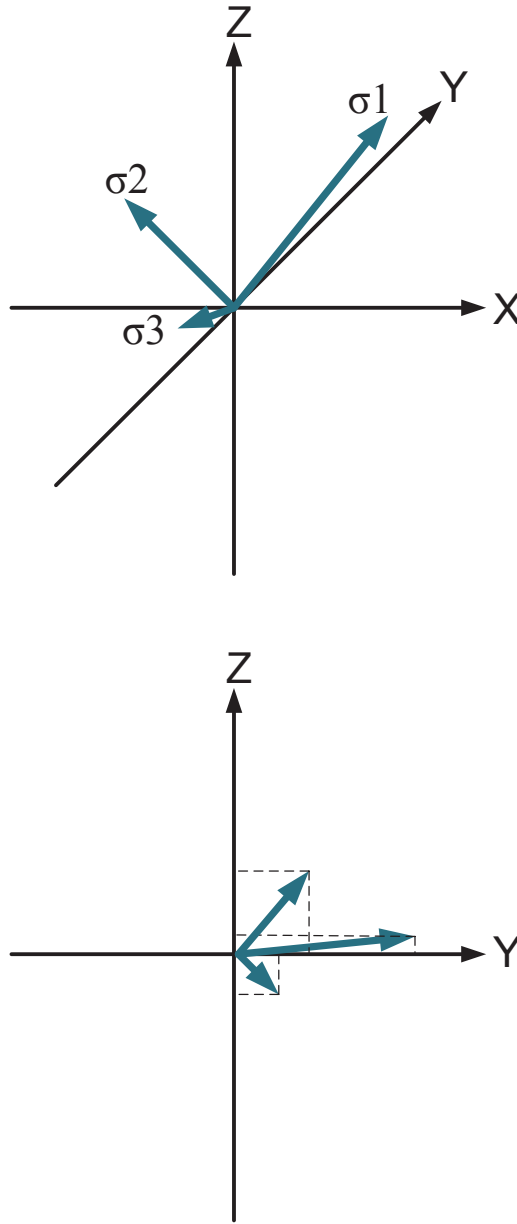


Figure 3-21 Principal stress projected to the YZ plan

#### 3.2.1.10 Mine Backfill Properties

The backfill material is treated, using elastic properties  $E=0.1\text{Gpa}$  and Poisson's ratio  $\nu = 0.30$  as numerical input parameters.

### 3.3 Flow Chart

As explained in Figure 3-22 below, there are three components in the system: database core, query algorithm and user interface. The query algorithm works like an engine from the database and subsequently display results on the user interface.

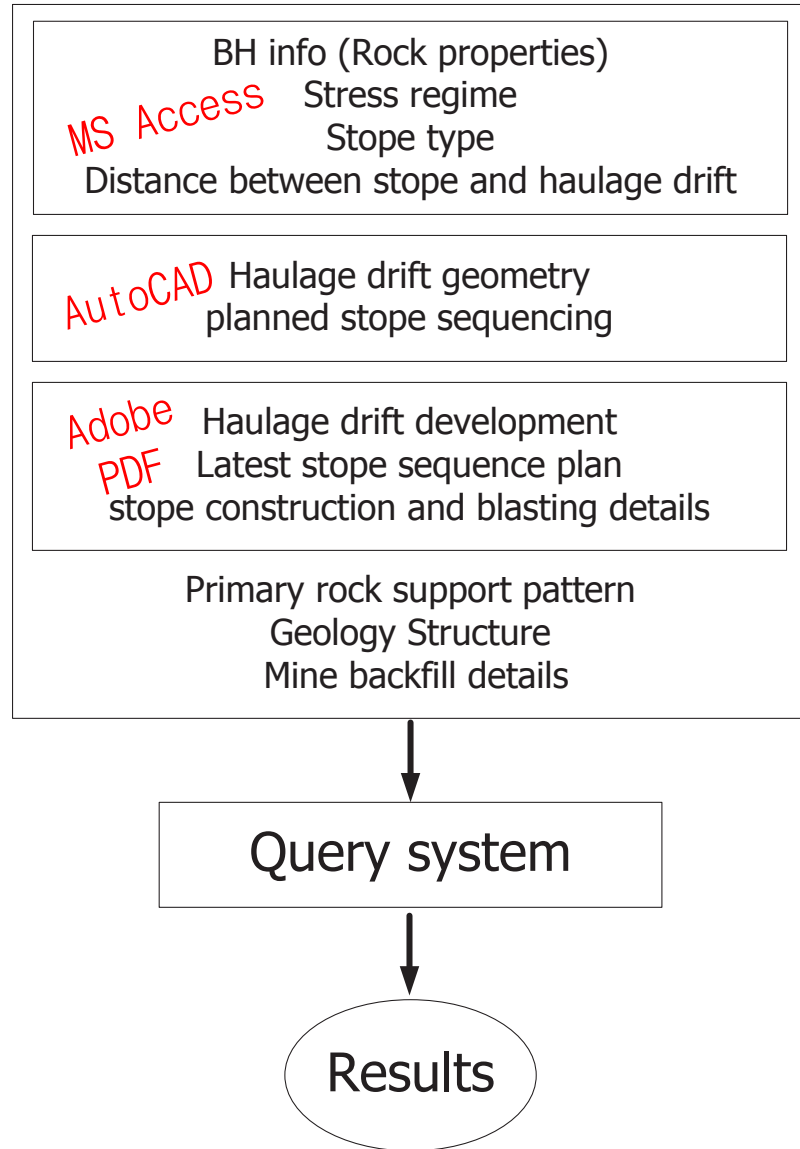


Figure 3-22 Flow chart of database

Generally all the raw data are in *Access*, including, for example, diamond drillhole data (Figure 3-23), which is used to define rock mass characterization, and which occupies a major portion of the total amount of data.

ID	X	Y	Z	BO	CO	LEVEL	FROM	TO	LENGTH	BCODE	COORDS	DEPTH	PR
1	2701.784668	175.622391	-525.614563	7087.970215	44.435291	0	4900	0	73.599998	73.599998		16	
2						0	4900					16	
3						0	4900					16	
4						0	4900					53	
5						0	4900					53	
6	2704.28125	175.960114	-559.550842	7055.119629	43.548363	0	4900	73.599998	94.599998	21		93	
7						0	4900					93	
8	2706.389404	176.263412	-590.563538	7025.842285	43.183468	0	4900	94.599998	159	64.400002		4	
9	2709.004639	176.678909	-632.970764	6986.067871	43.037815	0	4900	159	211	52		180	
10						0	4900					209	
11						0	4900					209	
12						0	4900					209	
13	2711.976074	177.225433	-688.80072	6934.590332	42.085548	0	4900	211	311	100		264	
14						0	4900					264	
15	2713.780273	177.648895	-728.859619	6898.872559	41.353588	0	4900	311	318.399994	7.399994		4	
16	2713.805273	177.690308	-731.935669	6896.164581	41.312706	0	4900	318.399994	319.200012	0.800018		4	
17	2713.935547	177.700409	-732.686216	6895.504395	41.302731	0	4900	319.200012	320.399994	1.199982		4	
18	2713.973145	177.713013	-733.624634	6894.679688	41.29026	0	4900	320.399994	321.700012	1.300018		4	
19	2714.122803	177.763916	-737.417603	6891.348633	41.23988	0	4900	321.700012	330.5	8.799988		329	
20						0	4900					329	
21	2714.329348	177.835861	-742.792969	6886.638672	41.168503	0	4900	330.5	336	5.5		4	
22	2714.578613	177.925659	-749.530151	6880.732441	41.073094	0	4900	336	348.399994	12.399994		4	
23	2715.286865	178.202682	-770.479736	6862.569336	40.80143	0	4900	348.399994	391.5	43.100006		371	
24						0	4900					371	
25	2715.955566	178.487122	-793.763672	6842.571289	40.485519	0	4900	391.5	409.799988	18.299988		398	
26	2716.207764	178.287523	-802.639465	6835.025879	40.225075	0	4900	409.799988	414.799988	5		4	
27	2716.301514	178.180054	-805.656128	6832.477051	40.136654	0	4900	414.799988	417.700012	2.900024		4	
28	2716.463867	178.054001	-810.589844	6828.325684	39.992157	0	4900	417.700012	427.700012	10		4	
29	2716.737549	177.859573	-818.258484	6821.914063	39.767834	0	4900	427.700012	437.700012	10		4	
30	2717.011475	177.682785	-825.295898	6816.074219	39.562279	0	4900	437.700012	446	8.299988		442	
31	2717.199951	177.569336	-829.844238	6812.322266	39.429592	0	4900	446	449.5	3.5		4	
32	2717.266113	177.530975	-831.387939	6811.053223	39.384586	0	4900	449.5	450	0.5		4	
33	2717.44458	177.430542	-835.444641	6807.726074	39.286388	0	4900	450	460	10		457	
34	2717.804932	177.240128	-843.18988	6801.413086	39.041023	0	4900	460	470	10		4	
35	2718.136475	177.077362	-849.869873	6796.007813	38.84697	0	4900	470	477.200012	7.200012		4	
36	2718.416748	176.947403	-855.242249	6791.687012	38.691135	0	4900	477.200012	483.799988	6.599976		4	
37	2718.576904	176.876099	-858.20575	6789.313965	38.605251	0	4900	483.799988	484.799988	1		4	
38	2718.619629	176.857361	-859.983637	6788.689941	38.582645	0	4900	484.799988	485.799988	1		4	
39	2718.684082	176.829269	-860.15741	6787.754395	38.548733	0	4900	485.799988	487.799988	2		4	
40	2718.782005	176.784504	-861.018121	6786.583812	38.510701	0	4900	487.799988	489.799988	2		4	

Figure 3-23 Diamond drillhole info

*AutoCAD* files like haulage drift geometry, planned stope sequencing, and PDF files like haulage drift development, latest stope sequence plans, stope construction and blasting details are stored in *Visual Basic* engineering files in the same folder so that they can be quickly reached, Figure 3-24.

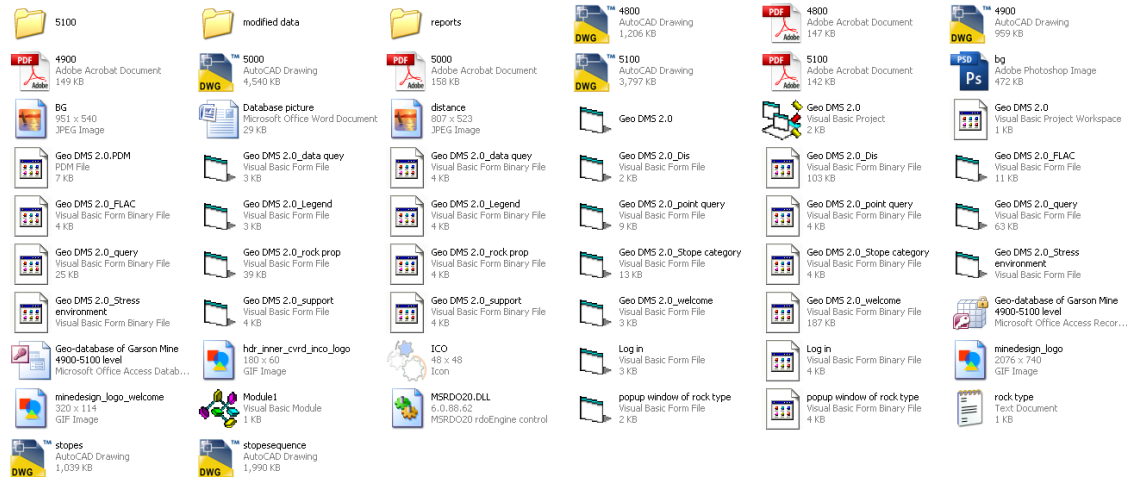


Figure 3-24 File content of the database

A certain query from a user is transformed into an understandable algorithm, from which *Visual Basic* is able to launch a series of calculations in order to find and select data (Figure 3-25).

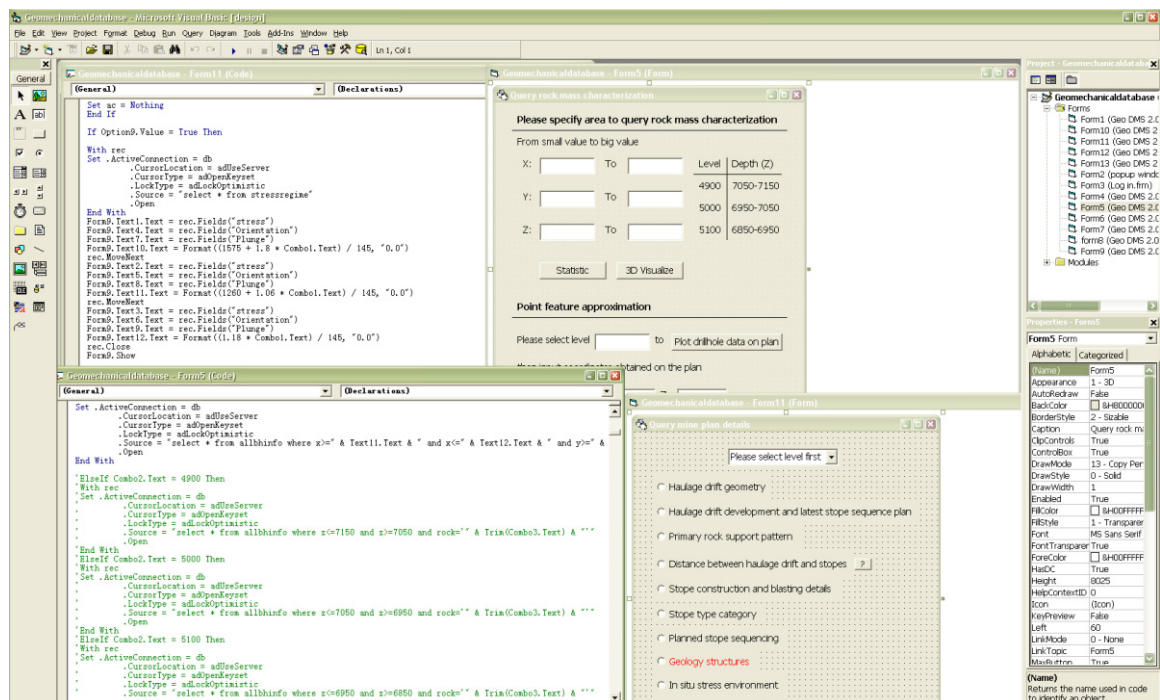


Figure 3-25 Searching engine of the database

### 3.4 Programming Technique in *VB* and Access

Basically, a database will not operate properly without programming. Engineers use various codes, such as *Visual Basic (VB)*, to do offstage control. There are two versions of *VB*, *VB* and *VBA*. In this project, *VB* was selected after a careful balancing of the advantages and disadvantages of each version, as explained below.

In the early days, only programmers could develop user-oriented software that fulfilled specific requirements, while normal users could only operate these ready-made programs. This meant that after the software had been developed and published, no more functions could be added by the user, unless the software were updated to a new version. In engineering fields like *AutoCAD* design, mine planning or numerical modeling, application software is usually weak delivering solutions to complex tasks, such as drawing a paraboloid, inputting duplicated data, integrating systems or assessing risk with complicated mathematical programming. To remedy this situation, *VBA (Visual Basic Application)* was developed as an embedded visual basic programming environment. Both *AutoCAD* and *Microsoft Access* provide *VBA* solutions. With the help of *VBA*, it became possible for engineers to write their own code within current software to adapt it to their work. For example, instead of drawing manually, an engineer could write *VBA* codes to design a mechanical part whose surface is a saddle paraboloid, as shown in Figure 3-26.

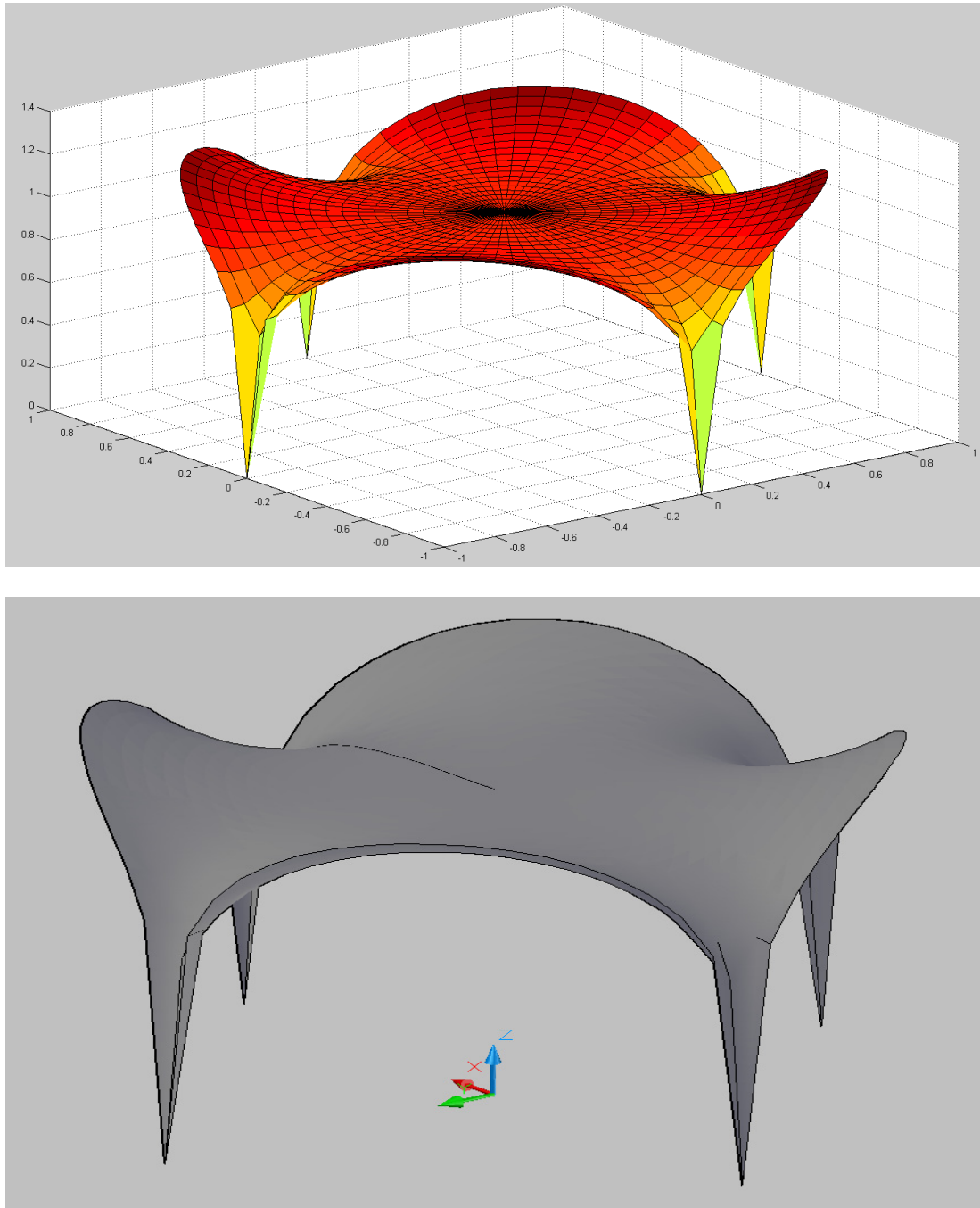


Figure 3-26 Drawing a part in *AutoCAD* with *VB* instead of manually

### 3.4.1 Programming Technique

Although *VBA* is a very strong embedded function within software like *AutoCAD* and *Access*, etc., it turns out to be a double edged sword as a programming language. *VBA*

only supports activities within the software itself, and this feature is inconsistent with the goal of this work, which consists in packing all sorts of relevant data from different software platforms into a single instrument.

Though *VB.net* is a powerful and widely used programming environment, it is optimized for developing web applications and is unnecessarily complicated for developing a local database. Thus it was finally decided to adopt *VB6 (Visual Basic 6.0)*, known as an event-driven programming language and integrated development environment (IDE).

A project named “GeoDB\_Garson” was created at first. Then four major techniques were used to guarantee that the database was running properly:

1. Linking *Access* with *VB*.

In *VB*, a path leading to the data source is necessarily instructed to allow query or management. For example,

```
Public db As New ADODB.Connection
```

```
With db
```

```
    .Provider = "MSDASQL"
```

```
    .CursorLocation = adUseServer
```

```
    .Mode = adModeReadWrite
```

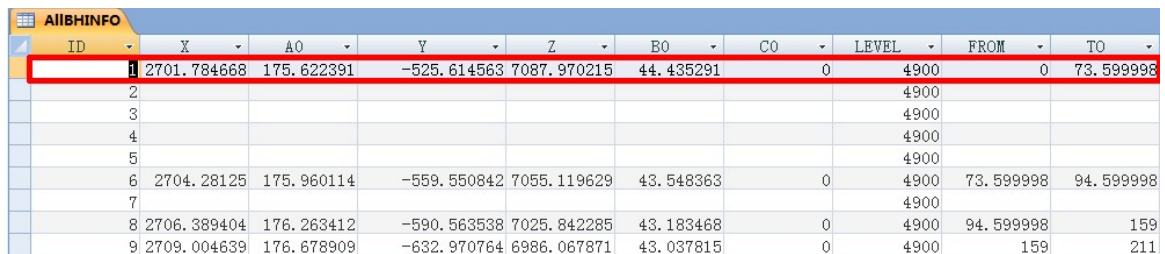
```
    .Open "Provider = Microsoft.Jet.OLEDB.4.0;Data Source=database  
location"
```

```
End With
```

This code admits that any application within *VB* may gain access to the data source, while maintaining the ability to overwrite the data source. A connection is set up allowing the user to browse or manipulate the database.

## 2. Scanning the data.

Once a gate was opened, and a path was set up, a cursor was employed by the user. A cursor is a certain memory set which, in brief, is a row in *Access* that gives the user full control of editing the data, as shown in Figure 3-27.



ID	X	A0	Y	Z	B0	C0	LEVEL	FROM	TO
1	2701.784668	175.622391	-525.614563	7087.970215	44.435291	0	4900	0	73.599998
2							4900		
3							4900		
4							4900		
5							4900		
6	2704.28125	175.960114	-559.550842	7055.119629	43.548363	0	4900	73.599998	94.599998
7							4900		
8	2706.389404	176.263412	-590.563538	7025.842285	43.183468	0	4900	94.599998	159
9	2709.004639	176.678909	-632.970764	6986.067871	43.037815	0	4900	159	211

Figure 3-27 illustration of a cursor

Since nearly eighty percent of the total operations depend on the cursor, it is very important to understand the mechanism of the cursor, as defined below:

```
Dim rec As New ADODB.Recordset
```

```
With rec
```

```
Set .ActiveConnection = db
```

```
.CursorLocation = adUseServer
```

```
.CursorType = adOpenKeyset
```

```
.LockType = adLockOptimistic
```

```
.Source = "select * from & table name"
```

```
.Open
```



End With

3. Calculation and presentation of results.

There is only one procedure to be followed no matter how complicated the query is, namely: moving the cursor according to the query, fetching the data in any column into memory, doing a calculation or a comparison and then displaying the query results. For example,

```
Dim rec As New ADODB.Recordset
```

```
With rec
```

```
Set .ActiveConnection = db
```

```
    .CursorLocation = adUseServer
```

```
    .CursorType = adOpenKeyset
```

```
    .LockType = adLockOptimistic
```

```
    .Source = "select * from & table name"
```

```
    .Open
```

```
End With
```

```
Do while not rec.eof
```

```
    ...
```

```
    Query demands
```

```
    ...
```

```
Loop
```

```
Rec.move
```

```
Label.caption = query results
```

Through the above codes, the user can easily query the rock mass characterization of any type of rock at any level, as shown in Figure 3-28.

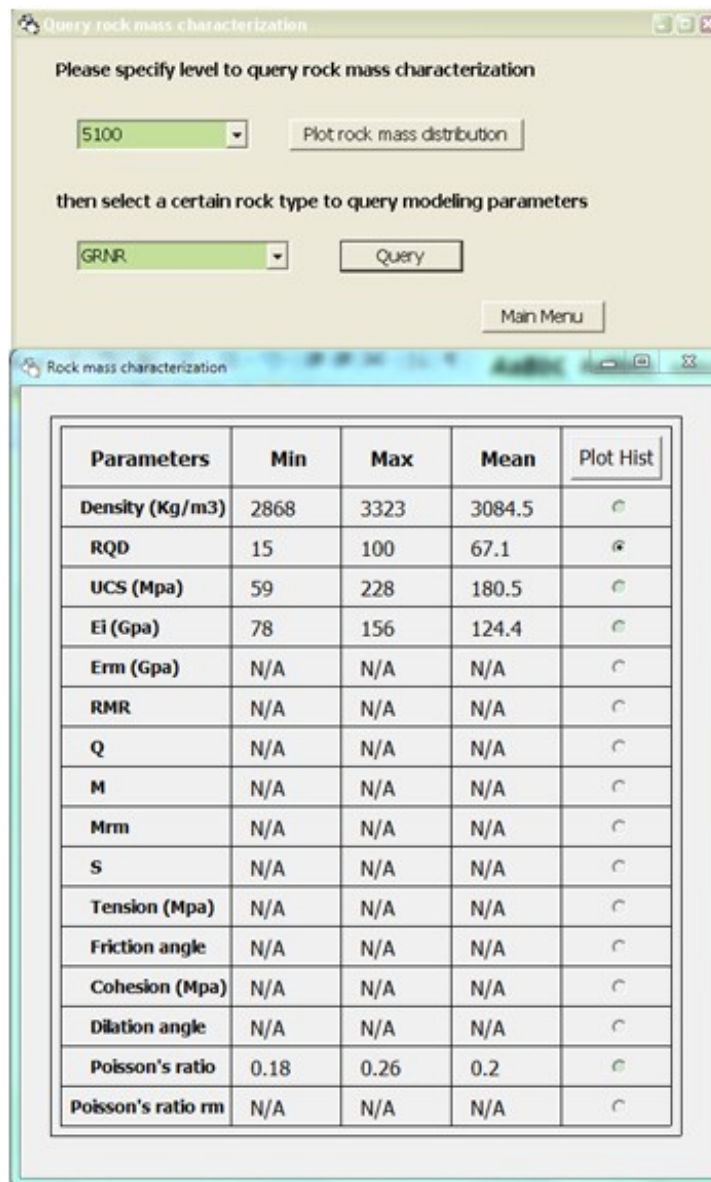


Figure 3-28 Rock mass properties of granite-norite on 5100 level

#### 4. Conjunctive programming between *VB* and other applications

The user may want to query mine plan details not stored in *Access*, but in other file formats, such as *AutoCAD* (Figure 3-29) or Adobe PDF (Figure 3-30).

Such demands can be fulfilled by using the following codes:

```
Dim ac as Object
```

```
Set ac = CreateObject("autocad.application")
```

```
ac.Documents.Open App.Path & "path ".dwg"
```

```
ac.Visible = True
```

```
Set ac = Nothing
```

To open an *AutoCAD* file:

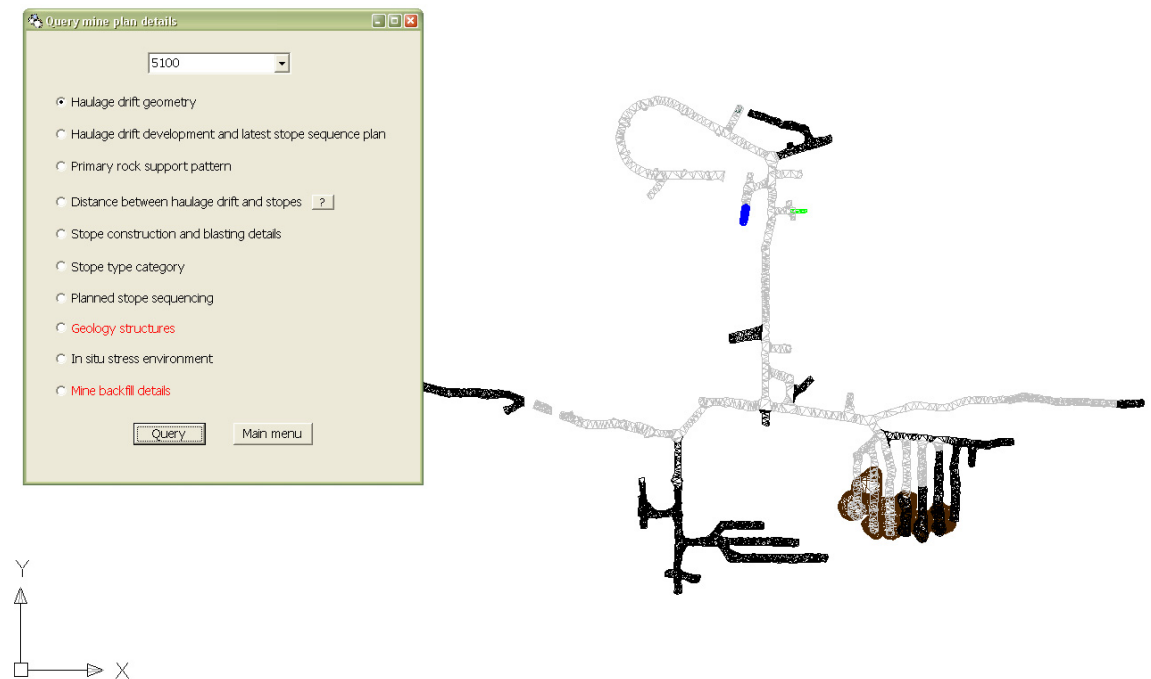


Figure 3-29 Query drift geometry

Or to open an Adobe PDF file:

Dim pdf as Object

Set pdf = CreateObject("AcroExch.AVDoc")

pdf.Open App.Path & "path".pdf", "pdf"

Set pdf = Nothing

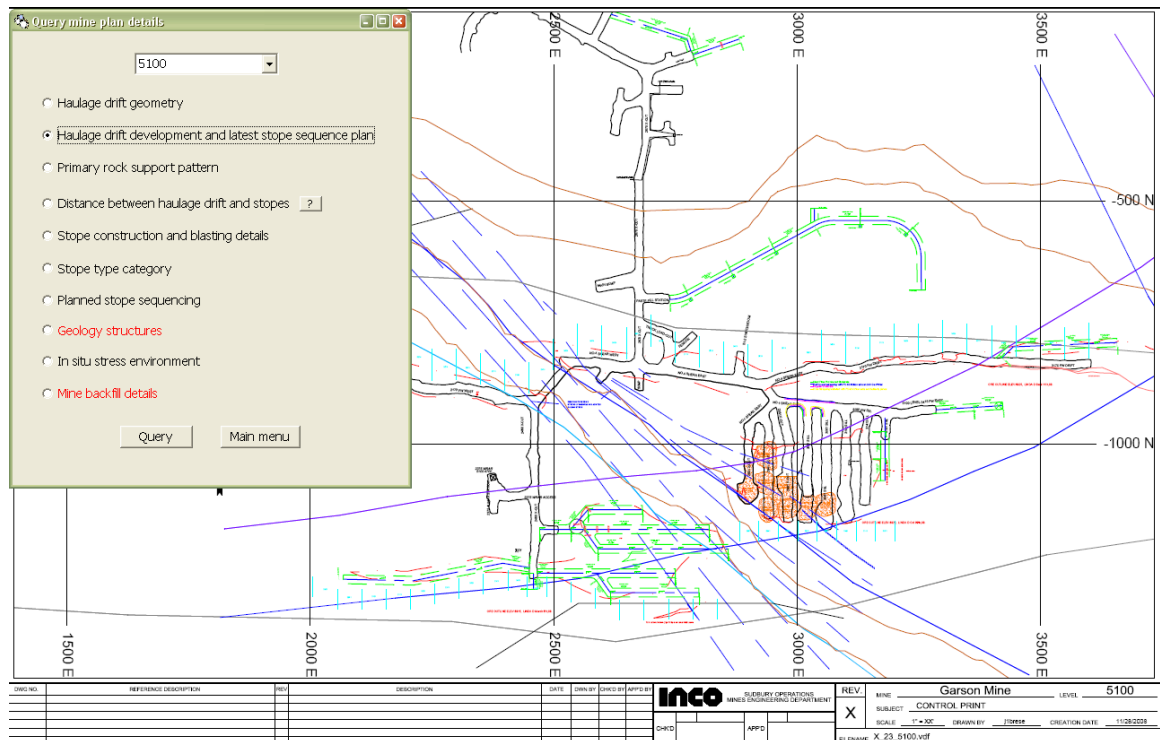


Figure 3-30 Query Haulage drift development and latest stope sequence

### 3.4.2 Error Handling

Errors can be characterized as major or minor.

A major error occurs when, due to insufficient diamond drillhole data, some columns or rows are left blank. If the cursor falls on the blank cell and was intended to draw data from it, an error happens that may lead to a crash of the query system.

Minor errors occur when some treatments of codes produce improperly rounded off calculated results.

### 3.5 Query Methodology

Using the database, a case study was launched, querying rock mass characterization of a cross section of the 5100 level (Figure 3-31) in order to carry out numerical modeling in *Phase2*.

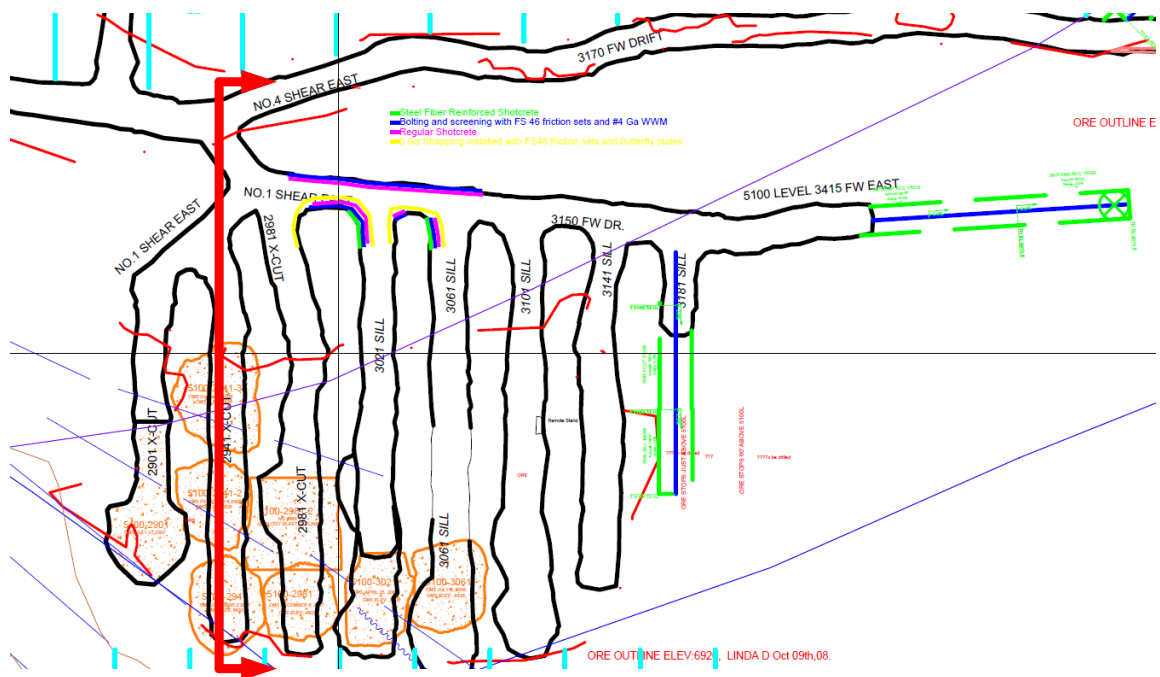


Figure 3-31 Location of numerical model

A welcome window of the database is presented in Figure 3-32.

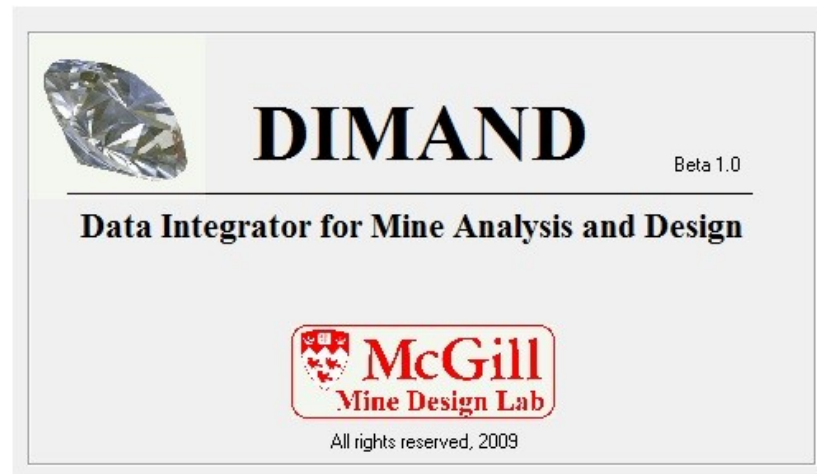


Figure 3-32 DIMAND of Garson Mine

“Data Query” was selected to launch rock mass characterization query. Then “Rock mass characterization” was selected and “5100” was entered in “plot rock mass distribution” for the 5100 level, as shown in Figure 3-33.

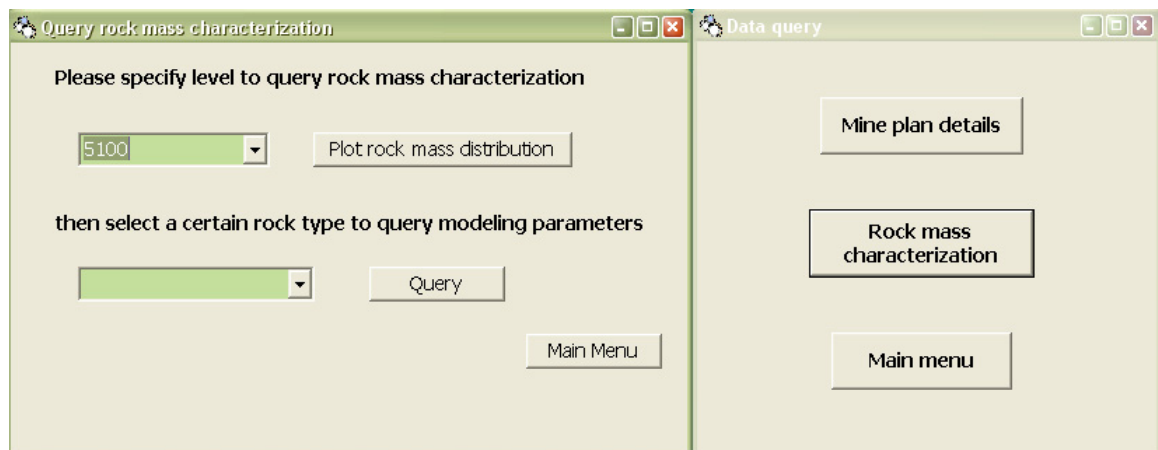


Figure 3-33 Query rock mass characterization by level

A haulage drift geometry of the 5100 level is opened, as shown in Figure 3-34, from which it can be found that there are ten different rock types at the north part of the haulage drift.

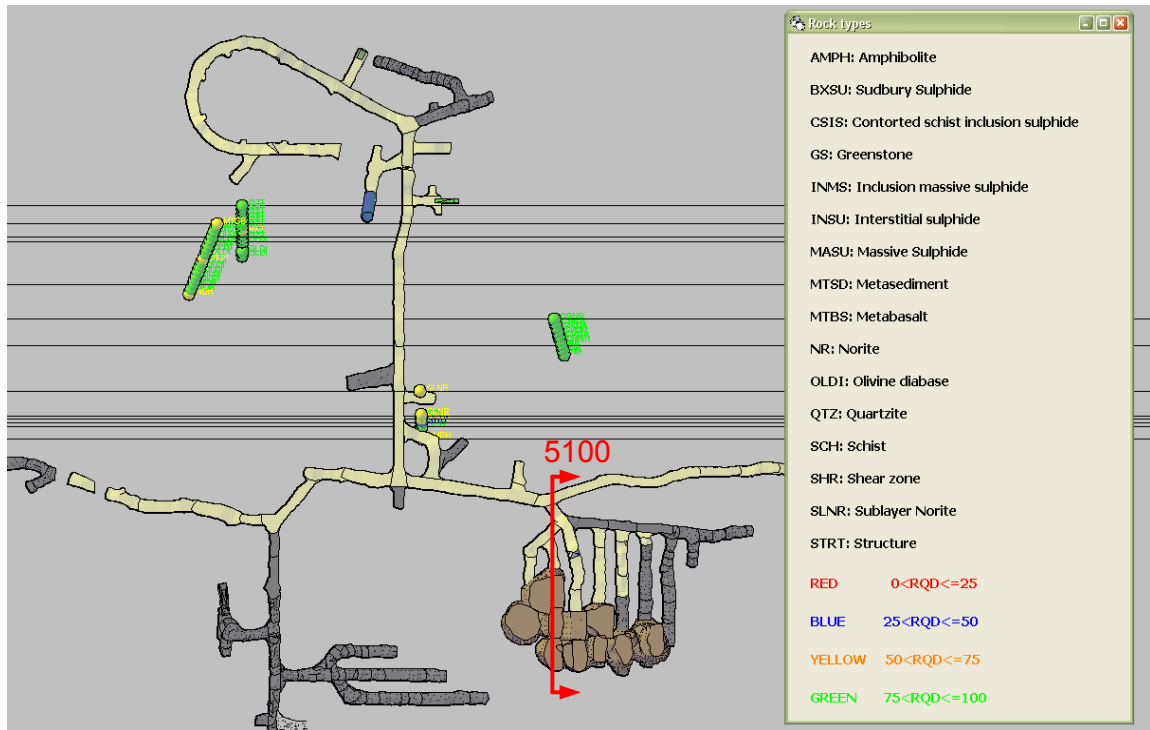


Figure 3-34 Query results of 5100 level

Finally, the real model of cross section 5100 (Figure 3-35) is transformed into *Phase2* (Figure 3-36) making it possible to run a numerical model for evaluating the stability of the haulage drift.

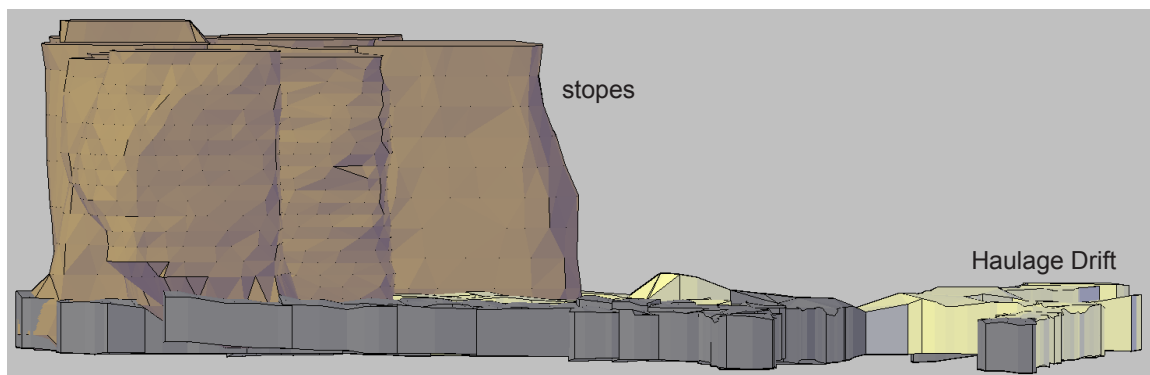


Figure 3-35 Real geometry of numerical model of 5100 level

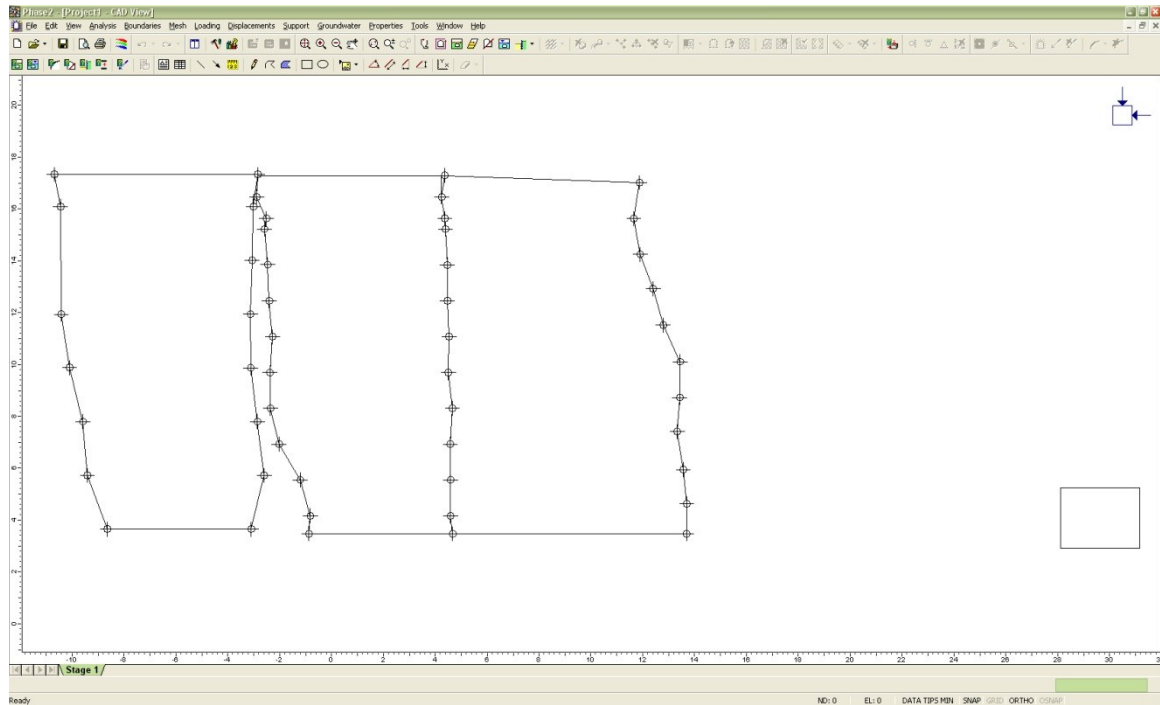


Figure 3-36 Transformed numerical model from real geometry of drift and stopes on 5100 level

### 3.6 Features of DIMAND

The information contained in DIMAND is distributed as follows:

- For each level, there is a 3D drift geometry, **three** in total at the moment in DIMAND, **ten more** in the future with respect to mine development.
- For each level, there is a plan of mining sequence, **three** in total at the moment in DIMAND, **ten more** in the future with respect to mine development.
- For each level, there is a few sets of blasting technical notes, one set in total at the moment in DIMAND, **ten more** in the future with respect to mine development.



- For each level, there are around **30** readings of the distance between drift and orebody contact regarding stope numbers, **90** in total at the moment in DIMAND, **ten times more** in the future with respect to mine development.
- For the diamond drillhole data, there are about **2000** readings distributed in **7** boreholes. For each reading, it contains information as **location, RQD, RMR, young's modulus, Q, average Q, Poisson's ratio, joints orientation, joints set number**, which means **18000** useful numbers to quantify rock mass quality. **Ten times more** in the future with respect to mine development.

The key function of DIMAND is to **quickly find a level plan**, plot diamond drillhole data on it, and **quantify the rock mass quality** for numerical modeling use.

### 3.7 Suggestions for Further Development

- Expand the scope of the database to include other ore zones at Garson mine.
- According to feedbacks from ground control engineers, update the database to query relevant daily production information.
- To facilitate multi-query, further development of the searching index that links all the information in *MS Access* is necessary.
- Develop a new visualization system to better present the rock mass characterization.

## **Chapter 4**

### **Stability of Haulage Drift During Nearby Mining Activities**

#### **4.1 Introduction**

Haulage drifts are used for the transportation of blasted ore from the draw point to nearby ore pass or dumping point. During production, haulage drifts are occupied by mine operators and mining equipment. Therefore the stability of haulage drift is important to the safe and uninterrupted production of a mining operation. It would be advantageous to know how stability is influenced by mining activities in the proximity of the drift. This chapter presents a case study of a haulage drift from the Garson mine of Vale Inco. The study is done with numerical modeling to help examine the performance of haulage drift during nearby mining activity in a sublevel stopping environment.

Zhang and Mitri (2008) reported that the distance between the stope and haulage drift has a great influence on the stability of a haulage drift. Following this track, numerical models are developed herein to evaluate the influence of mining sequences: from lower to upper levels, and from hanging wall to footwall in retreat, as well as the influence of drift orientation with respect to principal stress on the stability of haulage drift. The models represent a case study of the Garson deep mine, with mining depth currently at 5,100 feet below surface (Figure 4-1).

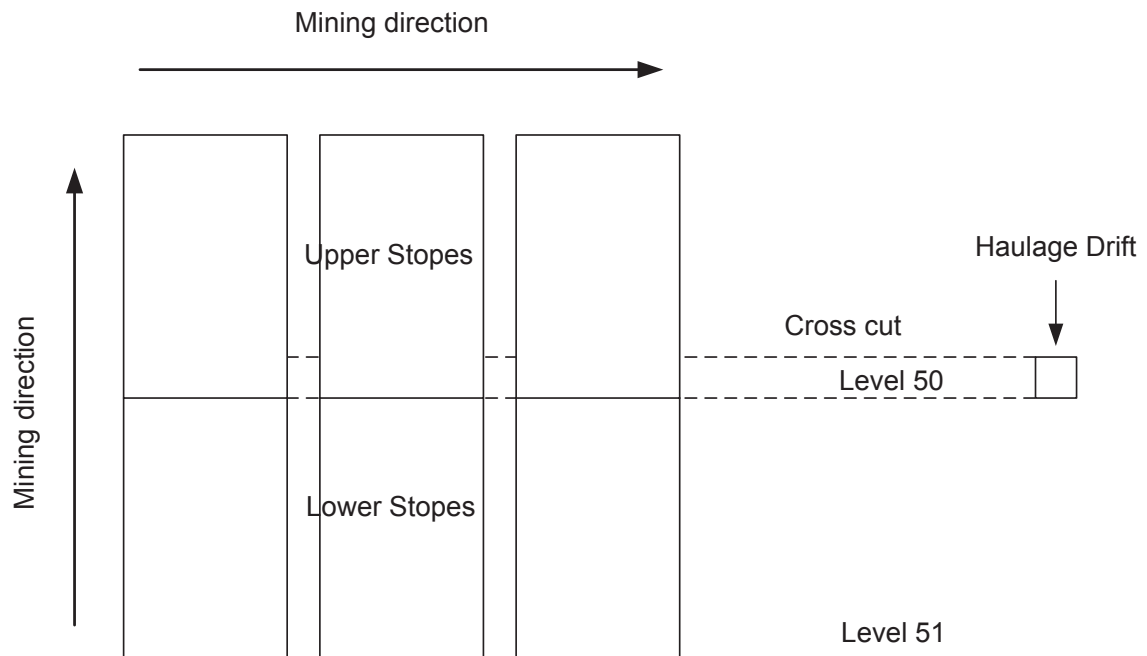


Figure 4-1 Layout of problem analyzed showing haulage drift in the vicinity of mining

## 4.2 Numerical Model

A case study from Garson mine, Vale Inco has been selected to examine the stability of the 5000 ft level (level50 – Figure 4-1) haulage drift as mining production proceeds on three stopes on level 51 and three stopes on level 50. According to the level plan shown in Figure 4-2, there is a shear zone intersecting the orebody in a south-east direction at the south-west part of the orebody. A typical section A-A passing through the 3150 footwall drift is selected to develop the finite element models in *Phase2* (RocScience, 1989)

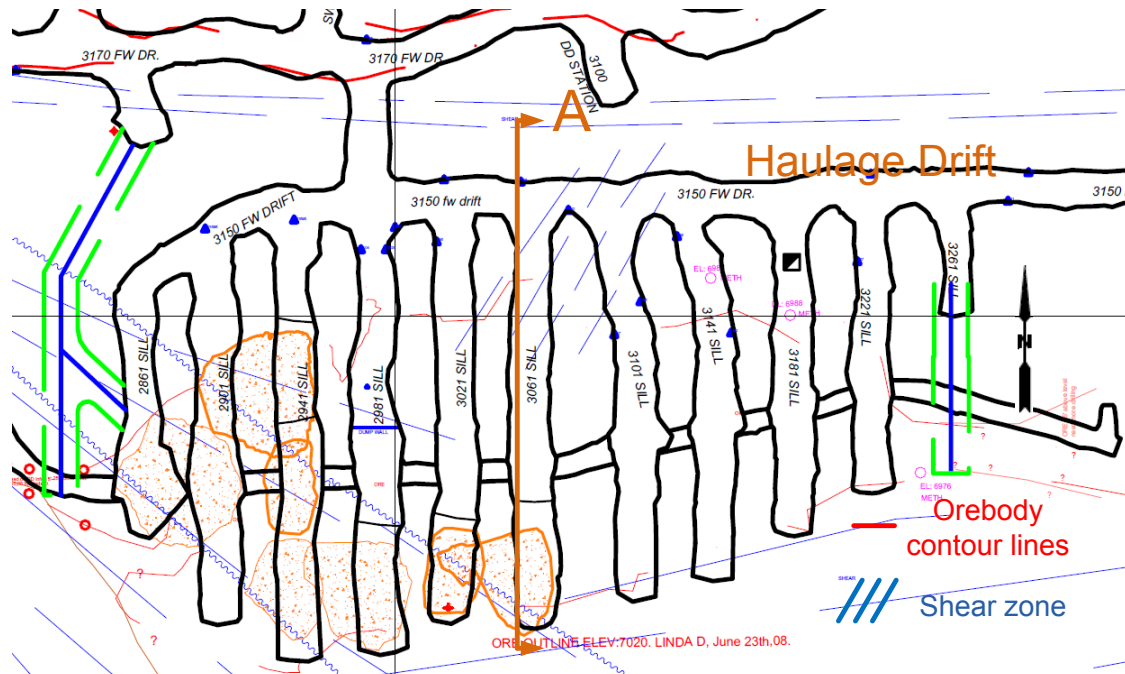


Figure 4-2 Plan view of level 50 – Garson mine

As part of the preparation of model input parameters, a DIMAND for Garson mine has been built to help organize and retrieve information in an orderly fashion. The layout of level 50 as depicted by the DIMAND is shown in Figure 4-3. In order to launch the numerical modelling analysis, orebody properties, rock mass and backfill properties as well as in situ stresses are required. The DIMAND presented in chapter 4 has been used to extract the required geomechanical data. These are listed in Table 4-1.

As for in situ stresses, Herget (1987) derived a set of empirical equations for the estimation of the horizontal-to-vertical in situ stress ratio  $k$  as a function of the mining depth  $H$  as follows.

$$k_{\max} = \frac{\sigma_{H\max}}{\sigma_v} = \frac{357}{H} + 1.46 \quad (1)$$

$$k_{\min} = \frac{\sigma_{H\min}}{\sigma_v} = \frac{167}{H} + 1.10$$

$k_{\max}$ : the maximum horizontal-to-vertical in situ stress ratio

$k_{\min}$ : the minimum horizontal-to-vertical in situ stress ratio

$\sigma_{H\max}$ : the maximum horizontal in situ stress

$\sigma_{H\min}$ : the minimum horizontal in situ stress

H: mining depth

In the current case study, the calculated  $k_{\max}$  and  $k_{\min}$  from equation (1) are 1.67 and 1.20, respectively at a depth of 1,670 m. As can be seen from the level plan of Figure 4-3, the haulage drift is not quite parallel to the orebody. In fact, the mine plans show that the distance between the haulage drift and the orebody contact ranges from 12 m to 18 m. Zhang and Mitri (2008) reported that this distance has a significant influence on the stability of the drift. Therefore it was decided to analyze this parameter in the present case study.

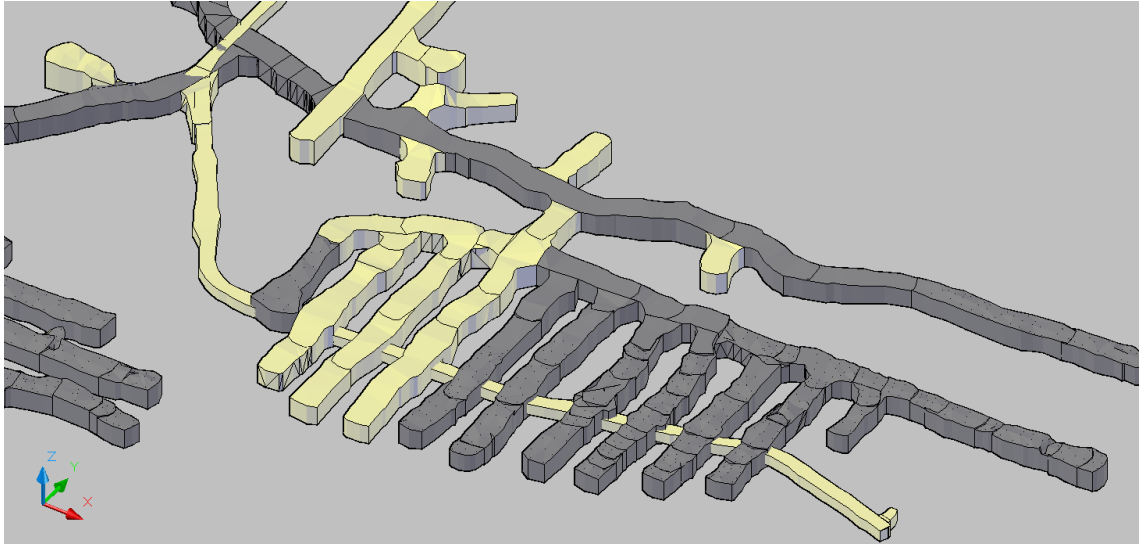


Figure 4-3 Three-dimensional view of level 50

Table 4-1 Mechanical properties of materials as obtained from the Garson Mine database

Material	Hanging Wall	Ore	Foot Wall	Backfill
Unit weight	0.03 MN/m <sup>3</sup>	0.03 MN/m <sup>3</sup>	0.03 MN/m <sup>3</sup>	0.03 MN/m <sup>3</sup>
Young's modulus	40000 MPa	10000 MPa	24000 MPa	100 MPa
Poisson's ratio	0.18	0.22	0.15	0.30
Dilation Parameter	0	0	0	0
Compressive strength	200 MPa	45 MPa	120 MPa	1 MPa
m <sub>b</sub> parameter	8.2	5	4.8	0.1
s parameter	0.06	0.02	0.04	0.001

#### 4.2.1 Finite Element Model

A finite element model was constructed using the eight-node-quadrilateral element with a mesh gradation factor 0.1. A zoom-in view of the mesh showing the drift under study on

level 50 (5000 ft) and nearby stopes is shown in Figure 4-4. Thirteen modelling stages are set to model the drift excavation followed by the mining and backfilling of six stopes in the order shown in Figure 4-4.

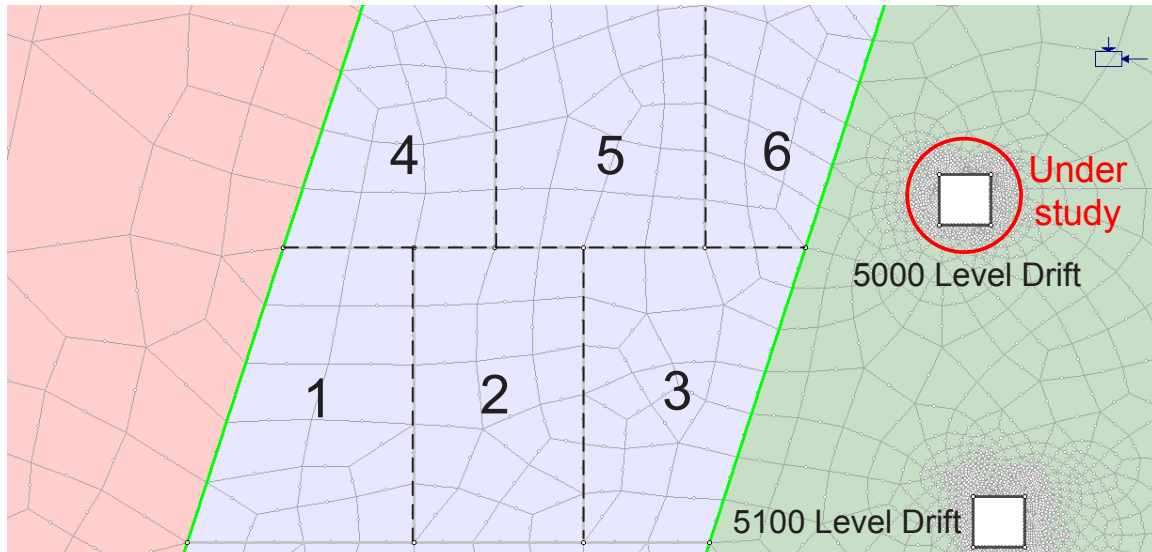


Figure 4-4 Finite element mesh showing the modeled mining sequence

### 4.3 Drift Stability Evaluation Criteria

Zhang and Mitri (2008) defined three criteria for the evaluation of drift stability in terms of stress, yielding and convergence. The stress criterion examines high compressive stresses as well as low confinement stresses leading to failure due to lack of confinement. The yielding criterion examines the extent of yield zones around the drift to help assess the need for secondary support. Three deformation-based criteria for floor, back and wall convergence were introduced, of which the wall convergence criterion (WCR) is defined as

$$WCR = \frac{W - W_m}{W} \times 100\% \quad (2)$$

Where  $W$  is the drift span and  $W_m$  is the shortest deformed span.

### 4.3.1 Model Parametric Study

The existence of dyke and shear zones at Garson mine may cause rotation of major principal in situ stress field. Therefore, a model parametric study is carried out to determine the influence of drift orientation with respect to principal stress. As the 3150 footwall drift axis is not parallel to the orebody (Figure 4-3), it was decided to study the influence of the drift proximity to the orebody contact. Thus, four numerical models are developed with the parameters shown in Table 4-2. As can be seen, models 1 and 2 serve to assess the influence of  $k$  for a drift-to-orebody distance  $L$  of 12m, whereas models 3 and 4 will do the same for  $L=18$ m. A comparison of models 1 and 3, and models 2 and 4 will reveal the effect of the drift-to-orebody distance. The modeled drift is 5 m high by 5 m wide.

Table 4-2 Numerical models analyzed

Model No.	$k$	$L$ (m)
1	1.67	12
2	1.2	12
3	1.67	18
4	1.2	18



### 4.3.2 Model Results

#### 4.3.2.1 Stresses

Figure 4-5 shows the major principal stress ( $\sigma_1$ ) distribution around the drift excavation under study. The low stress regime around the excavation (10-24 MPa) is indicative of postpeak stress which causes relaxation. Compressive stress field in the far drift back is in the range of 64-72 MPa, which is well below the rock mass strength under confinement.

As mining and backfilling modelling stages are implemented, sidewall stresses tend to rise gradually to the 25 MPa range, whereas the stress in the back continues to drop to less than 5 MPa. This may be attributed to the growth of postpeak zones as mining activities progress.

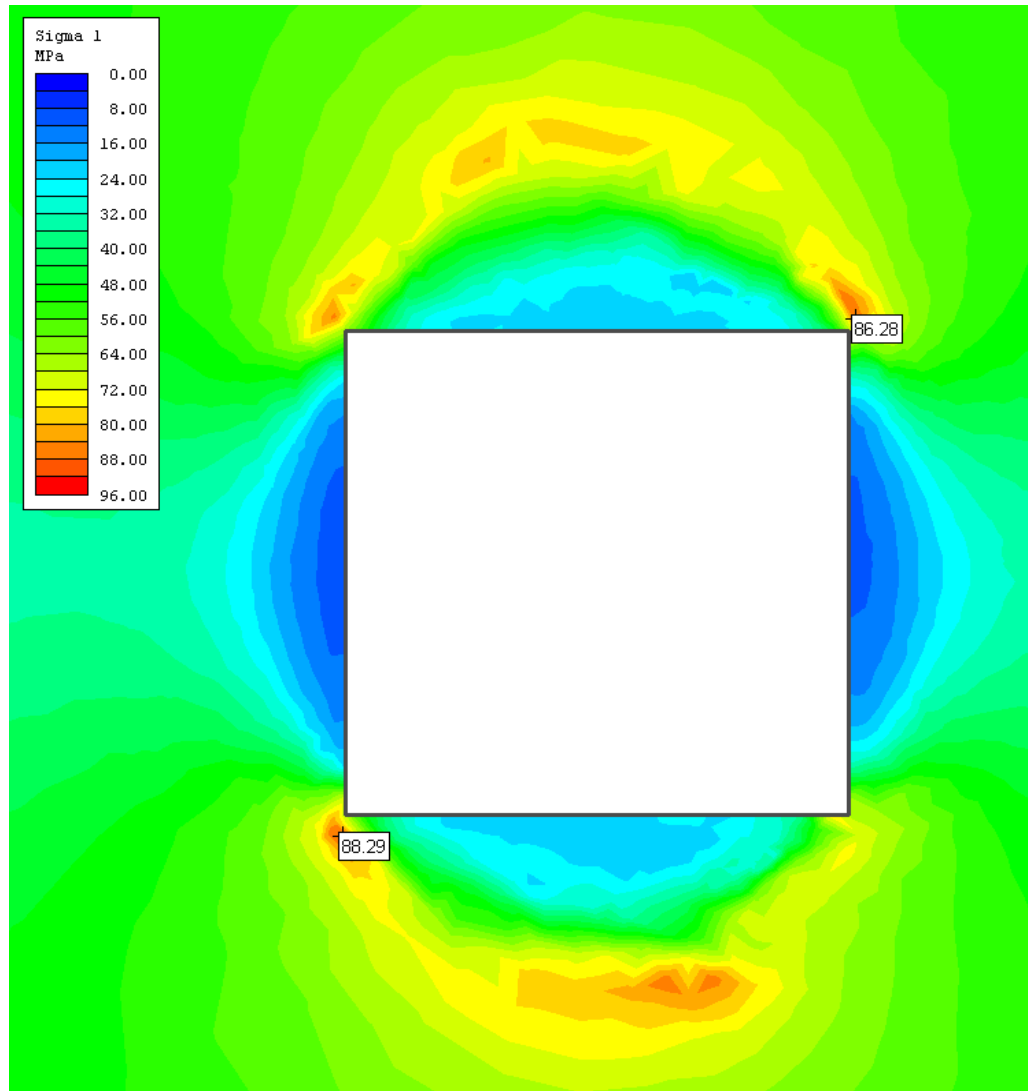


Figure 4-5 Major principal stress redistribution around the drift

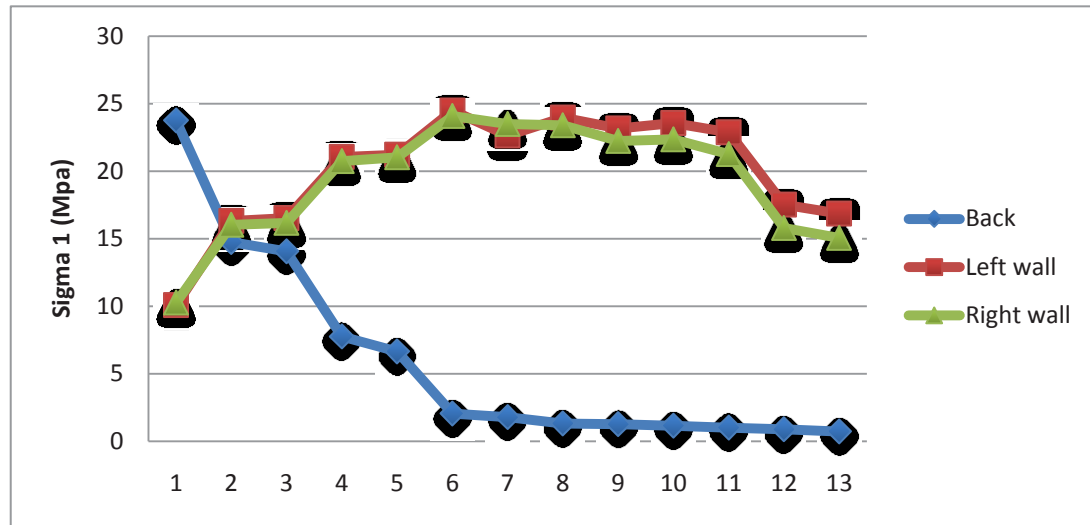
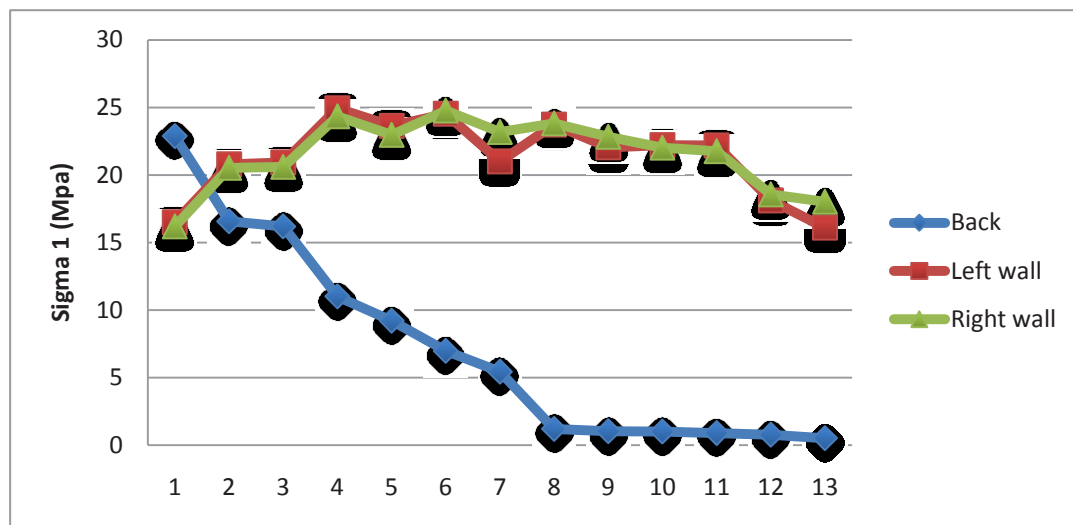
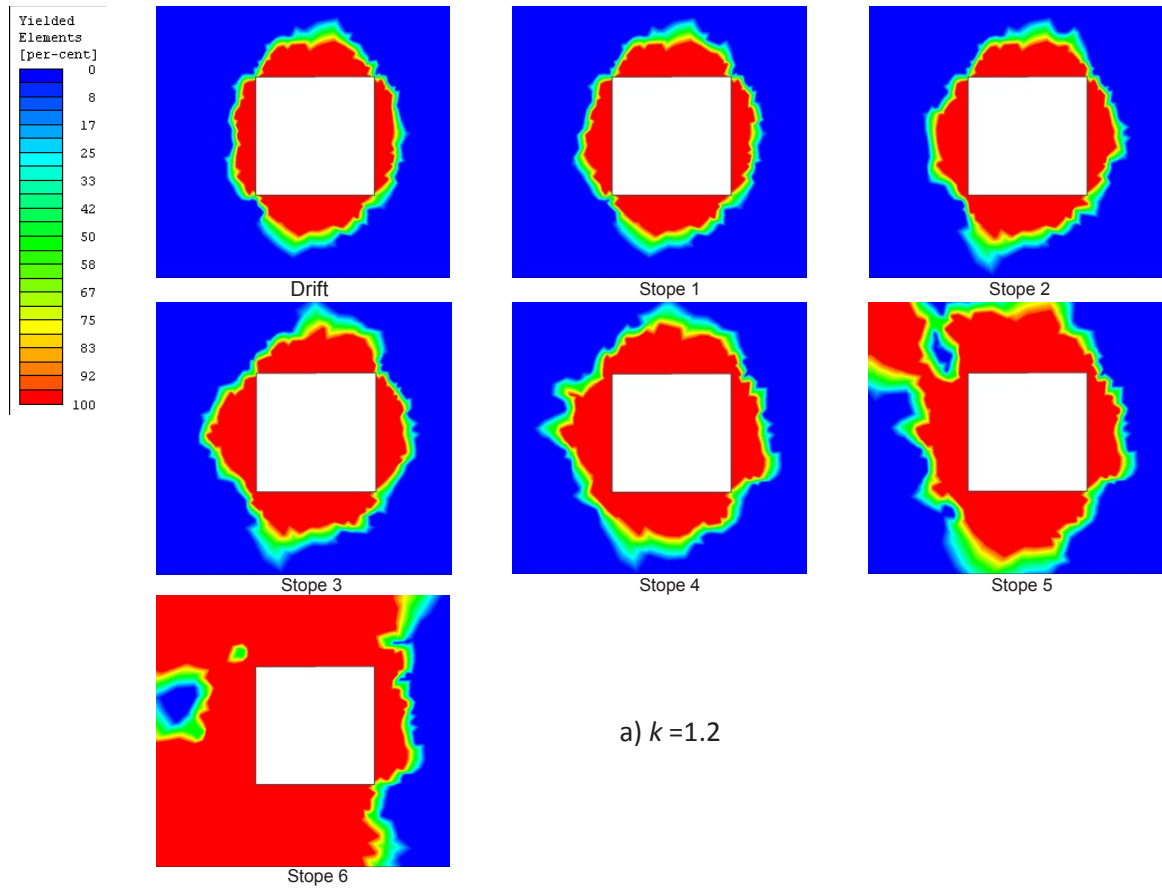
Figure 4-6 Major principal stress redistribution for  $k=1.67$ ,  $L=12$  mFigure 4-7 Major principal stress redistribution for  $k=1.2$ ,  $L=12$  m

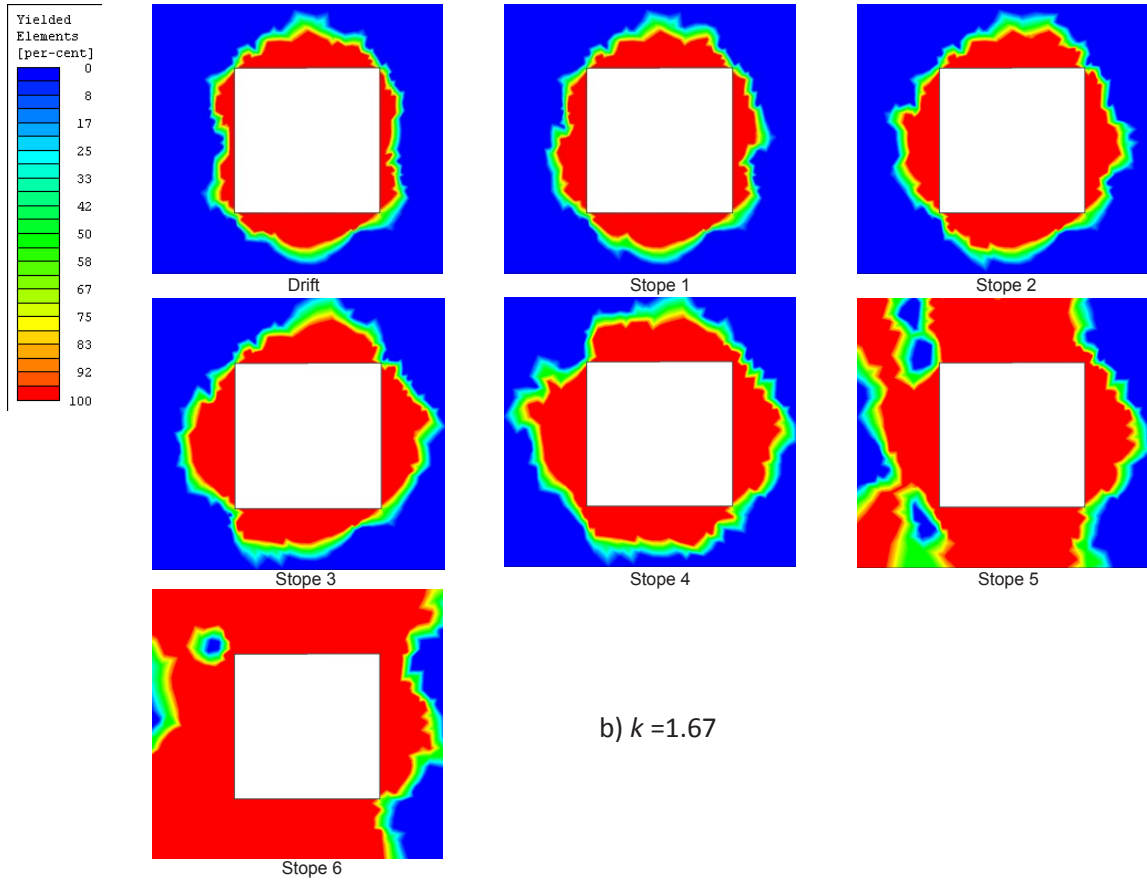
Figure 4-6 shows the distribution of  $\sigma_1$  around the drift for  $k=1.67$  and Figure 4-7 presents the same for  $k=1.2$ , and both for  $L=12$  m. As can be seen, the principal stress results are quite similar, and it can be concluded that the trend of low stress regime as a result of stoping activities is dominant in both cases.

#### 4.3.2.2 Extent of Yield Zones

Figure 4-8 shows the initial and subsequent progression of yield zones around the drift for  $k=1.67$  and 1.2, respectively. As can be seen, yielding spreads gradually with mining activity of stopes 1, 2 and 3. However, it was not until stages 9 to 11, where stope 5 and 6 are mined out and backfilled, that the haulage drift is affected severely with extensive yielding. It is also observed that the yielding pattern is not symmetric around the drift. Instead, it spreads more toward the orebody. This is especially true after the mining of stope 5. This trend is to be expected and is attributed to the influence of the large cavity created by mining the stopes.

These results imply that the drift is only slightly influenced by the mining of the lower stopes (1 to 3). On the other hand, the drift may require secondary support before mining of the 50-level stopes (4 to 6) is completed. It should be noted however, that the analysis is 2-dimensional, which inherently assumes that the stopes are infinitely long in the direction of the drift axis, which is not the case in reality. Thus, a more realistic evaluation of the influence of stopes 4, 5 and 6 on the extent of yield zones around the drift can only be done with three-dimensional analysis. This is beyond the scope of the current study.



Figure 4-8 Yield zone progression with mining sequence,  $L=12$  m

#### 4.3.2.3 Displacements

The initial deformation of the excavated drift is presented in Figure 4-9. The maximum total displacement recorded is 0.013m and takes place nearly at mid-height of the sidewall. As stopes been taken out, the total displacement of the drift walls increases. Figure 4-10 plots the variation of total displacement in the sidewall for each modelling stage. As can be seen, sidewall displacement reaches 0.16 m and 0.10 m for  $k = 1.67$  and 1.2, respectively. It is also observed that the rate of deformation is notably higher between modelling stages 7 and 8, which correspond to the mining of stope 4. Based on these

results, the wall convergence ratio WCR as calculated from equation (2) is 6.22% when stope 6 is mined out.

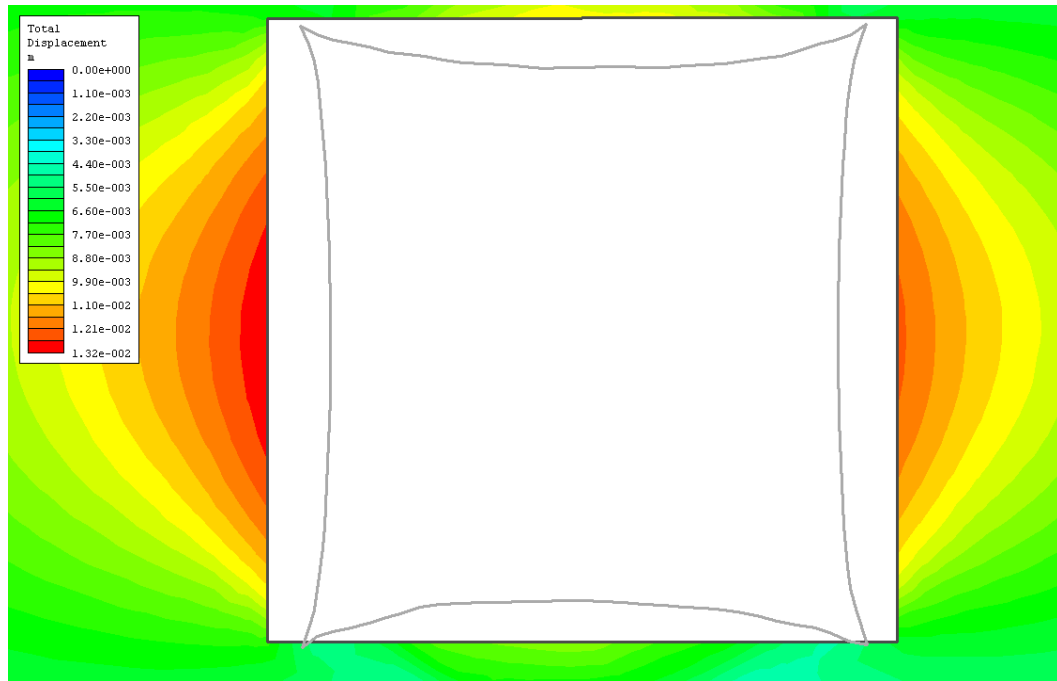


Figure 4-9 Initial drift displacements

#### 4.3.2.4 Effect of Drift Proximity to the Orebody Contact

In this case study, the shortest distance from the drift to orebody contact is 12 m and the longest distance is 18m. Figure 4-11 presents a comparison of the total sidewall displacements recorded after each modelling stage for both  $L = 12$  m and  $L = 18$  m, for the case of  $k = 1.67$ . As can be seen, the case of  $L = 12$  m show only slightly more displacements. It can be concluded from this results the distance to orebody contact has little influence on the drift sidewall deformations, or that mine induced stress changes are felt to within 18 meter of the ore body footwall contact.

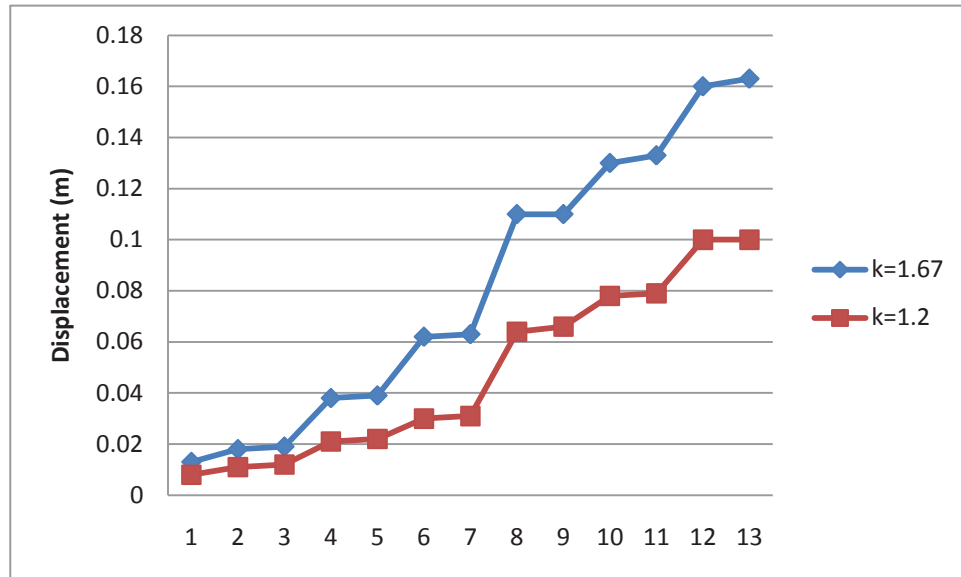


Figure 4-10 Total displacement variation with modelling stages,  $L=12$  m

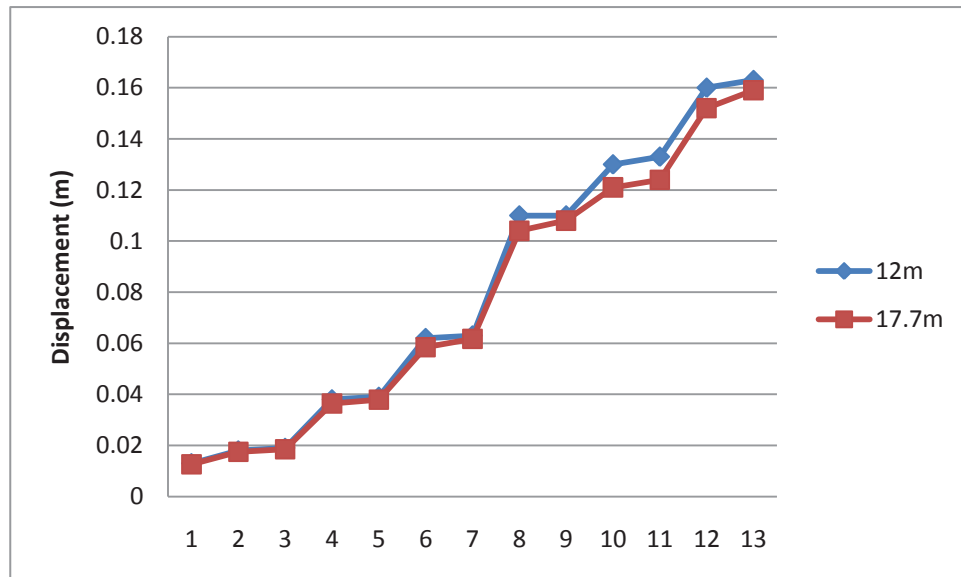


Figure 4-11 Total displacement variation with modelling stages,  $k=1.67$



#### **4.4 Conclusions and Discussions**

Serial numerical modeling analyses have identified key factors that infect the stability of a haulage drift: distance between orebody contact and haulage drift, in situ stress magnitudes and directions, drift span, rock mass quality and mining sequence. These are critical aspects for mine planners to examine carefully before producing drift layout. As a result of this study, methodology for designing a new haulage drift is developed, which is to

- 1) Analysis geomechanical data, such as RQD, UCS, joint sets information, where the haulage drift is to locate
- 2) Verify the magnitudes and directions of in situ stress to determine drift span
- 3) Finalize the location of haulage drift in conjunction with planned mining sequence

## Chapter 5

### Rock Supports for Mining Applications

#### 5.1 General Introduction of Various Rockbolts

Rock supports, like rockbolts, rebars, cablebolts and liners, are used to improve the stability and maintain the load-carrying capacity of rock near the boundaries of underground excavations. Rockbolts, rebars, cablebolts are known as structural elements which carry, in whole or in part, the weights of individual rock blocks isolated by discontinuities, or of zones of loosened rock. Designing a reliable rock support system based on advanced analysis of rock-support interaction is not only necessary, but is also vital for underground mining activities.

Support may be classified as being either active or passive. Active support imposes a predetermined load to the rock surface at the time of installation. Active support is usually required when it is necessary to immediately support the gravity loads imposed by individual rock blocks, or by a loosened zone of rock. Passive support or reinforcement is not installed with an applied loading, but rather, develops its loads as the rock mass deforms. According to specific demands, either active or passive support type is known in advance for rockbolt design.

The single **tensioned rock bolt** consists of an anchorage, a shank, a face plate, a tightening nut and, in some cases, a deformable bearing plate.

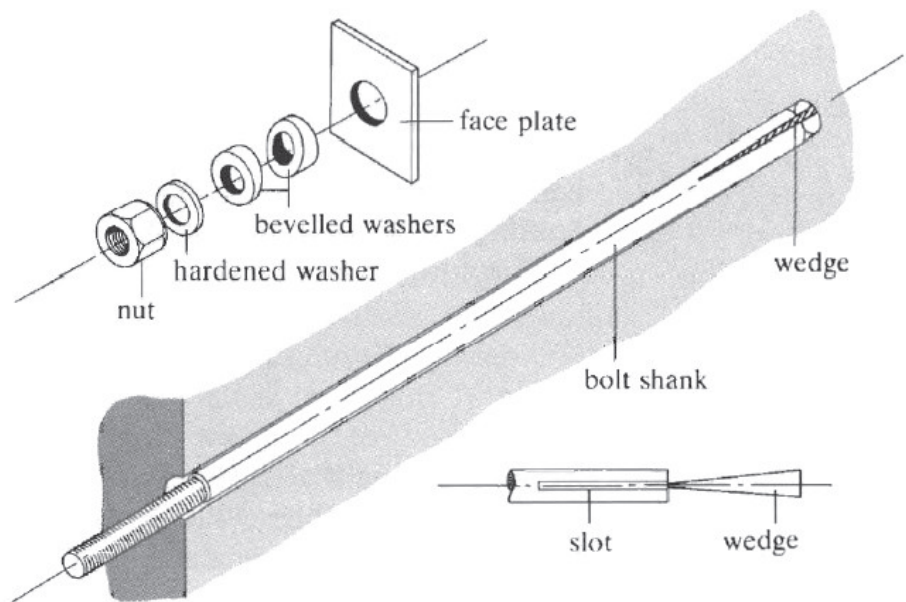


Figure 5-1 Rock bolt with a slot and wedge anchor (After Hoek & Brown 1980)

This is the earliest type of mechanically anchored rock bolt. It is very simple and inexpensive to manufacture and had been used throughout the world. The end of the bolt shank is slotted as illustrated and the wedge is driven home by pushing the assembly against the end of the drill hole. The wedge expands the end of the bolt shank and anchors it in the rock. Bevelled washers are used to accommodate an inclined rock face. The hardened washer is used when the bolt is tensioned by applying a measured torque to the nut. The advantages of the single tensioned rock bolt are:

- Simple and inexpensive
- Excellent anchorage in hard rock
- Immediate tensioning

But the anchor in poor-quality rock is unreliable.

The **Expansion shell mechanical anchors** were developed to provide more reliable anchorage in a wider range of rock conditions than those for which a slotted bolt and wedge system can be used.

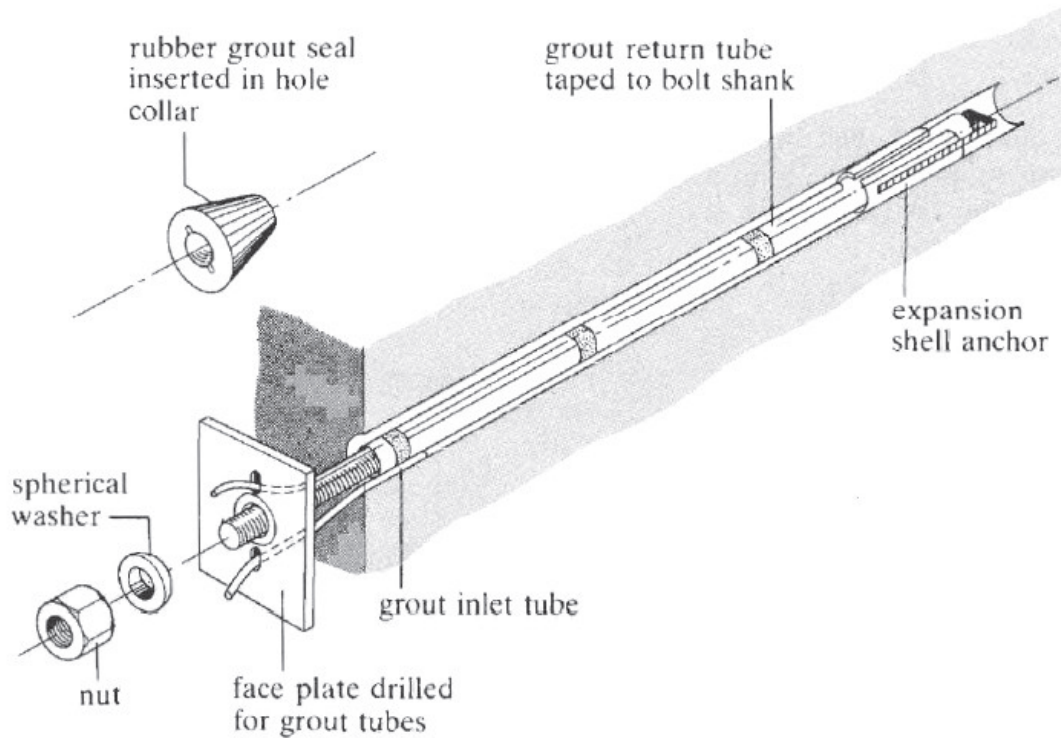


Figure 5-2 Rock bolt with an expansion shell anchor, tensioned and grouted (After Hoek & Brown 1980)

A wedge, attached to the bolt shank, is pulled into a conical anchor shell forcing it to expand against the drillhole walls. The rubber grout seal is used to centre the bolt in the hole and to seal the collar of the hole against grout leakage. An alternative system is to use a quick-setting plaster to seal the hole collar. The grout is injected into the collar end of the hole (except in down-holes) and the return pipe is extended for the length of the

hole. This kind of bolt can be tensioned immediately after installation and grouted at a later stage when short-term movements have ceased. The advantages are:

- Immediately tensioned
- Reliable anchorage
- High bolt loads

While disadvantages are:

- Correct installation requires skilled workmen
- Grout tubes are easy to be damaged

**The Grouted anchors** can be used in very poor quality rock masses. An alternative system is to inject a dry sand/cement mixture through one pipe and a measured water quantity through a second pipe, withdrawing both pipes as the anchor is formed. The load-indicating bearing plate is one of several designs which give visual load indication by progressive deformation with load. The advantages are:

- Good anchorage characteristics in a wide range of rock conditions
- Good visual indication of bolt load

But the stiffness of bolt and bearing plate may be too low for some applications. Hence, it is used in short-term support requirements.

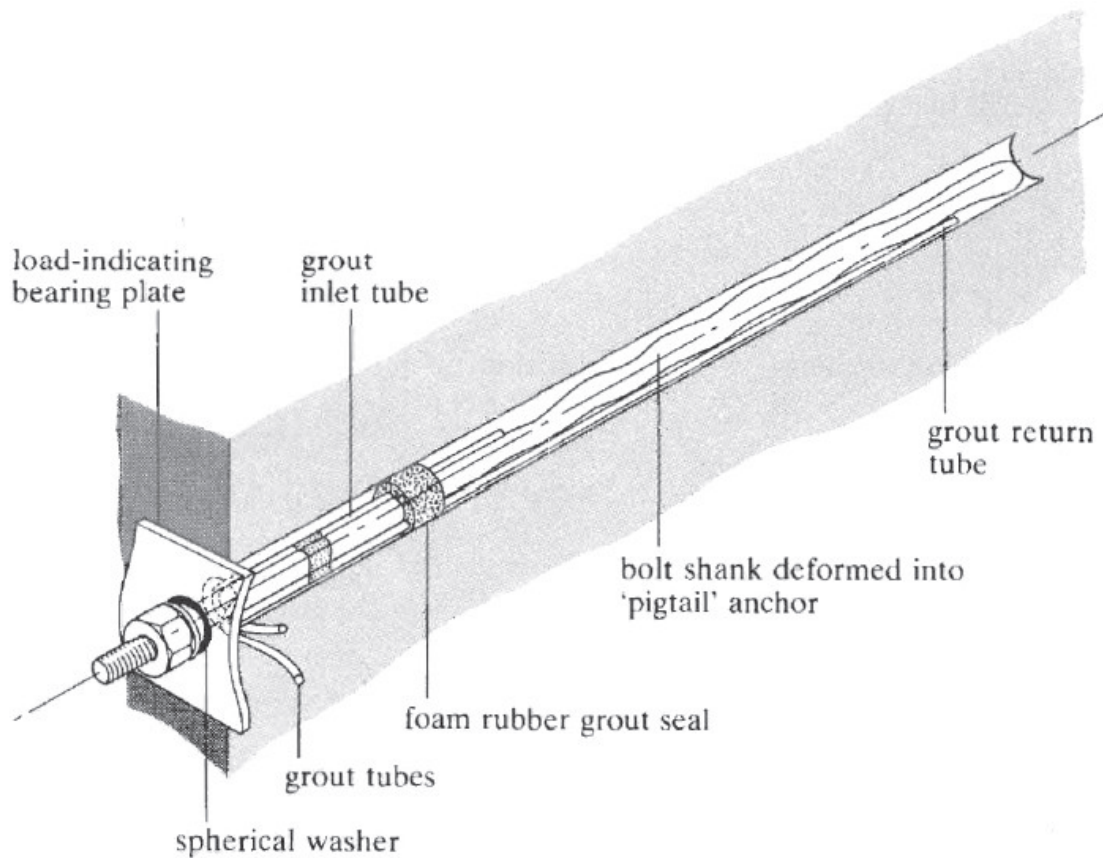


Figure 5-3 Rock bolt with a deformed section used to form a grouted anchorage (After Hoek & Brown 1980)

**The Rebar**, or reinforcing bar, is a common steel bar, and is commonly used in reinforced concrete, underground support and reinforced masonry structures. It is usually formed from carbon steel, and is given ridges for better mechanical anchoring into the concrete. It can also be described as reinforcement or reinforcing steel.

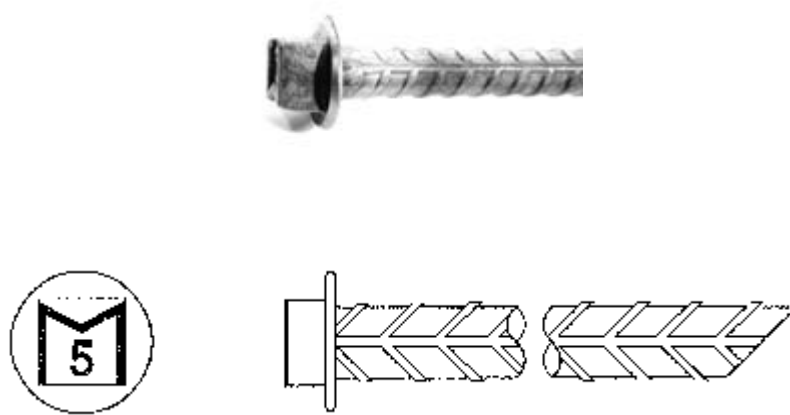


Figure 5-4 Forged Head Rebar (Mansour Group)

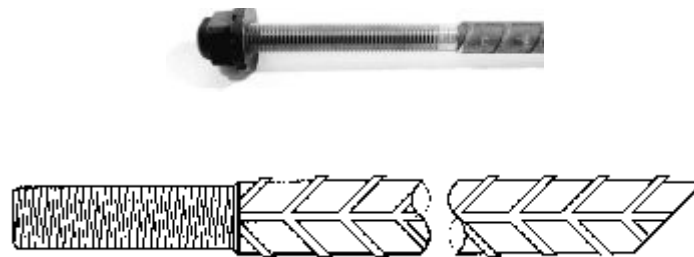


Figure 5-5 Threaded Rebar (Mansour Group)

**The Resin-grouted rock bolt** is the most sophisticated rockbolt system currently in use; it combines most of the advantages of other bolt systems. Resin and a catalyst are contained in plastic 'sausages', the catalyst being separated in a glass or plastic container in the resin. These capsules are pushed into the hole with a loading stick and the bar is then inserted. Rotation of the bar during insertion breaks the plastic containers and mixes the resin and catalyst. The bar has a very coarse rolled thread which gives good bonding and allows the length of the installation to be adjusted very easily. The advantages are:

- Convenient and simple
- High-strength anchors
- 'One-shot' installation

Although resins are expensive and are limited shelf-life, the resin-grouted rock bolt is used in critical applications in which cost is less important than speed and reliability.

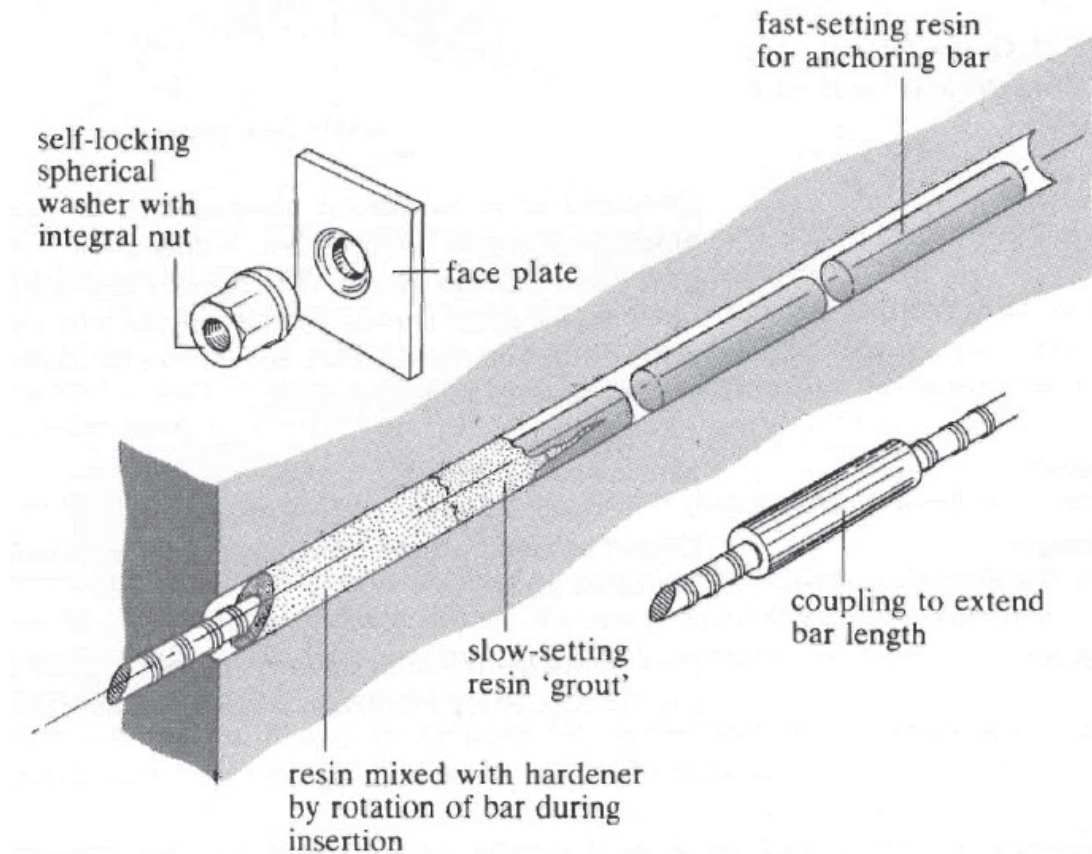


Figure 5-6 Resin-grouted rock bolt made from threaded bar (After Hoek & Brown 1980)

**The Split-set dowel** was developed by Scott, 1977 in conjunction with the Ingersoll-Rand Company in the USA. The 38mm diameter split tube is forced into a 35 mm diameter drillhole. The spring action of the compressed tube applies a radial force against



the rock and generates a frictional resistance to sliding of the rock on the steel. This frictional resistance increases as the outer surface of the tube rusts. The advantages are:

- Simple and quick to install
- Cheaper than a grouted dowel of similar capacity

While disadvantages are:

- Cannot be tensioned
- Drillhole diameter is critical

Which make the split-set dowel suitable for short-term support

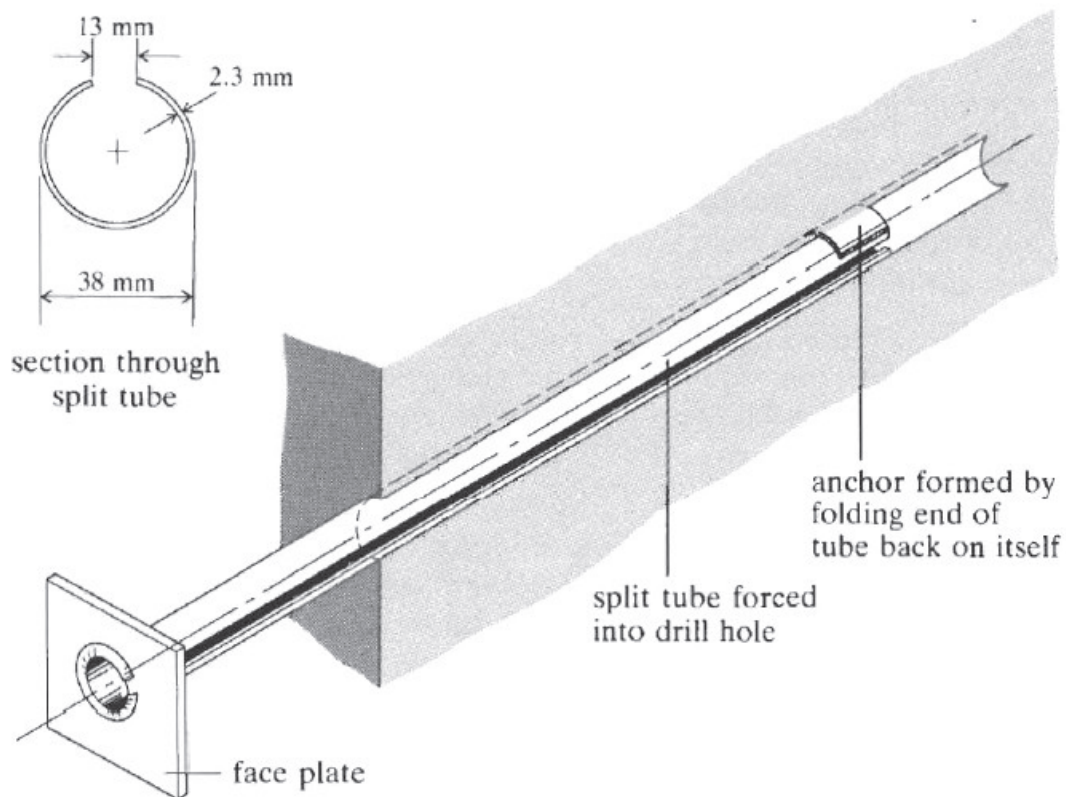


Figure 5-7 Split-set dowel (After Hoek & Brown 1980)

**The Swellex dowel** is a thin-walled tube folded into a collapsed shape of between 25 and 28 mm in diameter and then inserted into a 33-39 mm diameter borehole and expanded by injection of water at a pressure of about 20 MPa delivered by a small portable pump.

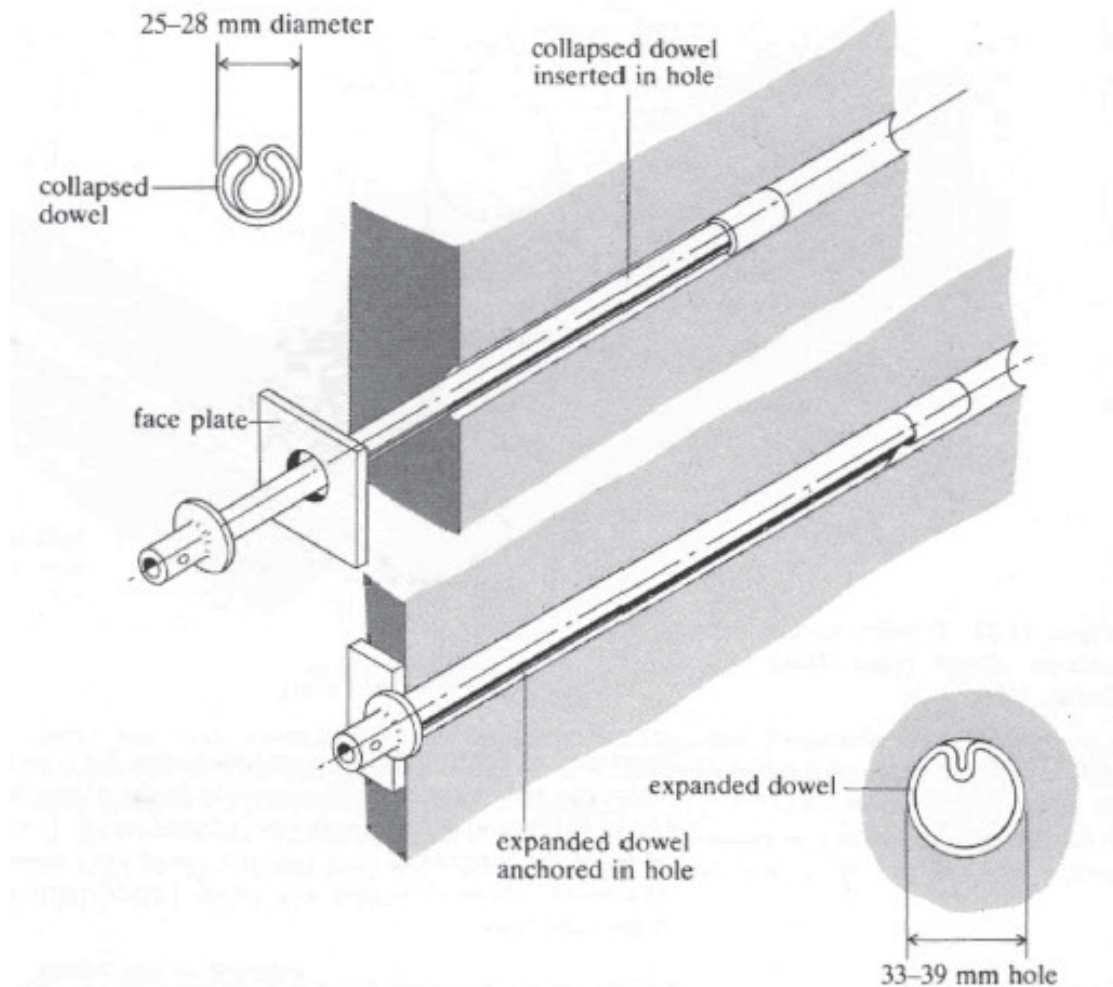


Figure 5-8 Swellex dowel, Atals Copco (After Hoek & Brown 1980)

Expansion of the dowel results in an overall length reduction which pulls the face plate tight against the rock and induces a small tension in the dowel. The advantages are:

- Anchoring force is high

- Simple to use

But the strength of the support system is limited by the strength of the thin-walled tube.

However, Swellex is capable of:

- Short-term reinforcement
- Stress releasing

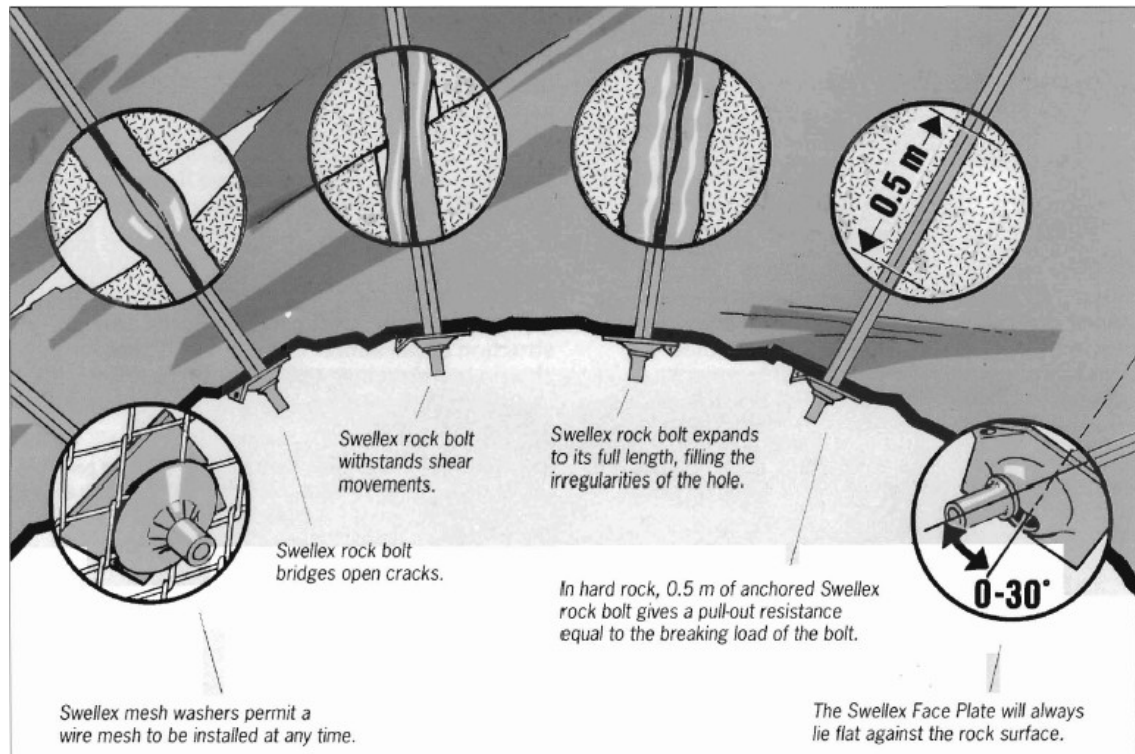


Figure 5-9 Applications of Swellex (Atlas Copco)

**The Cone Bolt** is a yielding tendon capable of providing effective support in areas prone to seismic events or high stress changes. Damage to tunnels normally resulting from, or associated with, rockbursts and large quasi-static rock deformations is consequently reduced. The cone bolt is designed with low stiffness, to yield under high dynamic loading conditions.

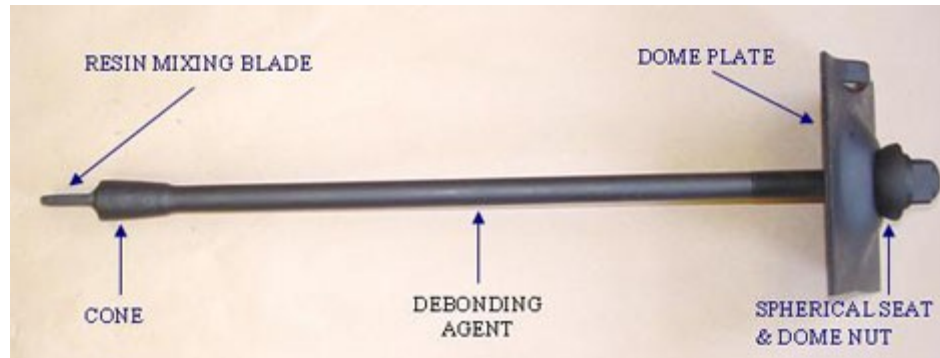


Figure 5-10 Modified Cone Bolt (Mansour Group)

**Cable bolting** is a technique used to fortify rock masses. In underground applications it is mainly used in the reinforcing of stope pillars, raises, drawpoints and haulage drifts.



Figure 5-11 Standard cable bolt (Mansour Group)



Figure 5-12 Nut cage cable bolt (Mansour Group)

The purpose of the support system is to maintain the quality of the rock mass by not allowing the displacement of discontinuities. Cable bolting is not meant to support the rock, but to create a self-supporting rock mass.



Figure 5-13 Dynamic Cable Bolt (DSI)

Yielding range up to 300mm

Static yield force capacity 150 - 180kN

Dynamic yield force capacity 80 - 120kN

Ultimate force capacity 250kN

Installed with cement grout in 45 - 51mm holes

Due to varying underground conditions, the support system varies. Existing bolts have been repeatedly updated to satisfy new supporting designs, as more new types of bolts are invented and come into service in the mining industry.

## **5.2 Cable bolt Installation In The Field**

There are two major methods for cable bolt installation in the field.

### 5.2.1 Using a Breather Tube

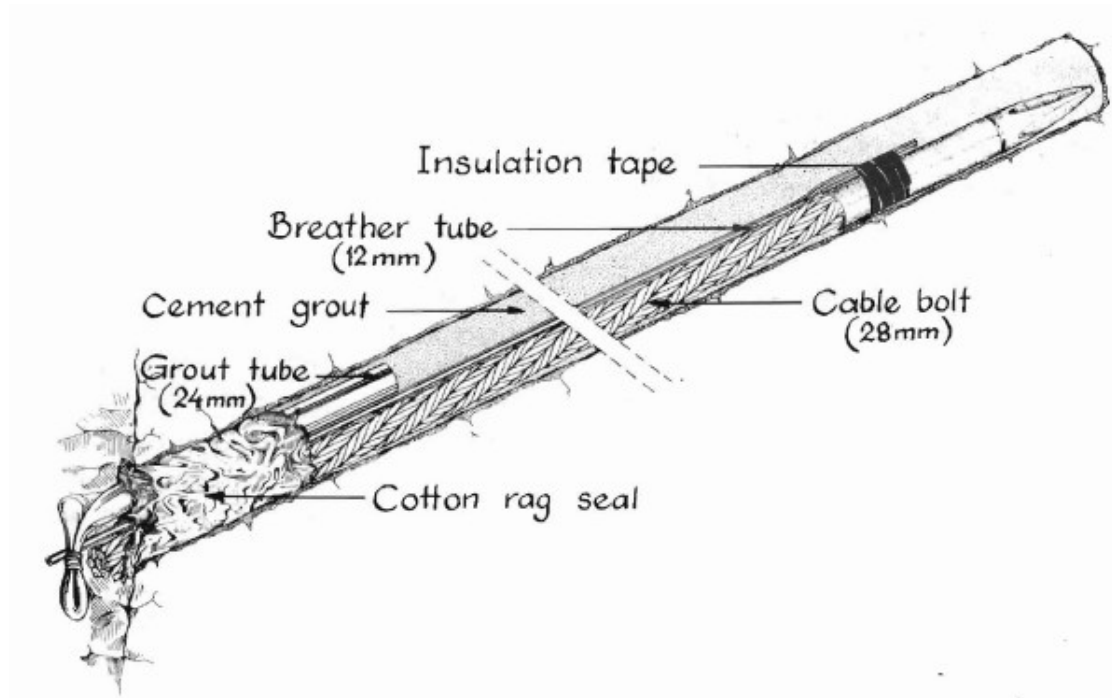


Figure 5-14 Principle of installation of a long fully grouted cable bolt

In this method, the cable is first inserted in the bottom of the borehole, together with a stiff nylon or polyethylene breather tube. After the grout tube has been inserted some 0.5 metres (1.5 ft) into the hole, the hole is sealed off at the collar. In steep upholes, it is necessary to lock the cable in place to prevent it from sliding out of the hole. The cable is locked by a top anchor arrangement or by some locking arrangement at the collar of the hole. Once the hole is sealed off, and the cable locked in place, the hole is filled with cement grout and the air trapped inside the hole escapes through the breather tube. The hole is filled with cement grout, when weak grout flows out of the breather tube. Finally, the grout tube is sealed and cut. The breather tube method is good for uphole installations

The installation machine is illustrated below,

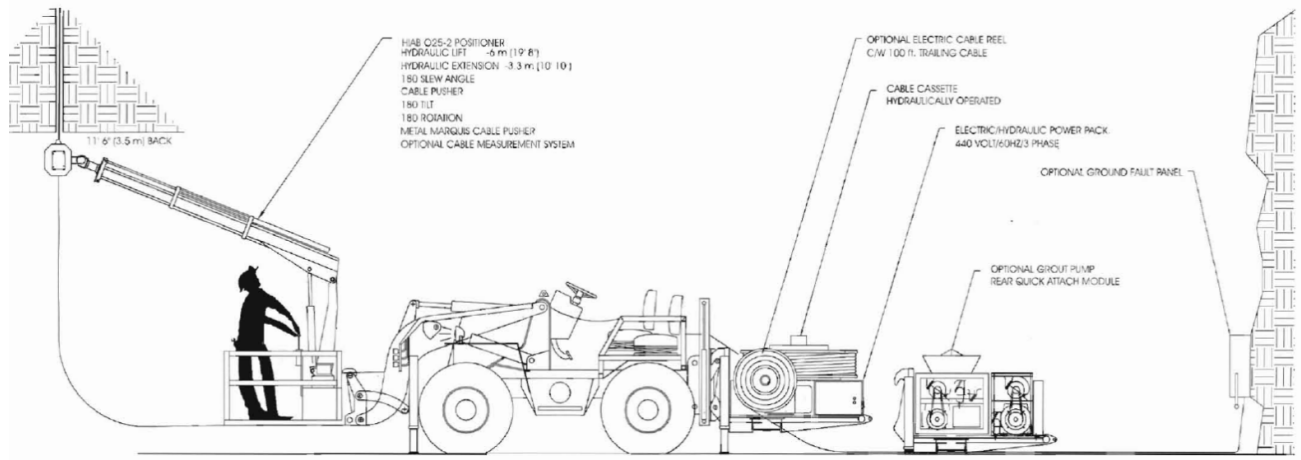


Figure 5-15 Rock bolts installation machine

### 5.2.2 Using a Grout Hose

In this method, the grout hose is inserted in the bottom of the borehole and retrieved as the hole is filled with cement.



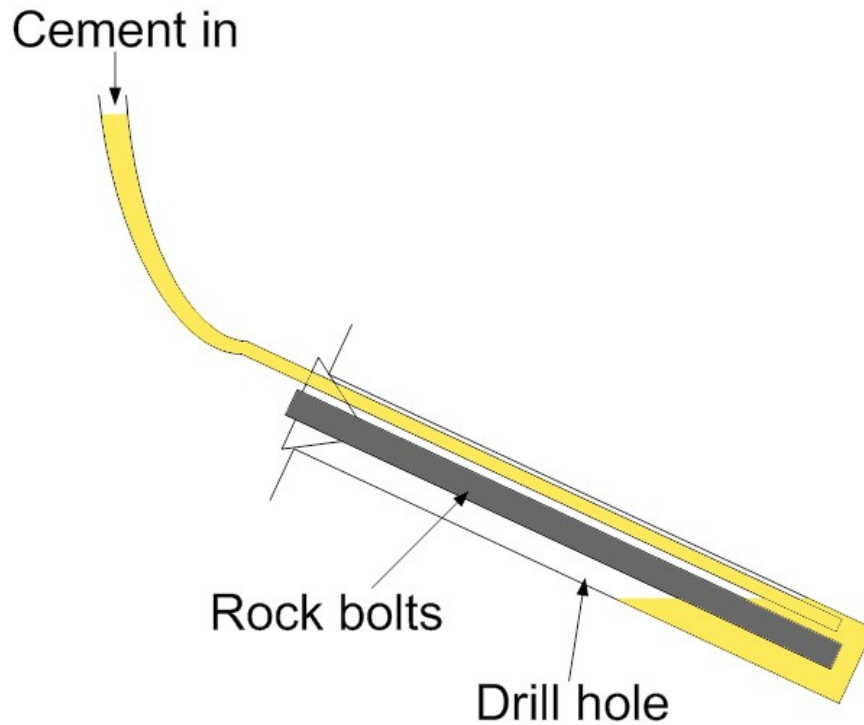


Figure 5-16 Grouting a cable bolt in down hole

After the hole has been filled, the cable is pushed down the hole until it reaches the bottom of the hole. It is recommended that the inserted length of cable be measured accurately, and compared with the driller's borehole log-sheet. This procedure will prevent the cable from not being fully inserted. To facilitate the installation of long cable bolts, a pointer made of steel or plastic is often attached to the end of the cable, see Figure 5-14. Although the grout hose method is good for downhole installations, there are a lot of uphole installations in the Garson mine, Vale Inco, where this method has been used.

### 5.3 Rockbolt Design

The evolution of rockbolts has never stopped. Many design criteria for rockbolts have been developed based on theory and real practice. Both analytical and empirical designs will be introduced in the following pages.



### 5.3.1 Analytical Design

#### 5.3.1.1 Suspension Design

As illustrated below, rock bolts may be used to suspend a potentially unstable roof beam in laminated rock.

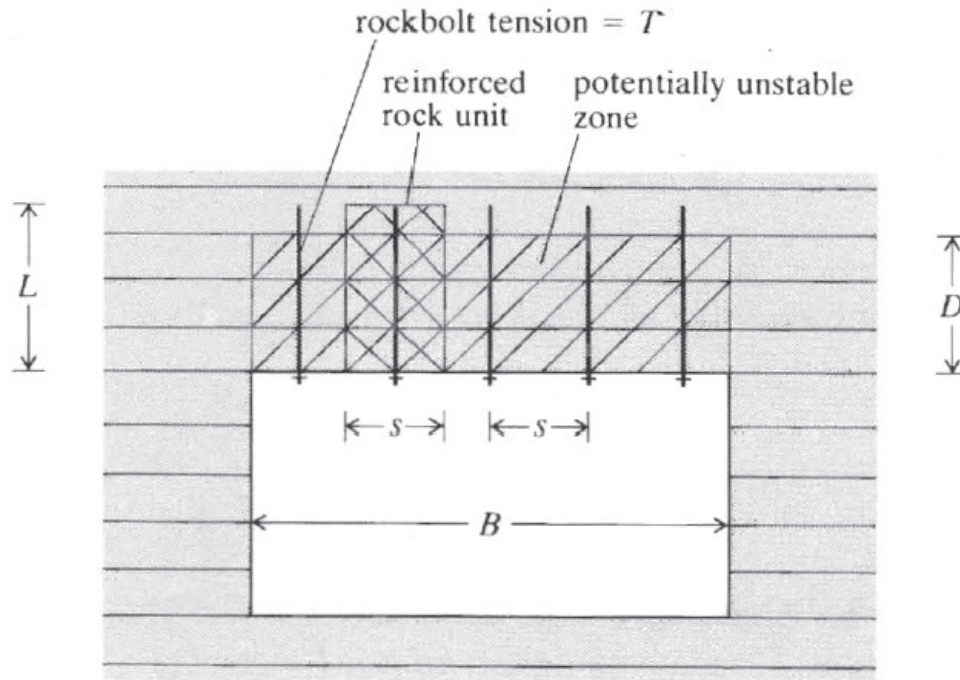


Figure 5-17 Rockbolt design to support the weight of a roof beam in laminated rock.

(After Hoek & Brown 1980)

If it is assumed that the weight of the rock in the unstable zone is supported entirely by the force developed in the rock bolts then,

$$T = \gamma D s^2 \quad (6.1)$$

$$s = \left( \frac{T}{\gamma D} \right)^{\frac{1}{2}} \quad (6.2)$$

where  $T$  = working load per rock bolt,  $\gamma$  = unit weight of the rock,  $D$  = height of the unstable zone, and  $s$  = rockbolt spacing in both the longitudinal and transverse directions.

Lang and Bischoff, 1982 have extended this elementary analysis to incorporate the shear strength developed by the rock mass on the vertical boundaries of the rock unit reinforced by a single rock bolt. The rock is assumed to be destressed to a depth,  $D$ , but variable vertical stresses,  $\sigma_v$ , and horizontal stresses,  $k\sigma_v$ , are assumed to be induced within the destressed zone. Typically,  $k$  may be taken as 0.5. The shear strength developed at any point on the perimeter of the reinforced rock unit is given by  $c + \mu k\sigma_v$ , where  $c$  is the cohesion and  $\mu = \tan\Phi$  is the coefficient of friction for the rock mass. Lang and Bischoff's analysis leads to the result

$$\frac{T}{AR} = \frac{\alpha}{\mu k} \left( 1 - \frac{c}{\gamma R} \right) \left[ \frac{1 - \exp(-\mu k D / R)}{1 - \exp(-\mu k L / R)} \right] \quad (6.3)$$

where  $T$  = rockbolt tension,  $A$  = area of roof carrying one bolt,  $R$  = shear radius of the reinforced rock unit,  $R = aP$ , where  $P$  is the shear perimeter,  $a$  is a factor depending on the time of installation of the rock bolts, and  $L$  = bolt length, often less than  $D$ , the height of the destressed zone of rock.

### 5.3.1.2 Wedge Design

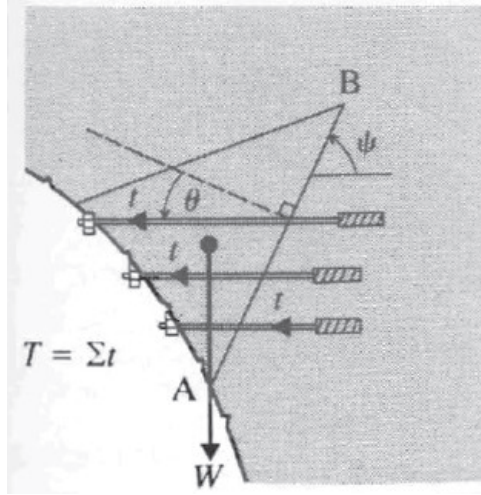


Figure 5-18 Design of a rockbolt or cable system to prevent sliding of a triangular prism.

(After Hoek & Brown 1980)

A two-dimensional wedge is free to slide on a discontinuity AB. If stresses induced around the excavation periphery are ignored, the tensioned rock bolt or cable support may be designed by considering limiting equilibrium for sliding on AB. If Coulomb's shear strength law applies for AB, the factor of safety against sliding is given by:

$$F = \frac{cA + (W \cos \psi + T \cos \theta) \tan \phi}{W \sin \psi - T \sin \theta} \quad (6.4)$$

where  $W$  = weight of the block,  $A$  = area of the sliding surface,  $T$  = total force in the bolts or cables,  $\psi$  = dip of the sliding surface,  $\theta$  = angle between the plunge of the bolt or cable and the normal to the sliding surface,  $c$ ,  $\phi$  = cohesion and angle of friction on the sliding surface.

The total force required to maintain a given factor of safety is given by:

$$T = \frac{W(F \sin \psi - \cos \psi \tan \phi) - cA}{\cos \theta \tan \phi + F \sin \theta} \quad (6.5)$$

### 5.3.1.3 Compression Arch Design

The concept of a rock arch assumes that rock reinforcement creates a load-carrying arch within the rock mass, stabilizing the tunnel roof. This allows the determination of the type and length of rock bolts as well as possible length reductions due to the arch effect (self-support as shown below). Spacing recommendations and minimum tension requirements are readily available.

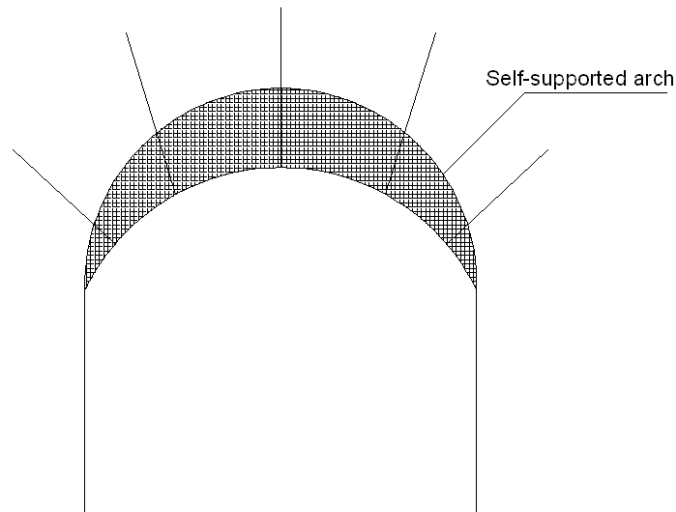


Figure 5-19 A self-supported arch occurring due to rockbolting

Based on earlier work, the conclusion was reached that the basic element of a rock bolted roof is the reinforced rock unit. This consists of an individual bolt and the immediately surrounding rock mass. A series of reinforced rock units constitutes a reinforced rock structure, and stability is ensured if the minimum rock-bolt tension is greater than a value  $T$ .

### 5.3.2 Empirical Design

Empirical design rules, based on precedent practice, are available for determining reinforcement or support requirements for 'permanent' excavations. Cording et al., 1971 reviewed support provided in a large number of underground power stations throughout the world and found that the equivalent uniform support pressures in the roof and side walls could be calculated as:

$$P_{i=nB\gamma} \quad (6.6)$$

and

$$P_{i=mH\gamma} \quad (6.7)$$

respectively, where  $0.10 < n < 0.25$  for the roof,  $0.05 < m < 0.12$  for the side walls,  $B$  = the span of the excavation,  $H$  = the height of the excavation, and  $\gamma$  = the unit weight of the rock.

The best known set of empirical design rules are those for pattern rock bolting developed by Lang, 1961 during the construction of the Snowy Mountains hydroelectric scheme in Australia. These rules are still widely used for determining bolt lengths and spacings for 'permanent' excavations. Lang gives the minimum bolt length,  $L$ , as the greatest of:

1. Twice the bolt spacing,  $s$ ;
2. Three times the width of critical and potentially unstable rock blocks defined by the average discontinuity spacing,  $b$ ;
3.  $0.5B$  for spans of  $B < 6\text{m}$ ,  $0.25B$  for spans of  $B = 18\text{-}30\text{ m}$ .

Using Lang's rules and the experience of others as a basis, Farmer and Shelton, 1980 compiled the rockbolt design guide-lines for excavations in rock masses having clean, tight discontinuity interfaces.

Rockbolt parameter design rules for rock masses with  $\leq 2$  and  $\leq 3$  discontinuity sets with clean, tight interfaces (after Farmer & Shelton 1980).

Excavation span (m)	Number of discontinuity sets	Bolt design	Comments
< 15	$\leq 2$ inclined at $0-45^\circ$ to horizontal	$L = 0.3B$ $s = 0.5L$ (depending on thickness and strength of strata). Install bolts perpendicular to lamination where possible with wire mesh to prevent flaking	The purpose of bolting is to create a load-carrying beam over span. Fully bonded bolts create greater discontinuity shear stiffness. Tensioned bolts should be used in weak rock; subhorizontal tensioned bolts where vertical discontinuities occur
	$\leq 2$ inclined at $45-90^\circ$ to horizontal	For side bolts: $L > h \sin \psi$ (installed perpendicular to discontinuity) $L > h \tan \psi$ (installed horizontally). See Figure 11.13a for $h$ and $\psi$ ; $L$ = bolt length; $s$ = bolt spacing; $B$ = excavation span	Roof bolting as above. Side bolts designed to prevent sliding along planar discontinuities. Spacing should be such that anchorage capacity is greater than sliding or toppling weight. Bolts should be tensioned sufficiently to prevent sliding
	$\geq 3$ with clean tight interfaces	$L = 2s$ $s = 3-4 \times$ block dimension. Install bolts perpendicular to excavation periphery with wire mesh to prevent flaking	Bolts should be installed quickly after excavation to prevent loosening and retain tangential stresses. Prestresses should be applied to create zone of radial confinement. Sidewall bolting where toe of wedge daylight in side wall
> 15	$\leq 2$	$L_1 = 0.3B_1$ primary bolting $s_1 = 0.5L_1$ $L_2 = 0.3s_1$ secondary bolting $s_2 = 0.5L_2$ install wire mesh to prevent spalling	Primary bolting conforms to smaller excavation design. Secondary (and tertiary) bolting supplements primary design (Fig. 11.13b)
	$\geq 3$ with clean tight interfaces	$L_1 = 0.3B_1$ primary bolting $s_1 = 0.5L_1$ $s_2 = 3-4 \times$ block size; secondary bolting $L_2 = 2s_2$	Primary bolting should have sufficient capacity to restrain major blocks. Decisions on block size for secondary bolting should be left to the section engineer

The Q-system, proposed by Barton, Lien, and Lunde, 1974, was developed specifically for the design of tunnel support systems. As in the case of the geomechanical applications, the Q-system has been expanded to provide preliminary estimates. According to this system, the rock mass quality,  $Q$ , can be obtained using six given parameters:

$$Q = \frac{RQD}{J_n} \frac{J_r}{J_a} \frac{J_w}{SRF} \quad (6.8)$$

where,

RQD= Rock quality designation;

$J_n$ =joint set number;

$J_r$ =joint roughness number;

$J_a$ =joint alteration number;

$J_w$ =joint water reduction number

SRF=stress reduction number.



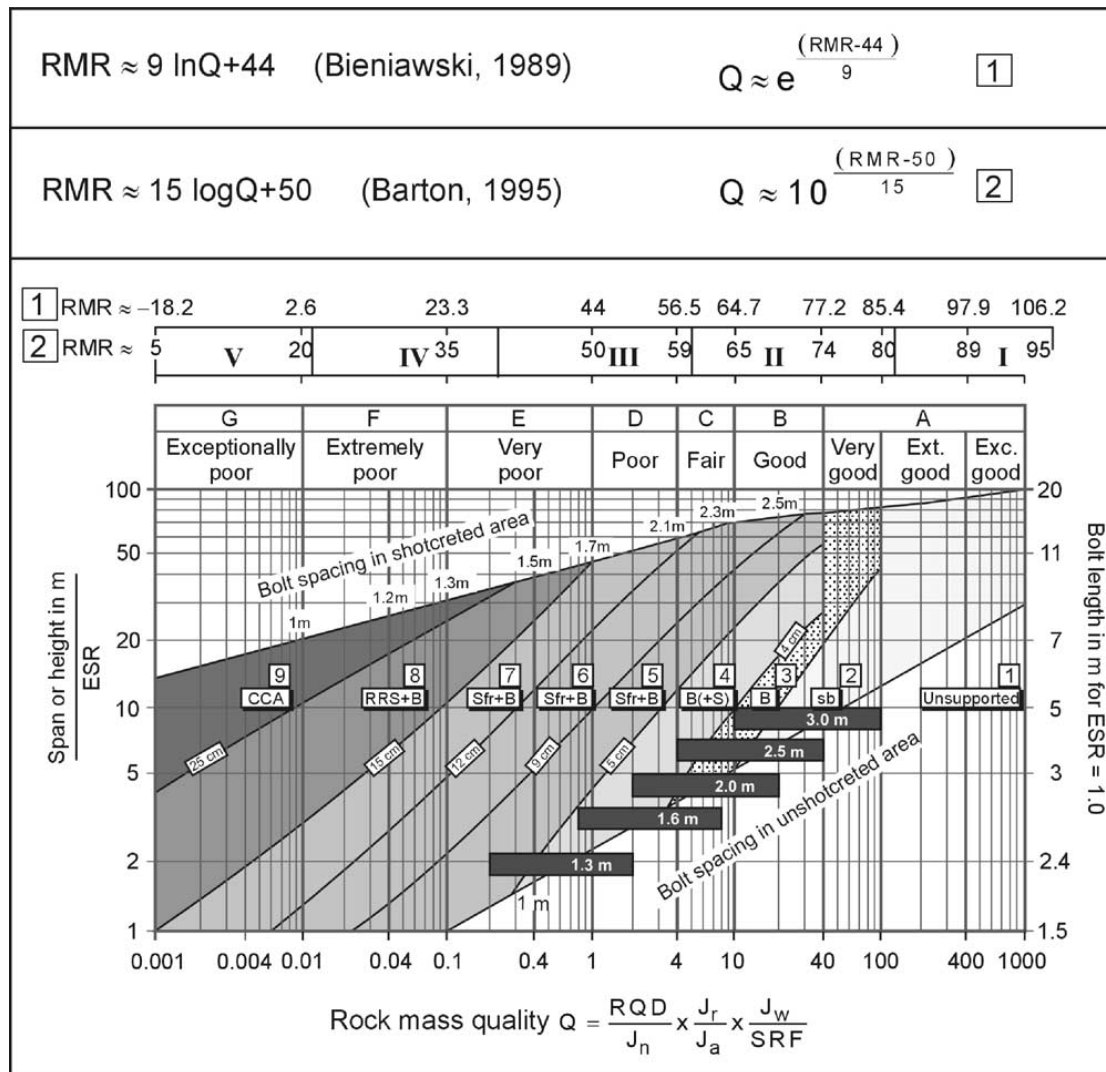


Figure 5-20 Q-support chart for selecting reinforcement and support, Barton 2002, where

B: systematically spaced steel rock bolt; S(fr): steel fiber reinforced sprayed concrete;

CCA: cast concrete arches; RRS: steel rib-reinforced shotcrete arches

Based on the calculated  $Q$  value, a proper preliminary rock support can be placed.

There is another available empirical design for underground opening, which is stability graphic method.

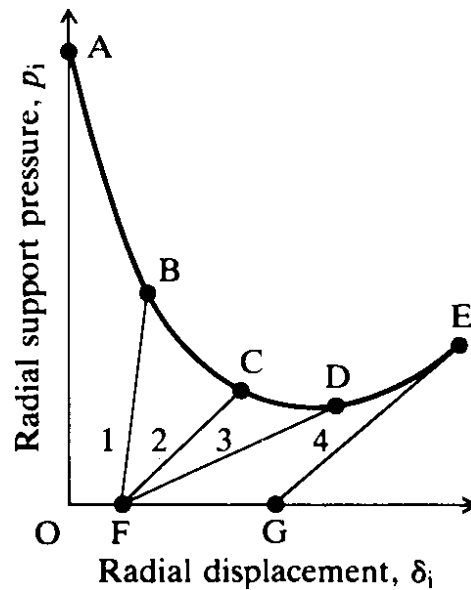


Figure 5-21 Rock support–interaction analysis (After Hoek & Brown 1980)

Enough displacement must be allowed to enable the rock mass strength to be mobilized sufficiently, so as to restrict the required support loads to practicable levels. However, excessive displacement, which would lead to a loosening of the rock mass and a reduction in its load-carrying capacity, must not be permitted to occur. The stiffness and the time of installation of the support element have an important influence on this displacement control.

As shown in Figure 5-21, support 1 is installed at F, and reaches equilibrium with the rock mass at point B. This support is too stiff for the purpose, and attracts an excessive share of the redistributed load. As a consequence, the support elements may fail causing catastrophic failure of the rock surrounding the excavation.

Support 2, having a lower stiffness, is installed at F and reaches equilibrium with the rock mass at C. Provided the corresponding displacement of the periphery of the excavation is

acceptable operationally, this system provides a good solution. The rock mass carries a major portion of the redistributed load, and the support elements are not stressed excessively. Note that if, as in the temporary/permanent support concept, this support were to be removed after equilibrium had been reached, uncontrolled displacement and collapse of the rock mass would almost certainly occur.

Support 3, having a much lower stiffness than support 2, is also installed at F, but reaches equilibrium with the rock mass at D, where the rock mass has started to loosen. Although this may provide an acceptable temporary solution, the situation is dangerous, because any extra load imposed, for example, by a redistribution of stress associated with nearby mining, will have to be carried by the support elements. In general, support 3 is too flexible for this particular application.

Support 4, of the same type and stiffness as support 2, is not installed until a radial displacement OG of the rock mass has occurred. In this case, the support is installed too late, excessive convergence of the excavation will occur, and the support elements will probably become overstressed before equilibrium is reached.

## **5.4 Numerical Modeling**

Mitri and Rajaie, 1990 have first introduced cable (support) elements into numerical modeling techniques presenting the effect of rockbolting. The assumption of the cable element is that the grout material and the slip occurring at the interfaces can be represented by a set of continuous tangential springs.

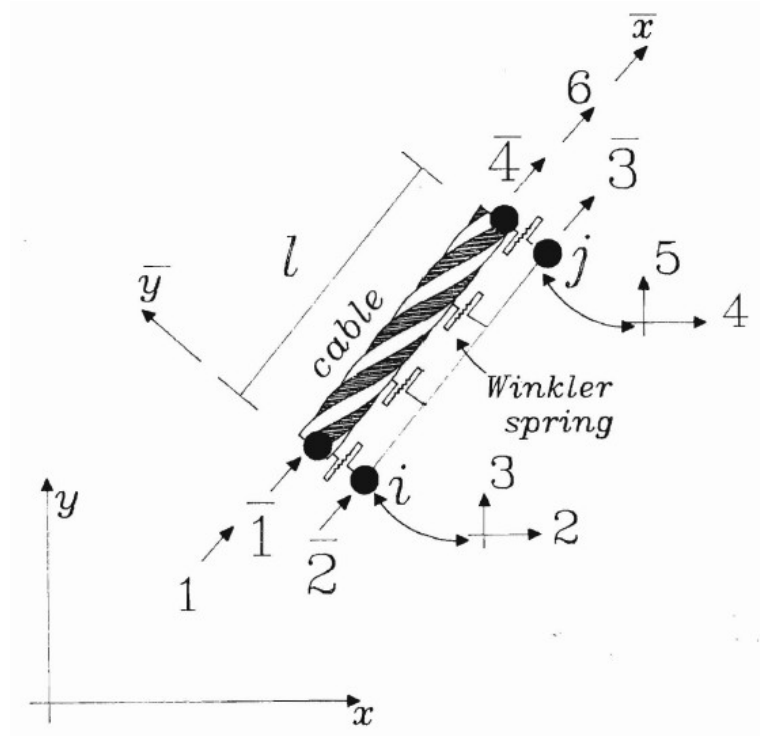


Figure 5-22 Geometry and degrees of freedom of cable element (Mitri and Rajaie 1990)

The total strain energy stored in the cable element is

$$U = \frac{1}{2} u^T k u$$

$$k = \frac{l}{12} \begin{bmatrix} 3k_i + k_j + \frac{12EA}{l^2} & -3k_i - k_j & -k_i - k_j & k_i + k_j - \frac{12EA}{l^2} \\ & 3k_i + k_j & k_i + k_j & -k_i - k_j \\ & & k_i + 3k_j & -k_i - 3k_j \\ & & & k_i + 3k_j + \frac{12EA}{l^2} \end{bmatrix} \quad (6.10)$$

For example, a problem is defined as illustrated in Figure 5-23 with a discretized finite element domain in Figure 5-24.

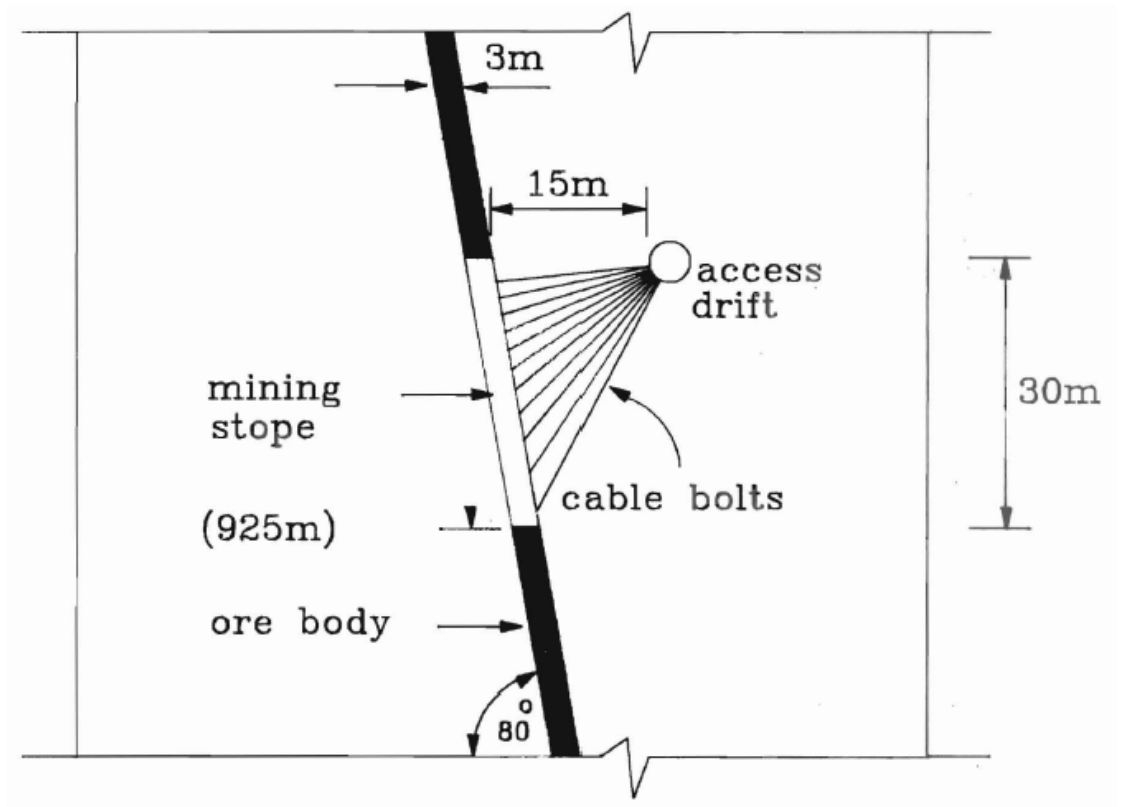


Figure 5-23 layout of case study (Mitri and Rajaie 1990)

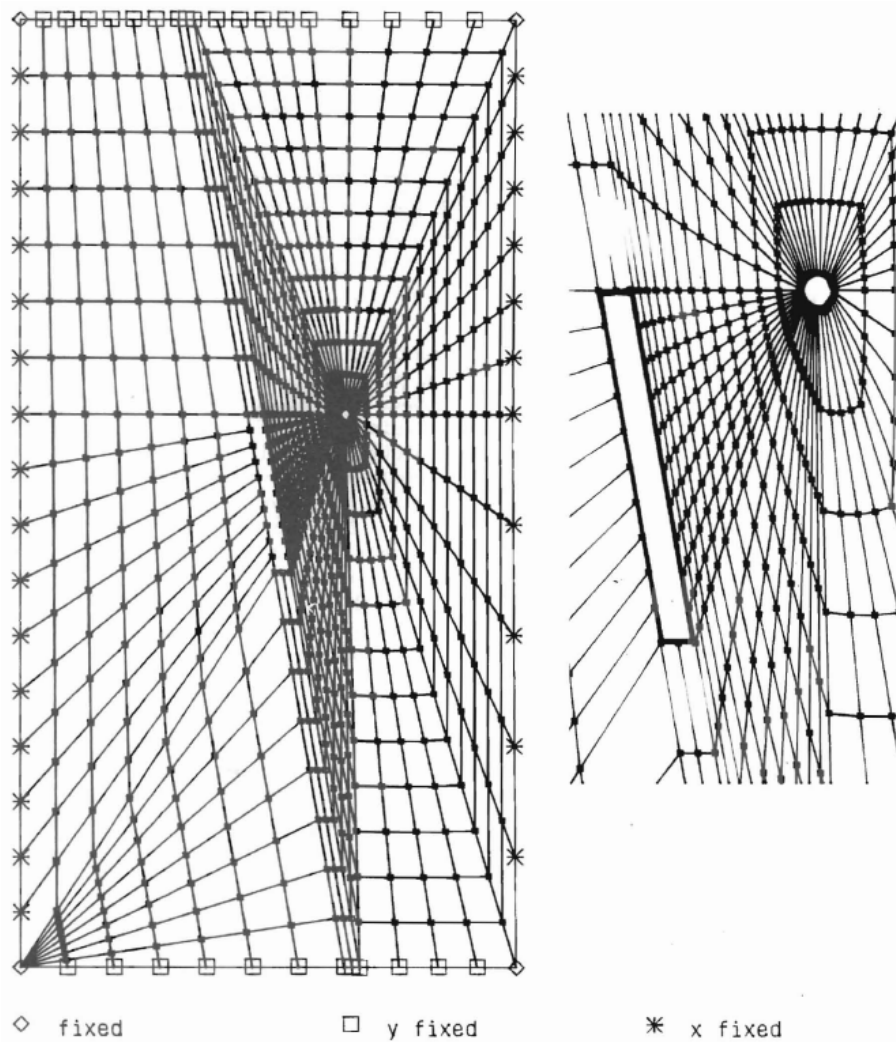


Figure 5-24 Finite element mesh (Mitri and Rajaie 1990)

Pretensioning is an important feature of mechanically anchored rock bolts, grouted rebars and cable bolts. Tang et al., 2000 described pretension numerically by setting up a model illustrated in Figure 5-25 below:

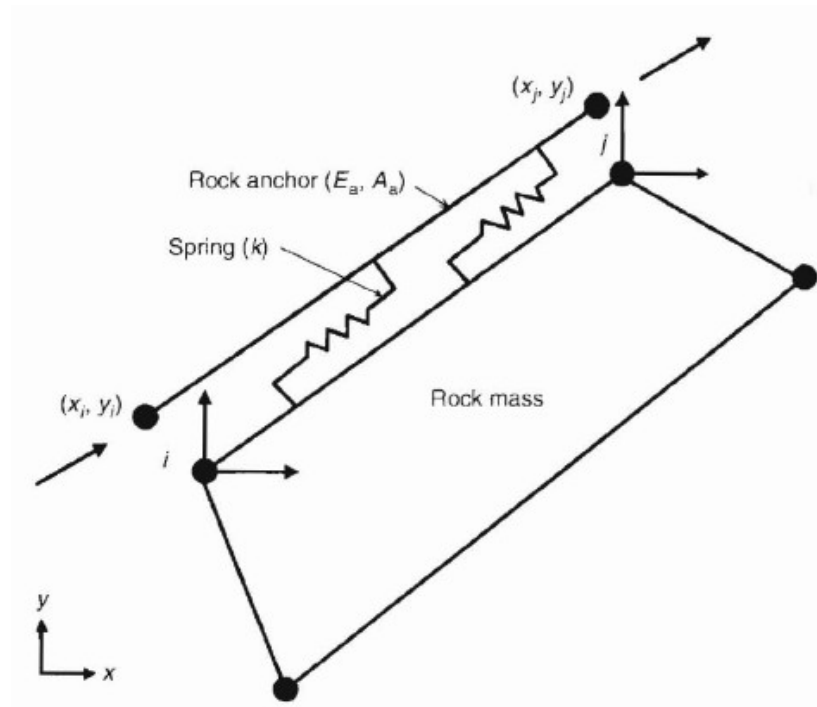


Figure 5-25 Rock anchor element (Tang 2000)

Different types of rock anchors were simulated to illustrate the effects of anchorage type, length of anchorage, and pretensioning, on the load distribution along the anchor and the maximum axial load attained.

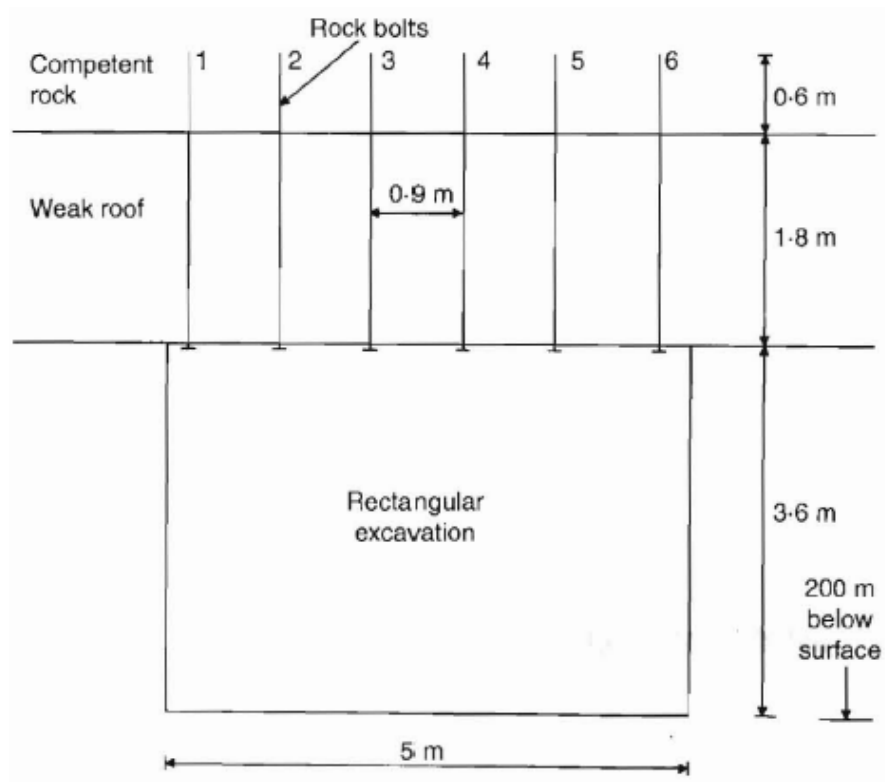


Figure 5-26 Definition of numerical example analysed (Tang 2000)

The simulated anchor models were assigned the same modulus of elasticity and cross-sectional area to permit a fair comparison, although this may not be the case in practice.

Another simple numerical model was developed and applied by Tannant et al., 1995 to study the waveforms recorded in the field, and to investigate the rockbolt-rockmass interaction under dynamic loading from a blast.



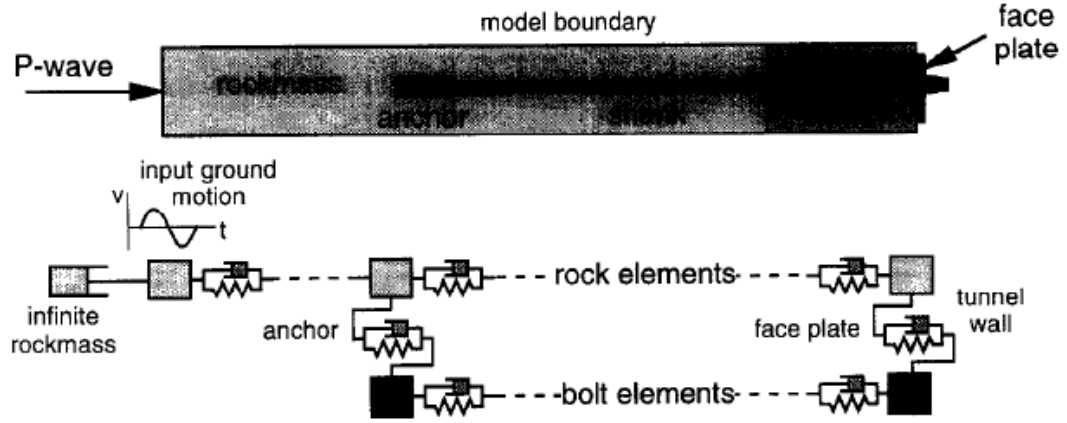


Figure 5-27 Rockbolt and surrounding rockmass (Tannant et al. 1995)

The model represents a combination of an end-anchored mechanical rockbolt and the rockmass at the wall of a drift. The drift wall is treated as a planar free surface. The end-anchored bolt is connected to the surrounding rockmass through the shell anchor and the face plate. It is assumed that a P-wave from the blast propagates towards the free surface in a direction parallel to the axis of the rockbolt.

The displacements of the  $j^{\text{th}}$  rock and bolt elements,  $D_{rj}$  and  $D_{bj}$  are expressed respectively as:

$$\begin{aligned} D_{rj} &= D'_{rj} + v'_{rj} \Delta t \\ D_{bj} &= D'_{bj} + v'_{bj} \Delta t \quad (6.11) \\ j &= 1, 2, \dots, N \end{aligned}$$

With the elastic stiffnesses of the rock,  $k_r$ , and the bolt,  $k_b$  known, the forces in the springs representing the rock and the bolt are:

$$\begin{aligned} F_{rj} &= k_r (D_{r(j+1)} - D_{rj}) \\ F_{bj} &= k_b (D_{b(j+1)} - D_{bj}) \quad (6.12) \\ j &= 1, 2, \dots, (N-1) \end{aligned}$$

The springs representing the anchor and head connections between the bolt and the rock

are non-linear. The forces in the anchor and face plate connections can be expressed as:

$$F_{anchor} = k_a \left( 1 + A \left| \frac{D_b - D_r}{D_n} \right| \right) (D_b - D_r)$$

$$F_{head} = k_h \left( 1 + H \left| \frac{D_b - D_r}{D_n} \right| \right) (D_b - D_r) \quad (6.13)$$

where  $k_a$ , and  $k_h$  are the initial stiffnesses of the anchor and head connection springs before dynamic displacements take place,  $D_r$  and  $D_b$  are the displacements of the connected rock and bolt elements,  $A$  and  $H$  are nonlinearity factors of the connection springs, and  $D_n$  is a normalizing factor given by the peak displacement amplitude of the input wave in the rockmass.

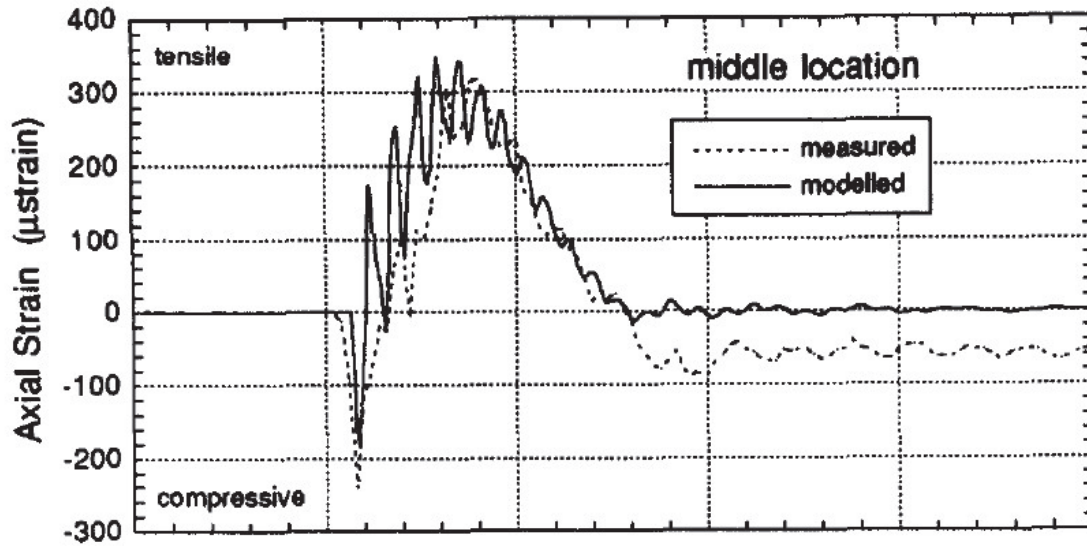


Figure 5-28 comparison between numerical and measured results (Tannant et al. 1995)

A comparison between the numerically predicted and measured axial strain waves at the middle location of the bolt is illustrated in Figure 5-28.

If the rock bolting effect has to be appropriately modelled in the numerical models, the rock bolts have to be represented as special elements. The action of the bolt in the

continuous rock mass and near the joint is so different, that it is necessary to be modelled as two different elements, Marencé and Swoboda 1995.

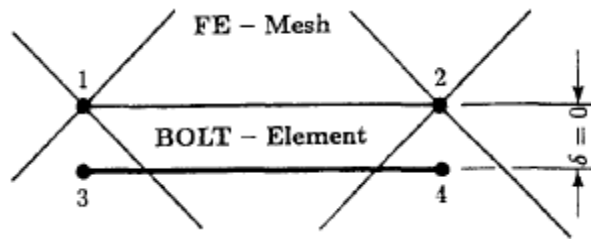


Figure 5-29 Four-node bolt element and connection with FE mesh (Marencé and Swoboda 1995)

Usually, the rock bolts in a continuous rock mass are simulated as truss or beam elements, Laabmayr and Swoboda, 1978. These elements are not appropriate to describe rock bolts, especially grouted bolts, because they do not take into consideration the stiffness of the grout. The main disadvantage of the method is that it is not possible to take into consideration different displacements in the bolt, and on the surface of the borehole (shear displacement which takes part in grout). To solve this problem some authors have attempted to apply special interface elements between the bolt, which is represented as a one-dimensional element, and the rock mass.

The bolt stiffness matrix  $[K]$  under consideration of expressed assumptions can be written as

$$[K] = \begin{bmatrix} 2k_g & 0 & k_g & 0 & -2k_g & 0 & -k_g & 0 \\ 0 & k_s + k_d & 0 & -k_s & 0 & -k_d & 0 & 0 \\ k_g & 0 & 2k_g & 0 & -k_g & 0 & -2k_g & 0 \\ 0 & -k_s & 0 & k_s + k_d & 0 & 0 & 0 & -k_d \\ -2k_g & 0 & -k_g & 0 & k_b + 2k_g & 0 & -k_b + k_g & 0 \\ 0 & -k_d & 0 & 0 & 0 & k_d & 0 & 0 \\ -k_g & 0 & -2k_g & 0 & -k_b + k_g & 0 & k_b + 2k_g & 0 \\ 0 & 0 & 0 & -k_d & 0 & 0 & 0 & k_d \end{bmatrix}$$

$$k_b = \frac{E_b A_b}{L}, \quad k_s = \frac{G_b A_b}{L}, \quad k_g = \pi G_g \frac{L}{3 \ln\left(\frac{r_h}{r_b}\right)} \quad (6.14)$$

$E_b$  and  $G_b$  are, respectively, the elasticity modulus and the shear modulus of the bolt,  $G_g$  is the shear modulus of the grout,  $A_b$  is the area of the bolt,  $L$  is the length of the element,  $r_b$  and  $r_h$  are the radii of the bolt and the hole respectively, and  $k_d$  is the "dowel" stiffness. The "dowel" stiffness is important only at the place where the bolt intersects the rock joint. A special element, the Bolt Crossing Joint (BCJ) element, has been developed to incorporate all the important factors. The BCJ element is the element which connects the bolt elements on both sides of the discontinuity, as shown below:

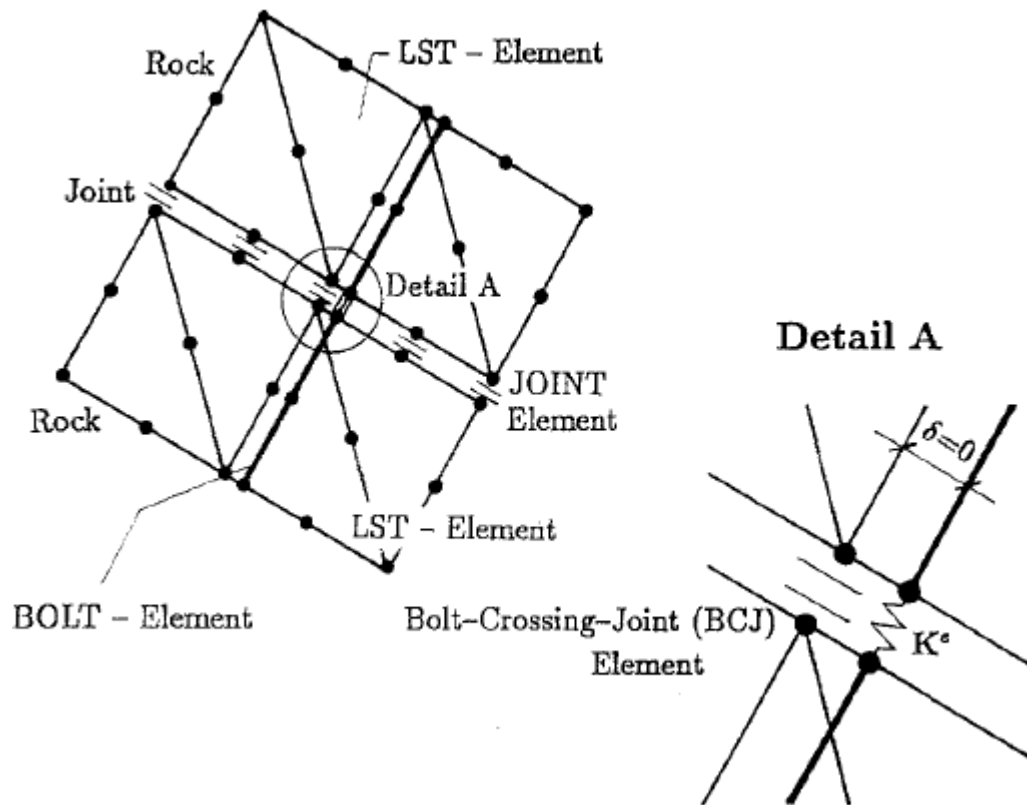


Figure 5-30 Bolt crossing joint element and connection with finite element mesh

(Marence et al.)

The BCJ element is modelled as springs which describe the bolt resistance according to the movements on the joint.

The axial spring stiffness describes the behaviour of the bar under the displacement in the direction of the bolt axis. The bar-grout interface plays the main role in this case, because in most cases slip occurred on this plane.



## **Chapter 6**

### **Assessment of Drift Support System Performance**

#### **6.1 Introduction**

Although the finite element method has been successfully used to model rock anchors in the past (e.g. Tang et al., 1999), trial simulations with Phase 2 showed the current version of Phase 2 software does not accurately simulate the rock support. This is because the nodes representing the bolts do not coincide with the FE mesh nodes. Thus, the finite difference method software FLAC has been selected. It has the modelling capability for both rock anchors and shotcrete. The case study level is situated 1.5 km below surface and the haulage drift is 5 m by 5 m. Primary support system consists of rebars, whereas secondary or enhanced support system includes modified cone bolts and shotcrete liner. Elastoplastic finite difference modeling is carried out in the first place to assess the state of stress and deformations around the drift, and the response of primary support system to drift development. A multi-stage simulation of mine and fill sequence in the vicinity of the haulage drift is then performed to examine the performance of enhanced support systems. Mining sequences are simulated in two directions: from lower to upper levels, and from hanging wall to footwall in retreat. Model results are discussed and analyzed to help identify the most critical mine design parameters and validated the proposed rock support systems.

Finite difference modeling software *FLAC* of Itasca is chosen as the numerical analysis tool as it has the capability of modeling the interaction between the rock support elements and the rock mass.

## 6.2 FLAC Model

The standard support pattern from Garson mine, Vale Inco was selected for the case study to analyze the variation of axial loads in the bolts and stresses in the shotcrete liner with respect of mining sequences. Figure 6-1 shows the layout of the problem to be modeled, whereby three lower level stopes and three same-level stopes are mined and filled in the sequence shown in the vicinity of the haulage drift located on the 5000 ft level.

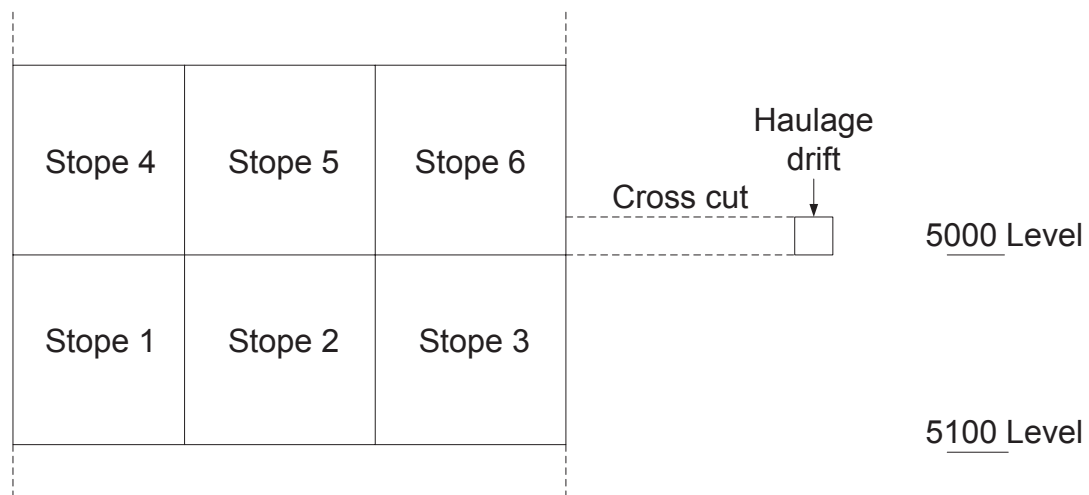


Figure 6-1 Layout of numerical modeling problem

Figure 6-2 presents two of the mine standard primary support patterns used in for drifts driven in regular rock (footwall) and ore rock. The current study concerns itself with the footwall drift. A total of fifteen 6-ft rebars are used with nine in the back, and three on each of the drift side walls. The enhanced support pattern consists of four eight-foot-long



modified cone bolts (MCB) installed in the back, three ten-foot-long MCBs on each side of the drift side walls and a shotcrete liner applied to the drift back and sidewalls; see Figure 6-3.

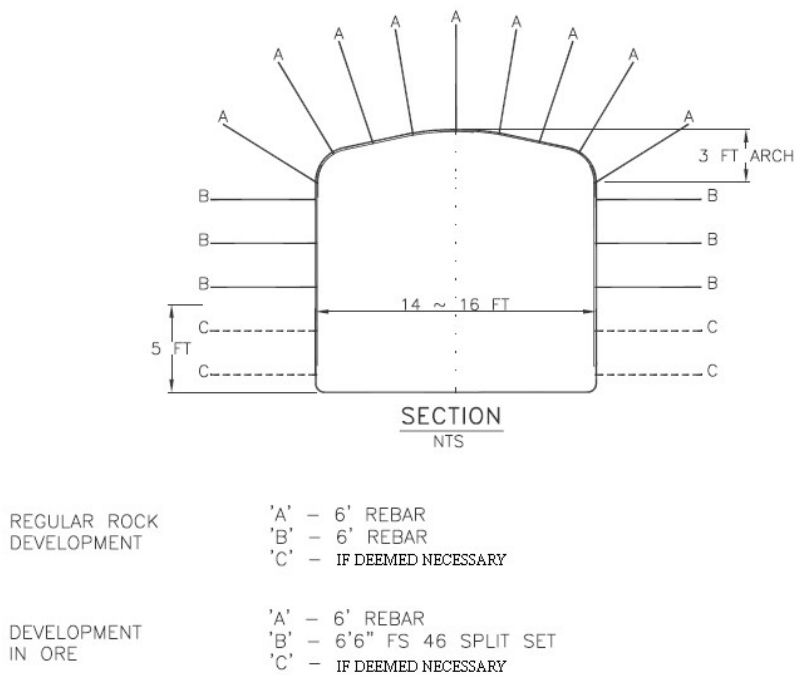


Figure 6-2 Drift primary support pattern

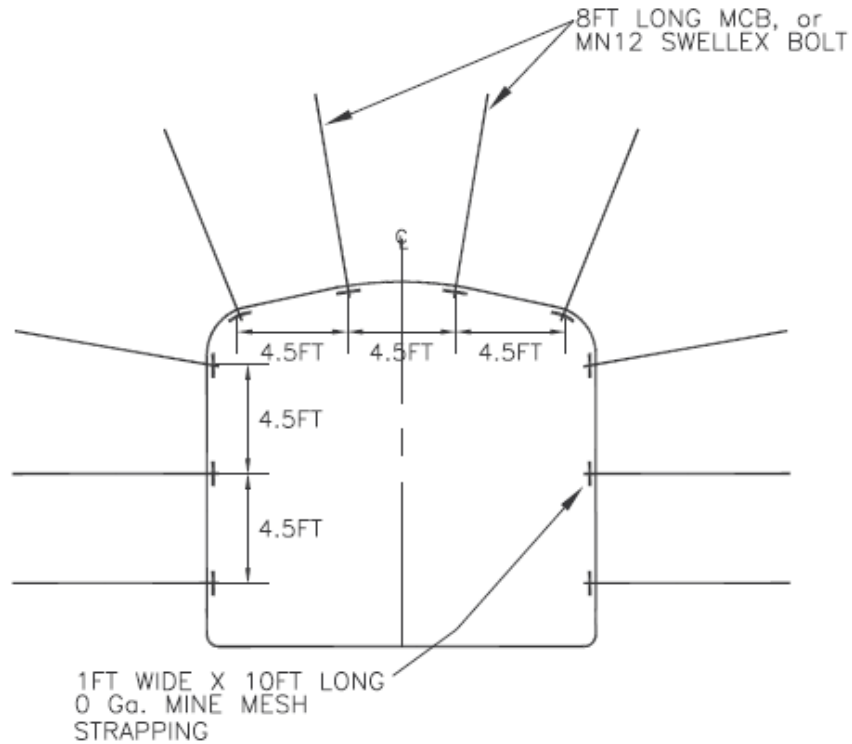


Figure 6-3 Enhanced support pattern

The primary support pattern mentioned above is installed on the 3150 footwall drift shown in Figure 6-4 on the 5000 level. Based on section A-A that is marked on Figure 6-4, a 2-dimensional finite difference model in *FLAC* is built (see Figure 6-5). In this model, three rock mass materials are found: footwall, orebody and hanging wall. The rock mechanical properties of these rock masses as well as those of the mine backfill are listed in Table 6-1. These properties are derived in a previous study by Wei et al. from the geotechnical parameters provided by the Garson mine. All geomaterials are treated as Mohr-Coulomb elastoplastic with zero angle of dilation.

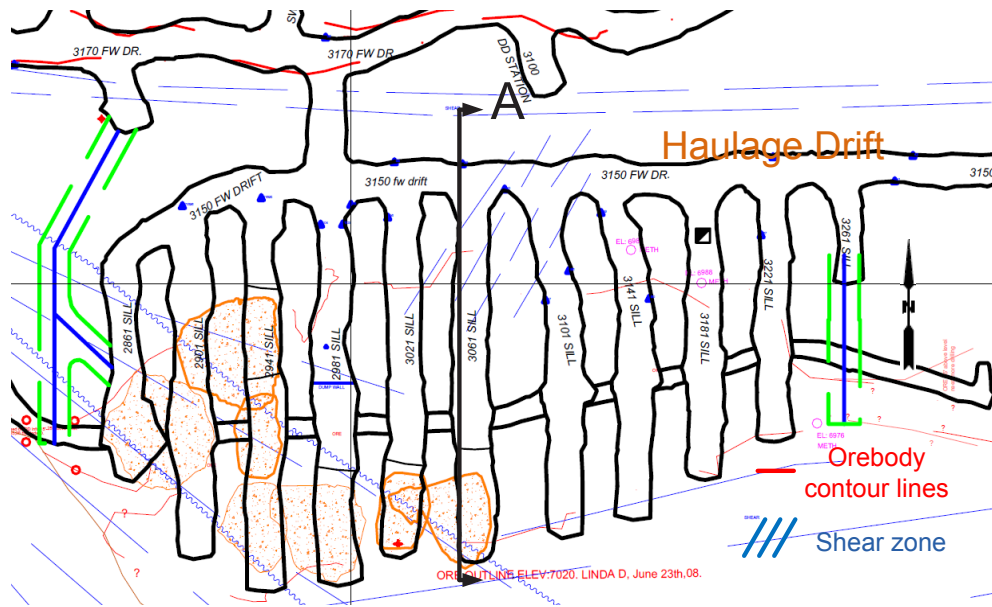


Figure 6-4 Plan view of 5000 level - Garson mine

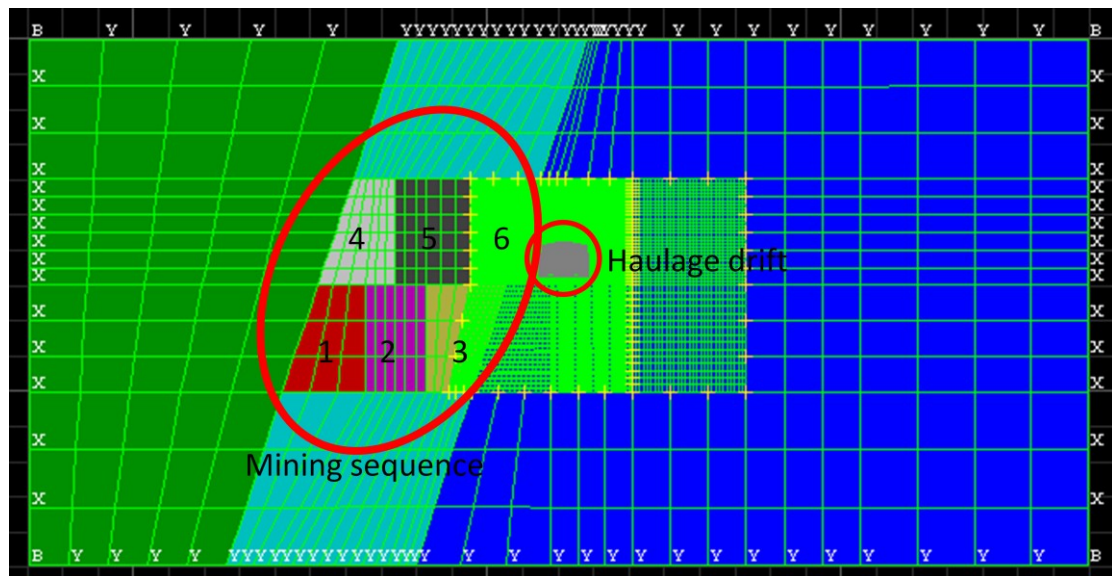


Figure 6-5 *FLAC* model of section A-A (see Figure 6-4)

Table 6-1 Mechanical properties of geomaterials used in *FLAC* models

Rock mass	HW	ORE	FW	BF
Unit weight (MN/m <sup>3</sup> )	0.03	0.03	0.03	0.02
Young's modulus (MPa)	40,000	10,000	24,000	100
Poisson's ratio	0.18	0.22	0.15	0.30
Dilation angle	0	0	0	0
Friction angle	30	30	30	30
Tensile strength (MPa)	1.52	1.80	0.99	0.01
Cohesion (MPa)	16.5	16.5	16.6	1

### 6.2.1 Rockbolt Modeling Technique

The modeling technique of rock support elements is based on the assumption that the rock support is attached to the rock mass through a set of continuous shear springs representing the shear bond stiffness of the rock-grout interface, the grout shear stiffness as well as the grout-bolt interface; see Figure 6-6.

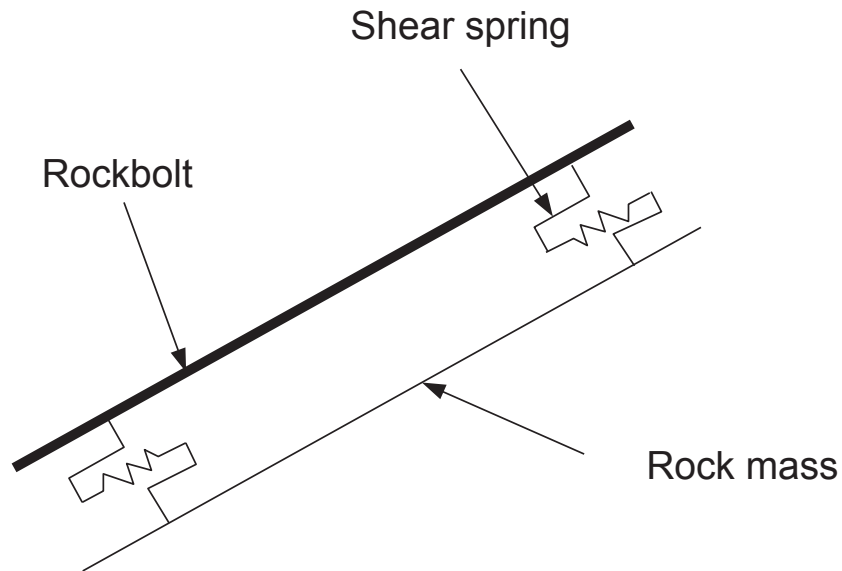


Figure 6-6 Basic model of a rockbolt element

In *FLAC*, a rock bolt is treated as a beam-column element with six degrees-of-freedom as shown in Figure 6-7. This formulation allows for tension and bending of the rock bolt element to be simulated. Modeling of the plated bolt head is done by "locking" the node representing bolt head onto a node of the finite difference grid representing the rock mass. Figure 6-8 shows the layout of simulated rebars on the drift section.



Figure 6-7 Degree of freedom of a rockbolt element

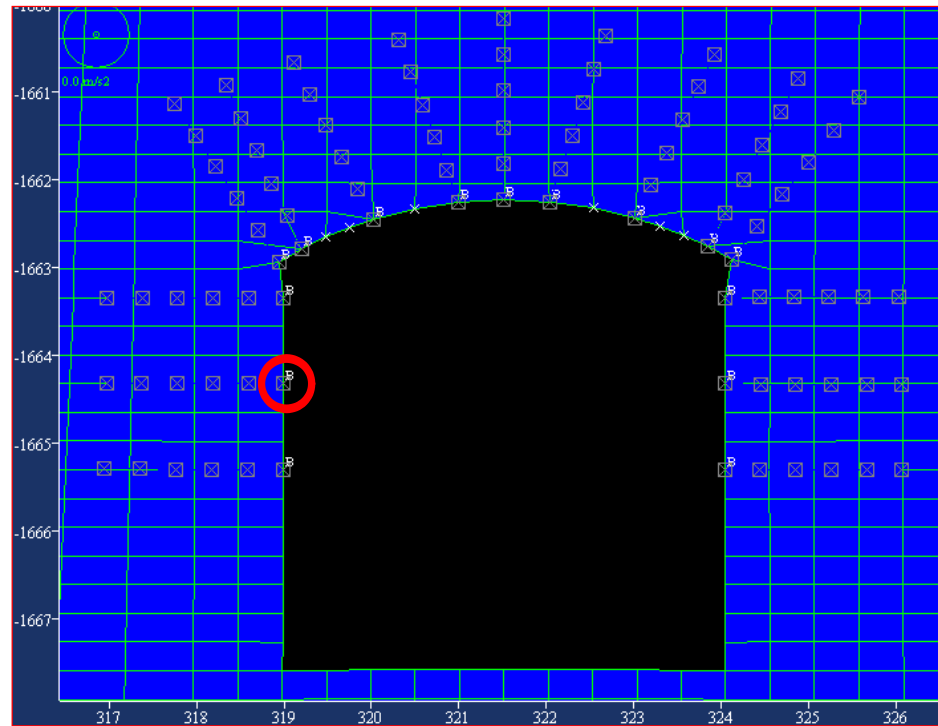


Figure 6-8 Fixed boundary condition of rockbolts

In order to model the grouted rebar more accurately, each rebar is divided into five elements, which are linked to the rock mass with shear springs.

### 6.3 Support System Analysis

#### 6.3.1 Primary Support

Primary support with grouted rebars is installed during the haulage drift development. Rebar mechanical properties are reported in Table 6-2. The shear spring stiffness of resin grouted rebar is obtained from a previous study by Chen and Mitri, 2005.

Table 6-2 Model input parameters

Properties	Primary support (Rebar)	Enhanced support (MCBs)	Enhanced support (Shotcrete)
E (MPa)	200,000	200,000	5,500
L (feet)	6	8-10	
D (inch)	$\frac{3}{4}$	$\frac{3}{4}$	
A (in <sup>2</sup> )	0.44	0.44	
Yield strength	125 KN	155 KN	
Shear spring stiffness (MN/m/m)	33.85	40	
Thickness (m)			0.1
Compressive strength (MPa)			40
Poisson's ratio			0.18

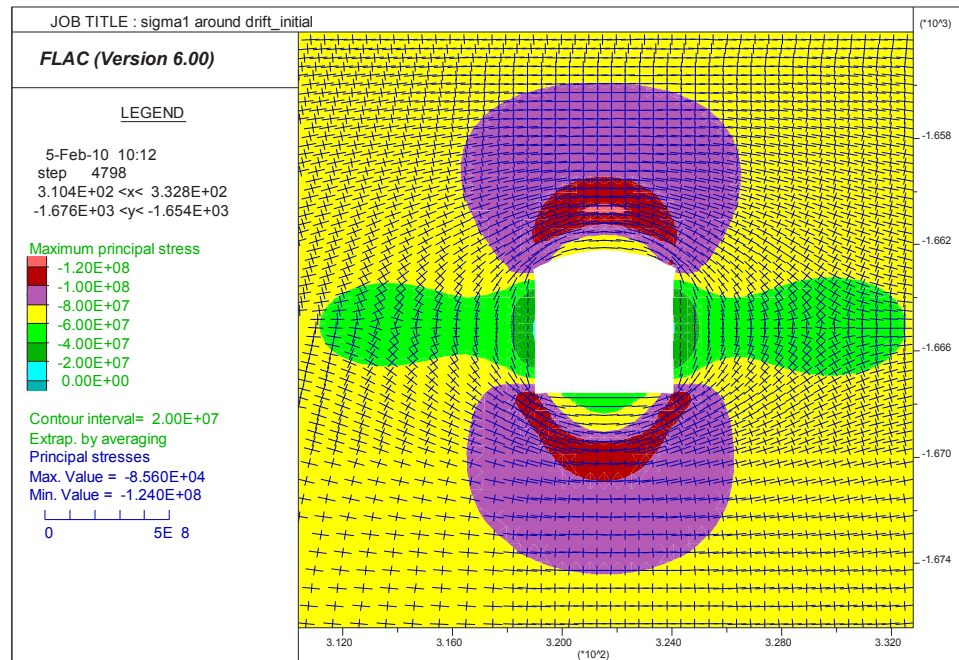


Figure 6-9 Principal stress distribution around haulage drift

As can be seen from Figure 6-9, high stress concentrations develop at approximately 1.5 m above the drift back and 2 m below the drift floor. Drift deformation can be viewed in Figure 6-10, from which it is observed that the drift walls and floor experience much more deformations than the arched drift back.



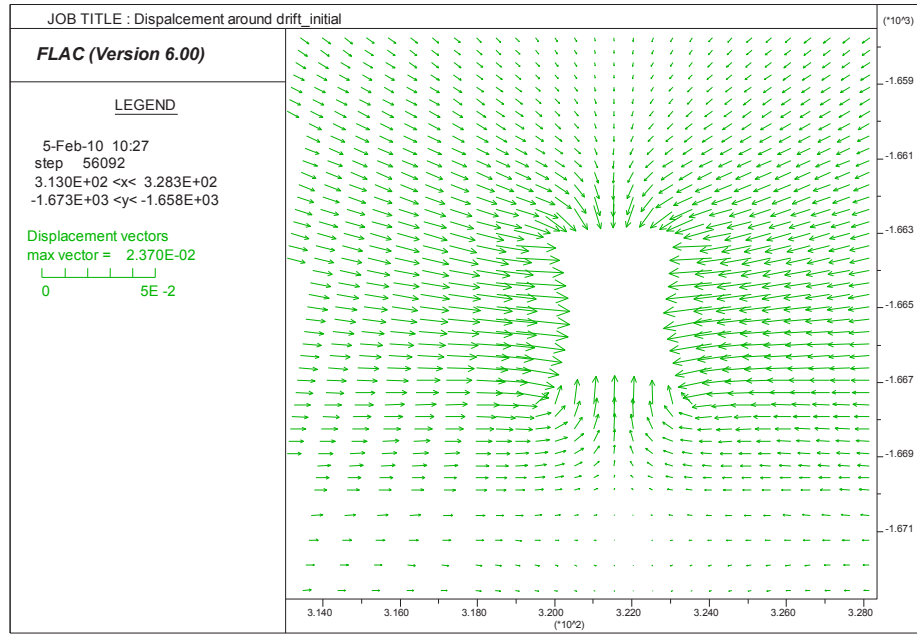


Figure 6-10 Initial deformations around haulage drift

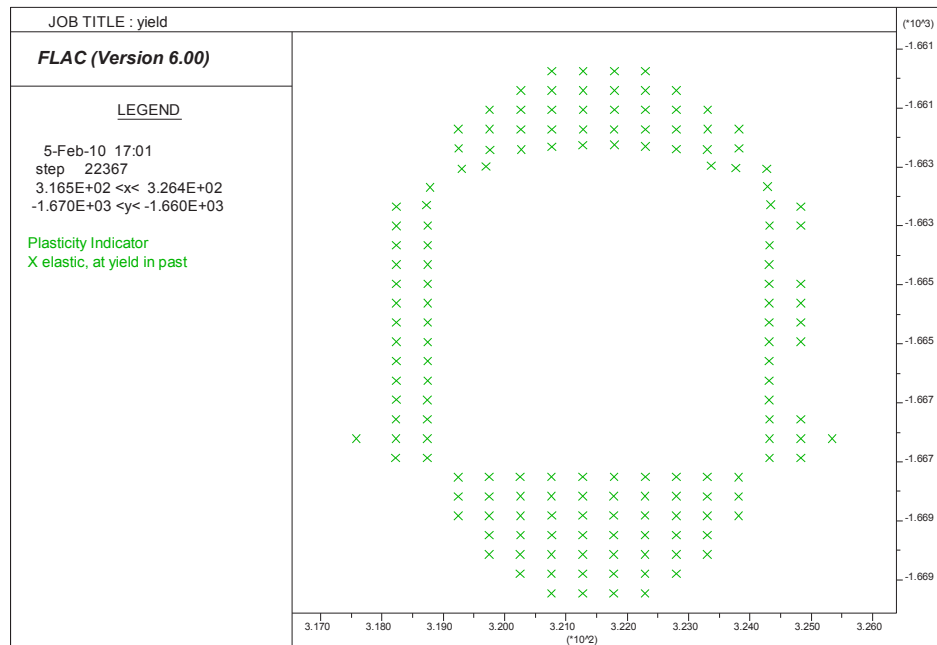


Figure 6-11 Rock mass yielding around haulage drift

As shown in Figure 6-11, yielding is observed more at two locations: drift back and floor where high mining induced stress concentrations are found.

It should be noted that the results shown in Figures 6-9, 6-10 and 6-11, change only slightly with the modeling of the drift primary support system of rebars. This suggests that the rebars have little influence on reducing the drift deformations. This can be explained by the fact that the drift overall stiffness (resistance to convergence) is much higher than those of the rebars. Thus, the primary support system of rebars can only resist some of the drift deformation or convergence.

Seven rebars are selected for plotting the results. These are located in the drift back (3), walls (2) and shoulders (2). Initial axial loads in the rebars – plotted in Figure 6-12 – show that the axial load is at a maximum at the rebar head where it is plated and nearly vanishes at the toe of the rebar. This response was expected. It is noted that the maximum axial load takes place at the back (right) and wall (right).

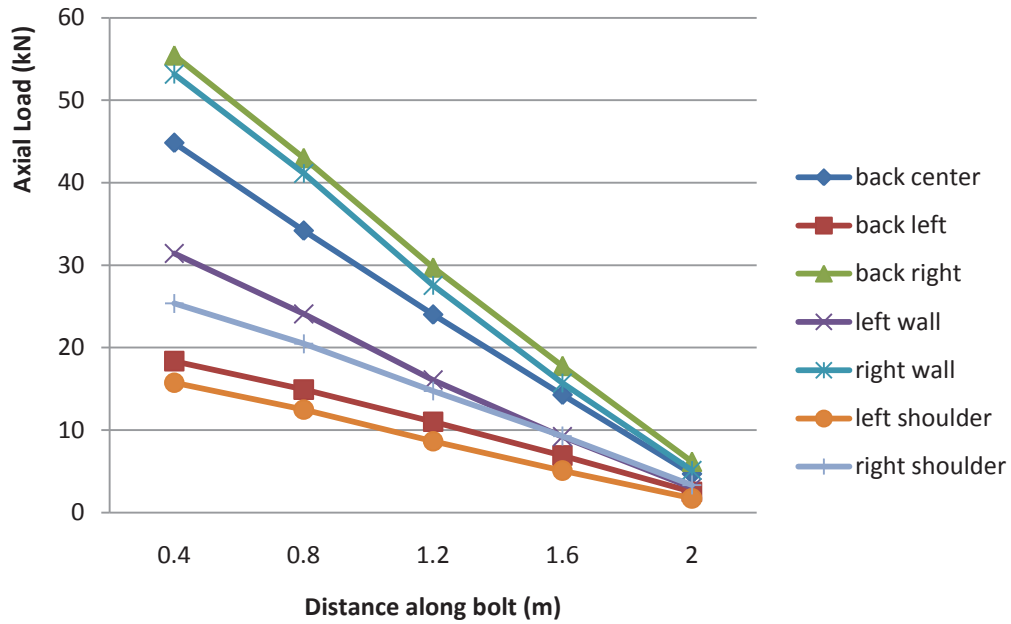


Figure 6-12 Axial loads in rebars after drift excavation

As mining activities continue with the primary support in place, the axial loads in the rebars continue to increase and approach the rebar yield load. After all six stopes have been mined out and backfilled, most of the rebars experience yielding to a depth of 0.8 m to 1.2 m - see the results in Figure 6-13.

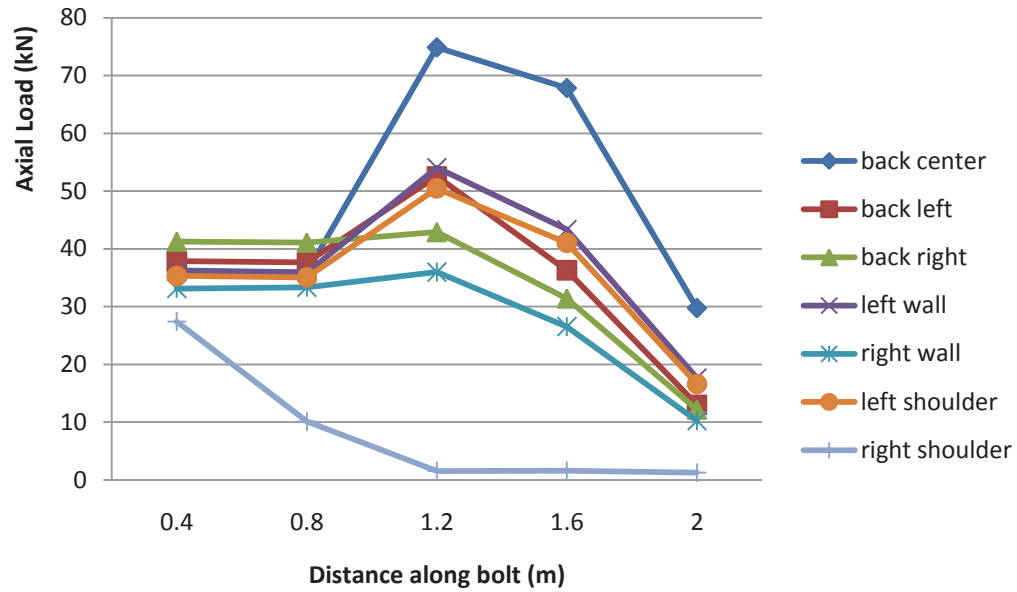


Figure 6-13 Axial loads of rebars after stope 6 is mined out

Although the rebars can still hold some of the axial loads transferred from rock mass, they cannot be considered as a reliable support system for haulage drift. Thus, it is expected that the enhanced support system is play a key role in drift stability.

The deformed drift periphery is presented in Figure 6-14. This will be referred to later.

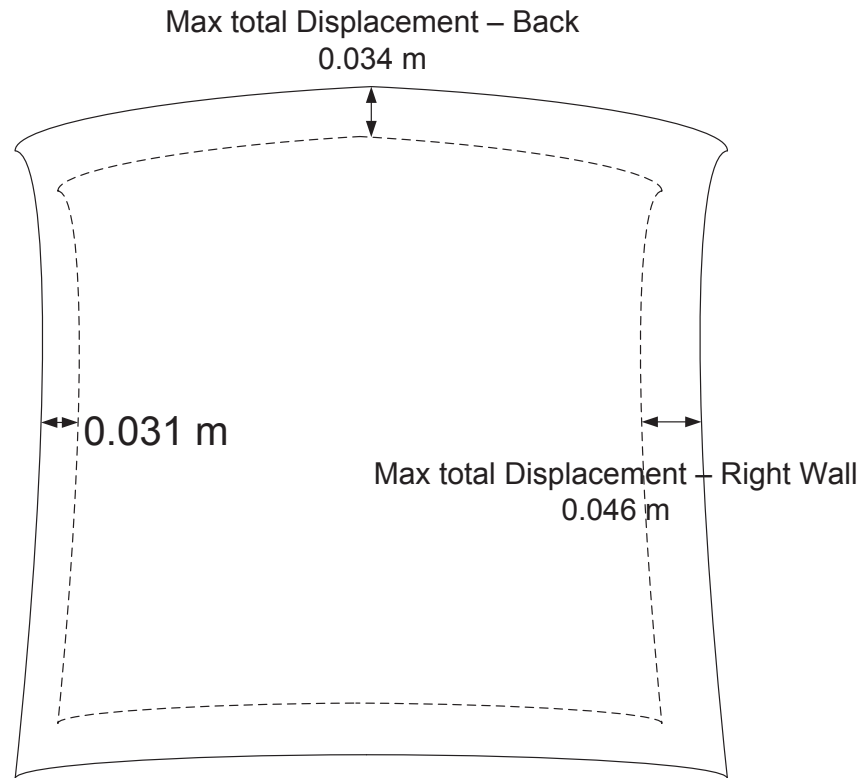


Figure 6-14 Deformed drift profile after stope 1 is mined out - primary support system

### 6.3.2 Enhanced Support

The current practice at the mine necessitates that enhanced support be installed simultaneously with the primary support. As presented in Figure 6-3, the enhanced support pattern consists of four eight-foot-long modified cone bolts (MCB) installed in the back, three ten-foot-long MCBs on each side of the drift side walls and a 10 cm shotcrete liner applied to the drift back and sidewalls. In this case study, MCBs are set up with one layer of shotcrete. Another maximum total displacement plotting is as below in Figure 6-15, from which the effect of enhanced support can be easily told.

In order to have an appreciation of the role of enhanced support system on drift deformations, the drift deformed profile after the mining of stope 1 is plotted for the case

of primary support system in Figure 6-14, and is then compared to the same when the enhanced support system is added to the model - Figure 6-15. As can be seen, deformations are reduced with the introduction of the enhanced support system, with the maximum reduction of 11% being on the left sidewall.

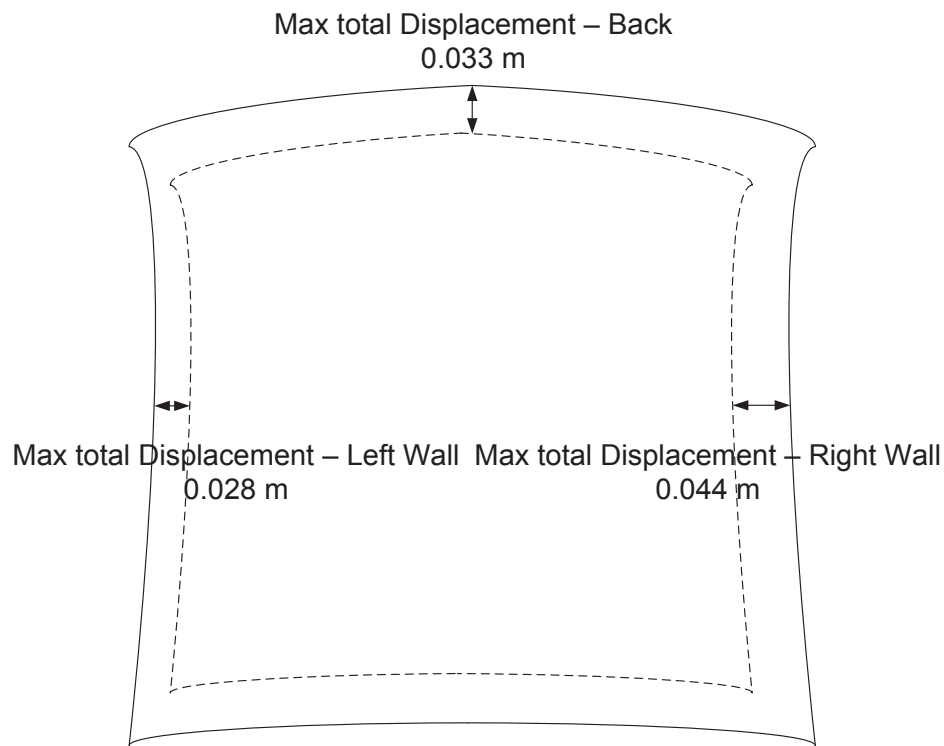


Figure 6-15 Deformed drift profile after stope 1 is mined out - primary and enhanced support systems

### **Deformation of Haulage Drift**

A serial of comparisons of maximum total displacement of the haulage drift with respect to mining sequence is presented in Figures 6-16 to 6-18 to examine the effect of enhanced support system. It is obvious from these results that the enhanced support system consistently offers more resistance to drift deformations with mining sequences.

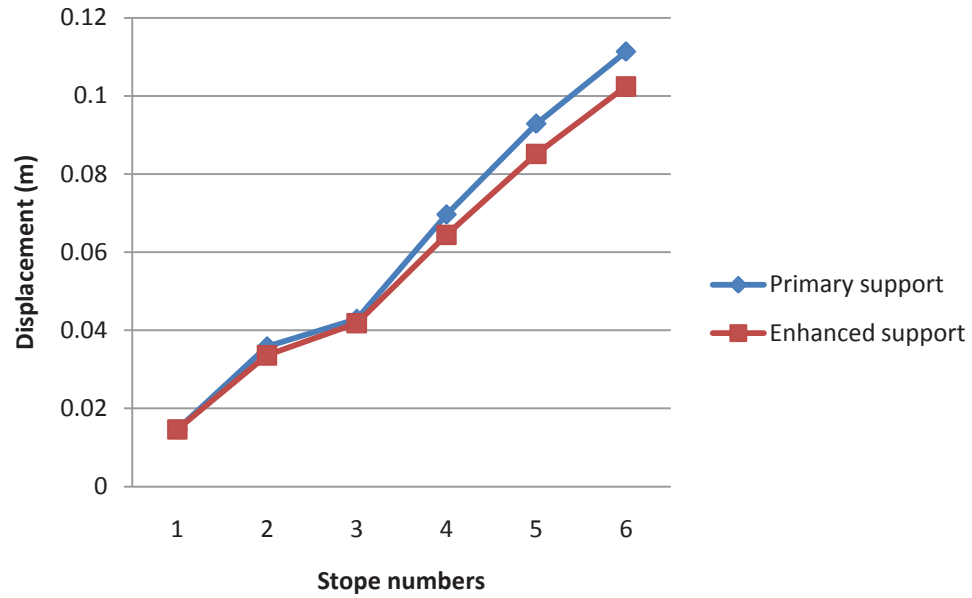


Figure 6-16 Maximum total displacements at drift back with respect to mining sequence

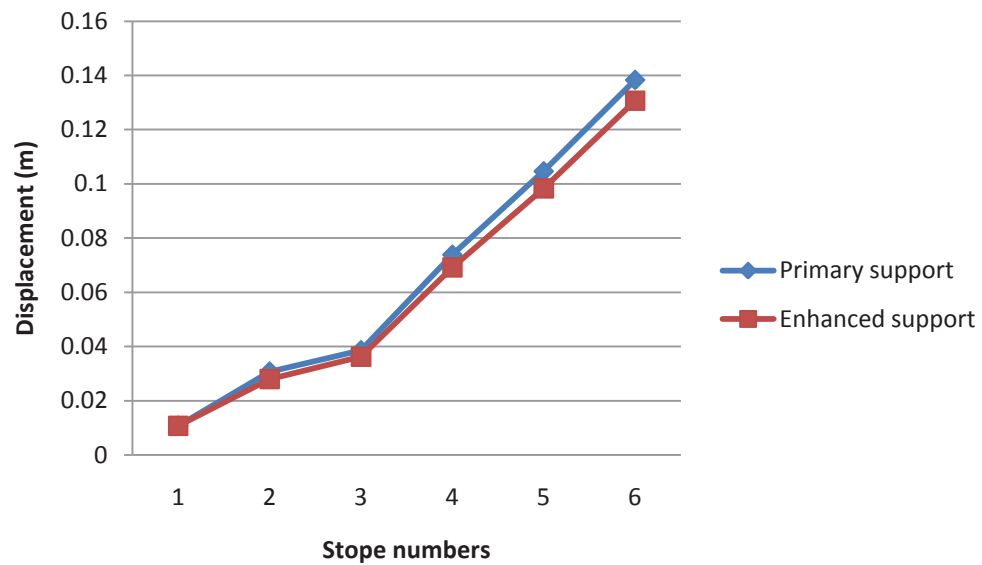


Figure 6-17 Maximum total displacements at left wall with respect to mining sequence

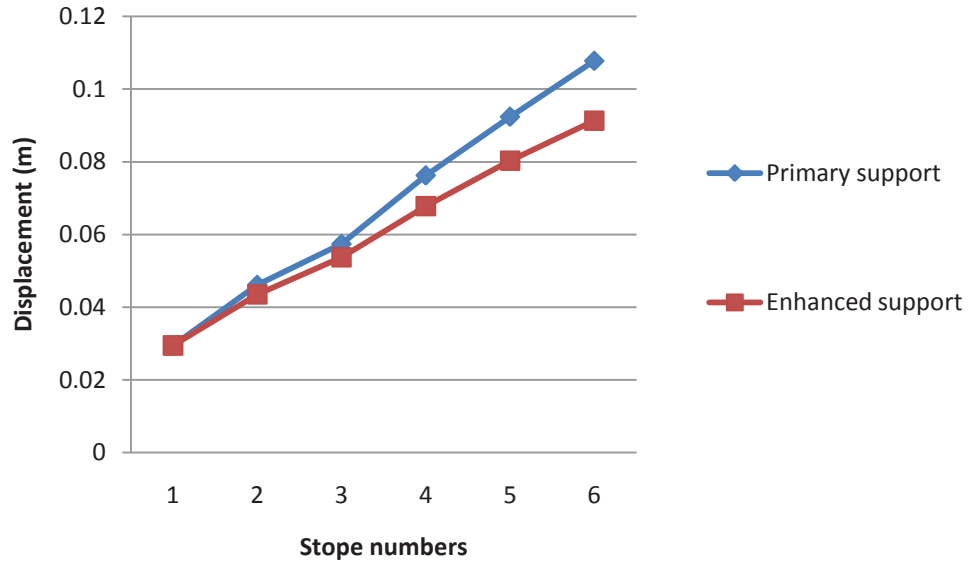


Figure 6-18 Maximum total displacements at right wall with respect to mining sequence

To better quantify the drift deformation, the wall convergence ratio (WCR) proposed by Zhang and Mitri is used and applied to the location of maximum displacement.

$$WCR = \frac{W - W_m}{W} \times 100\% \quad (7.1)$$

Where  $W$  is the drift span and  $W_m$  is the shortest deformed span as illustrated in Figure 6-19.



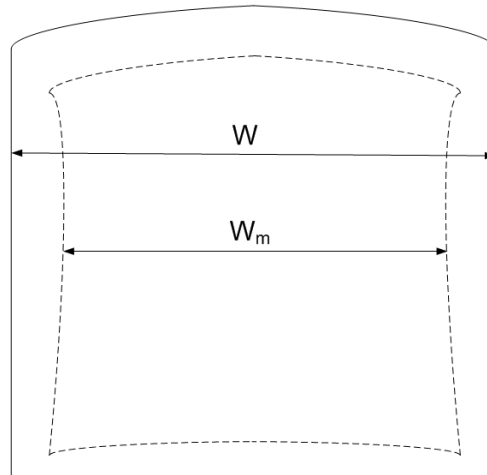


Figure 6-19 Wall convergence ratio (WCR)

The drift deformation is plotted in Figure 6-20 in terms of WCR and with respect to mining sequence. It is noteworthy that WCR increases gradually with mining sequence to a maximum of 4.5% for the case of enhanced support system, and 5% for case of primary support alone serving the haulage drift.

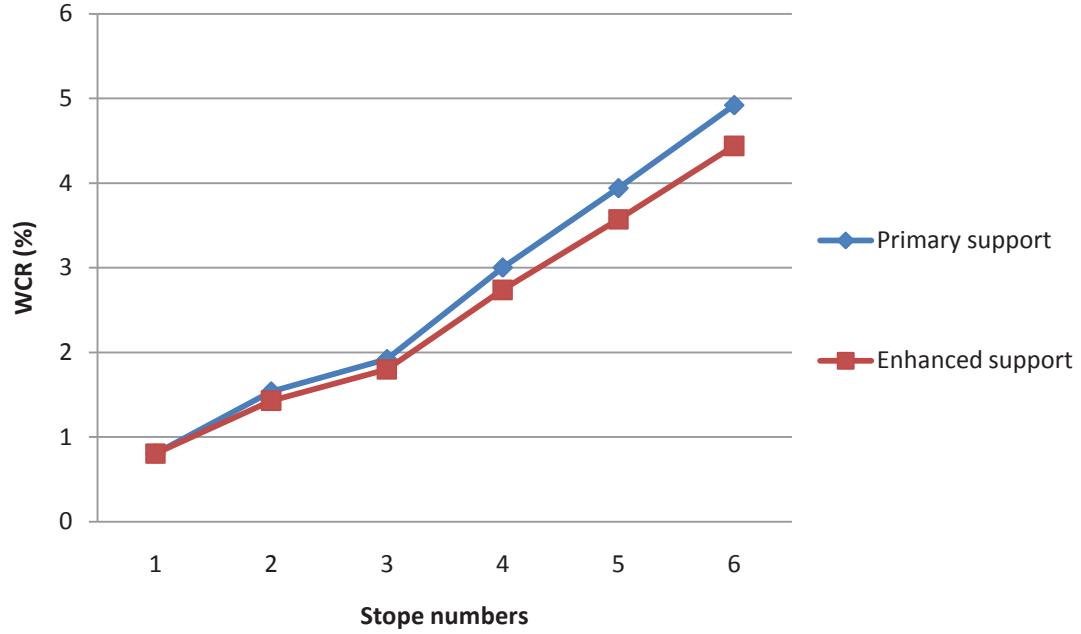


Figure 6-20 Variation of wall convergence ratio (WCR) with mining sequence

### Shotcrete Stresses

In addition to the MCBs, shotcrete also contributes to the strength of the drift boundary. In *FLAC*, shotcrete is modeled as a liner element that must be bonded to the grid which represents rock mass. Axial and shear loads in the shotcrete layer with respect to different mining stages are calculated by *FLAC*; these can be viewed in Figures 6-21 and 6-22, respectively. Axial and shear stresses are then calculated from.

$$\sigma_n = \frac{F_n}{S} \quad (7.2)$$

$$\sigma_s = \frac{F_s}{S}$$

Where,  $F_n$  is axial load,  $F_s$  is shear load and  $S$  is the cross sectional area of the shotcrete layer.

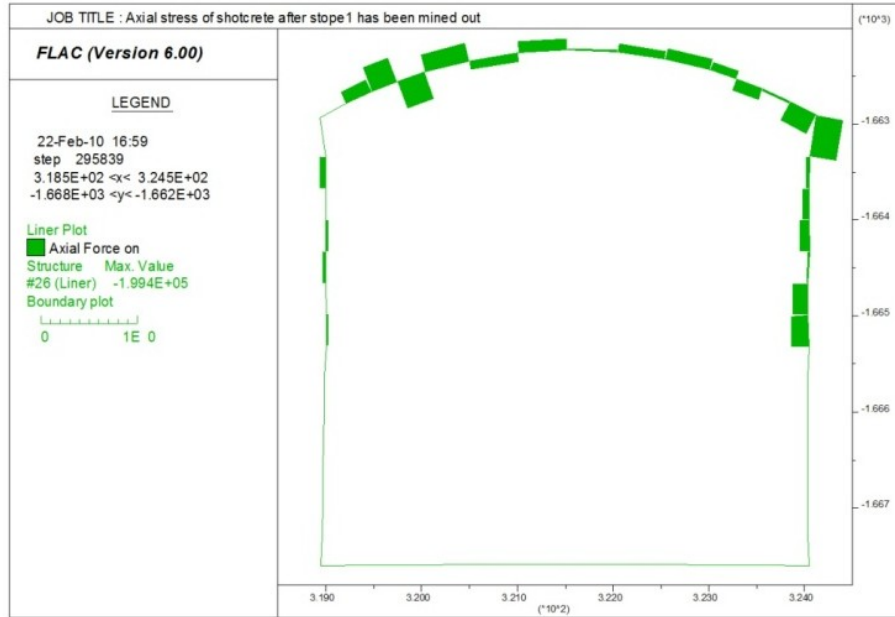


Figure 6-21-a Axial stress in shotcrete after stope 1 is mined out

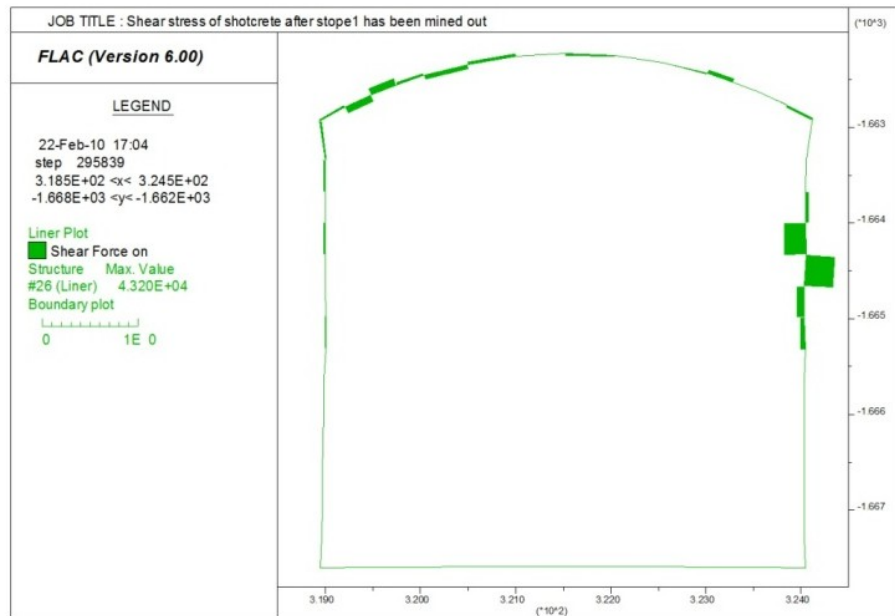


Figure 6-21-b Shear stress of shotcrete after stope 1 is mined out

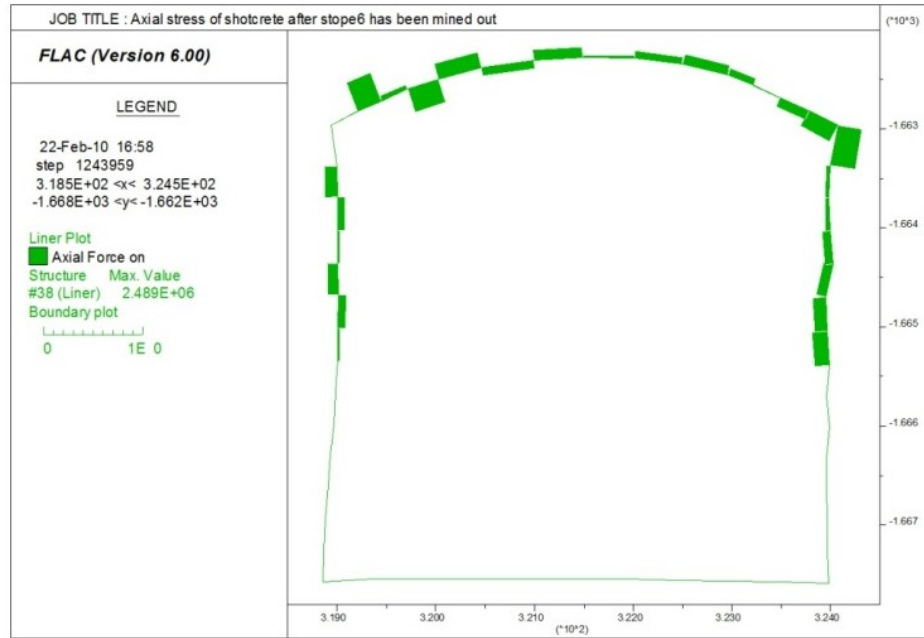


Figure 6-22-a Axial stress of shotcrete after stope 6 is mined out

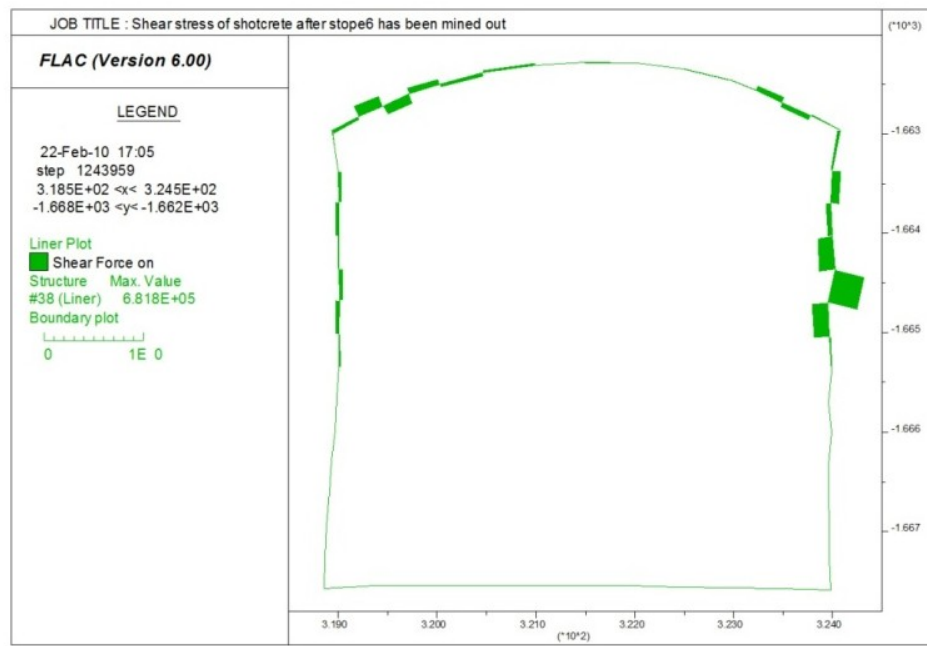


Figure 6-22-b Shear stress of shotcrete after stope 6 is mined out

In order to locate the most critical sections in the drift perimeter, the normal and shear stress acting on the shotcrete section are calculated in Table 6-3. Figure 6-23 shows node numbers around the drift perimeter and the locations of severe bending, which indicated from Table 6-3 are the highest compressive stresses and tensile stresses in the shotcrete layer.

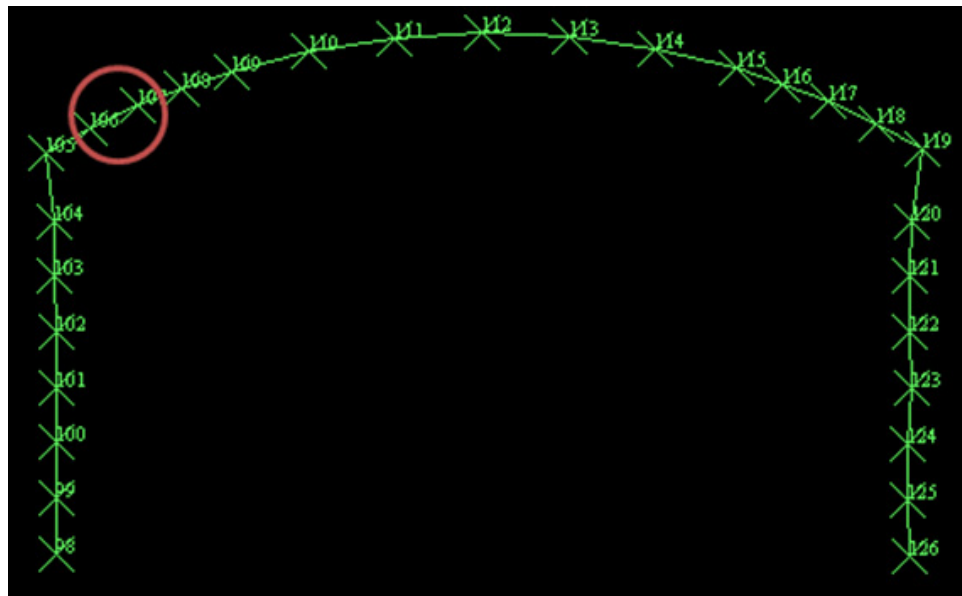


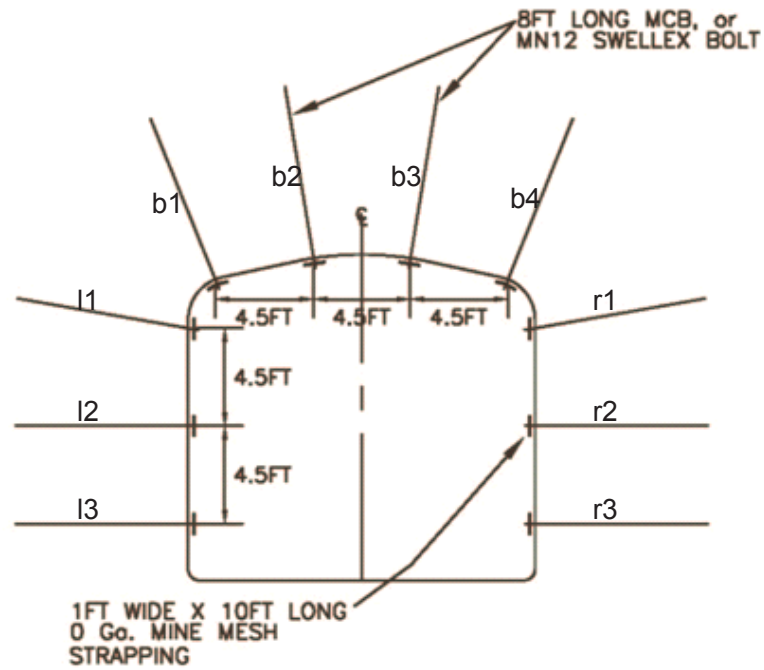
Figure 6-23 Location of potential failure of shotcrete layer

Table 6-3 Axial and shear stresses location of shotcrete layer

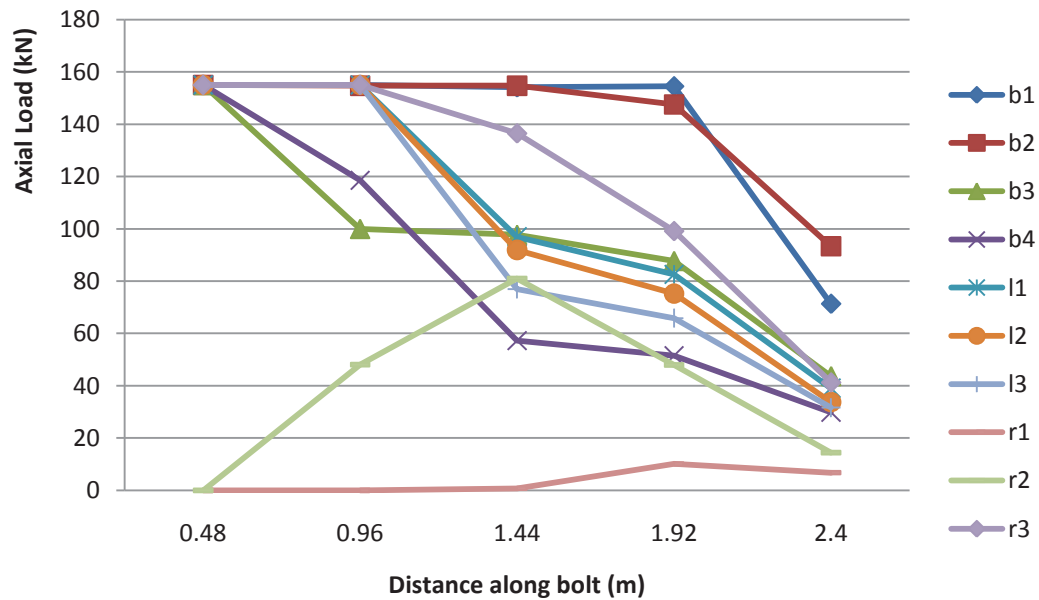
Node number	Axial stress	Shear stress	Node number	Axial stress	Shear stress
98	-1.38	-0.25	112	1.16	-0.22
99	-6.40	0.74	113	5.76	-0.08
100	8.15	-0.87	114	7.86	-0.13
101	-1.87	0.14	115	5.98	0.19
102	-6.14	0.67	116	-1.03	1.26
103	10.15	-0.59	117	-8.37	-1.12
104	-0.12	0.02	118	-14.70	0.21
105	0.17	-0.79	119	20.50	-0.49
106	24.89	2.36	120	-3.70	1.90
107	4.08	-2.27	121	-3.74	-1.17
108	-20.22	1.38	122	-7.22	-3.57
109	13.49	-0.77	123	-7.58	6.82
110	-6.63	0.46	124	-10.23	-3.57
111	8.46	0.02	125	-12.57	0.22

### **Axial Loads of Enhanced Support**

Axial loads along the MCBs are examined after stope 6 is mined out. The results are shown in Figure 6-24. As can be seen, the MCB  $r_1$  and  $r_2$  in the right shoulder have yielded.



a) Identification of MCB's



b) Axial load results

Figure 6-24 Simulation results of MCBs after stope 6 is mined out

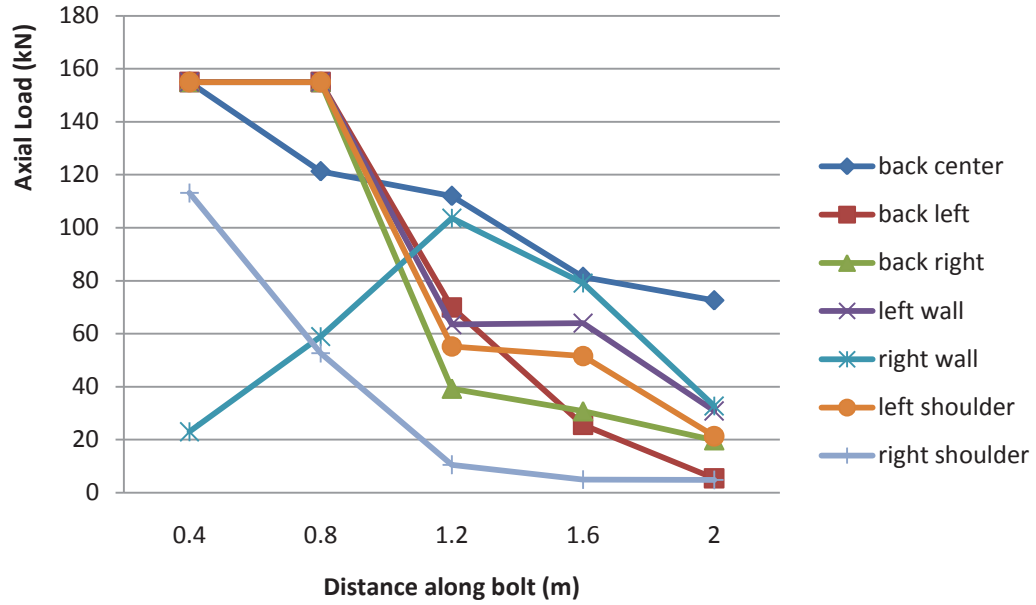


Figure 6-25 Axial loads of rebars after stope 6 is mined out

Figure 6-25 presents the axial loads in the rebars, from which it is observed that only the rebar in the right wall has yielded. This is a significant improvement over the results depicted in Figure 6-13 whereby most of the rebars yielded after stope 6 is mined out. Thus, it can be concluded that the enhanced support system not only increases the stability of haulage drift but also helps strengthen the primary support system.

### 6.3.3 Effect of Enhanced Support Installation

The following analysis examines an alternative timing of enhanced support system installation. Figure 6-26 shows a plot of rebar axial loads after stope 1 is mined out. At this stage, most of the rebars experience yielding. Checking the loads in the rebars again while stope 2 is being mined out, *FLAC* generates intermediate nodes along the rebars oriented towards the orebody, thus indicating that they have yielded; see Figure 6-27.



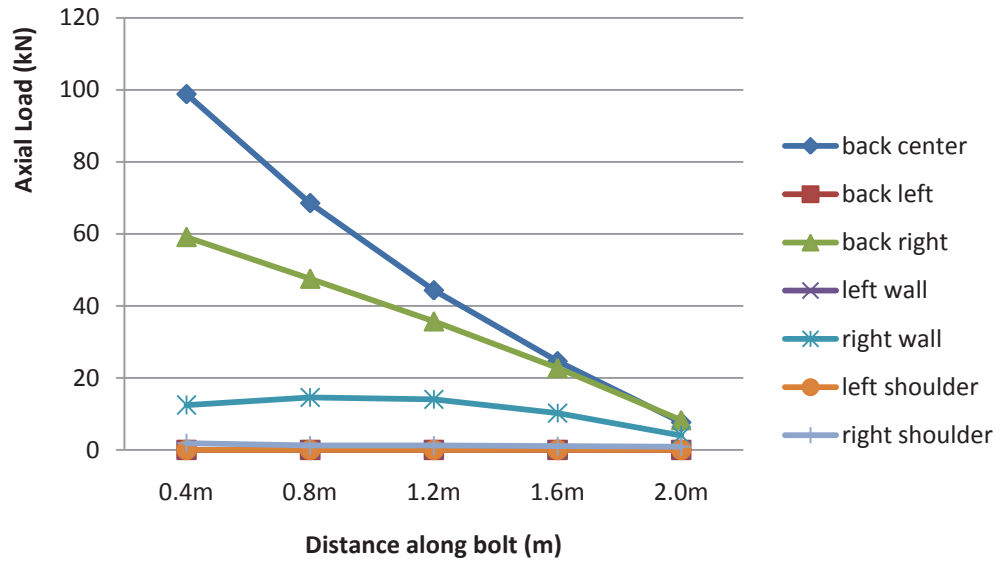
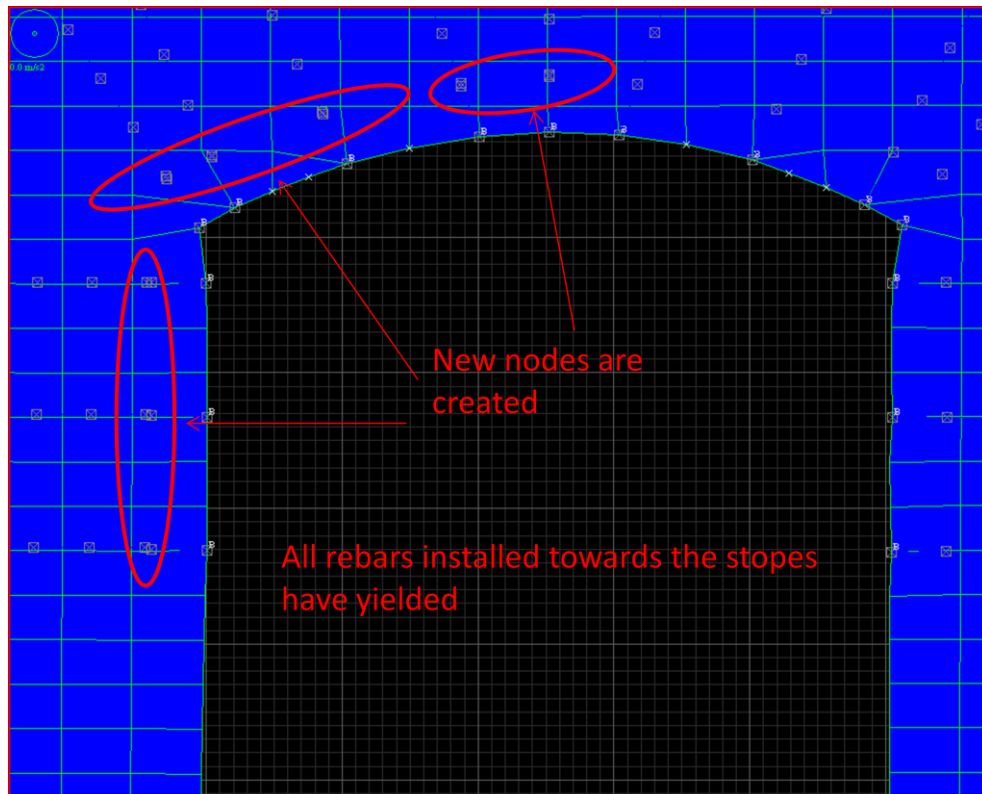


Figure 6-26 Axial loads of rebars after stope 1 is mined out

Figure 6-27 Presentation of yielding rebars in *FLAC*

Numerical modeling results imply that primary support is not working sufficiently after stope 2 has been mined out.

After stope 1 is mined out, enhanced support is installed. As can be seen from the results plotted in Figure 6-28, the enhanced support not only works effectively but also takes lesser loads than when installed right from the start.

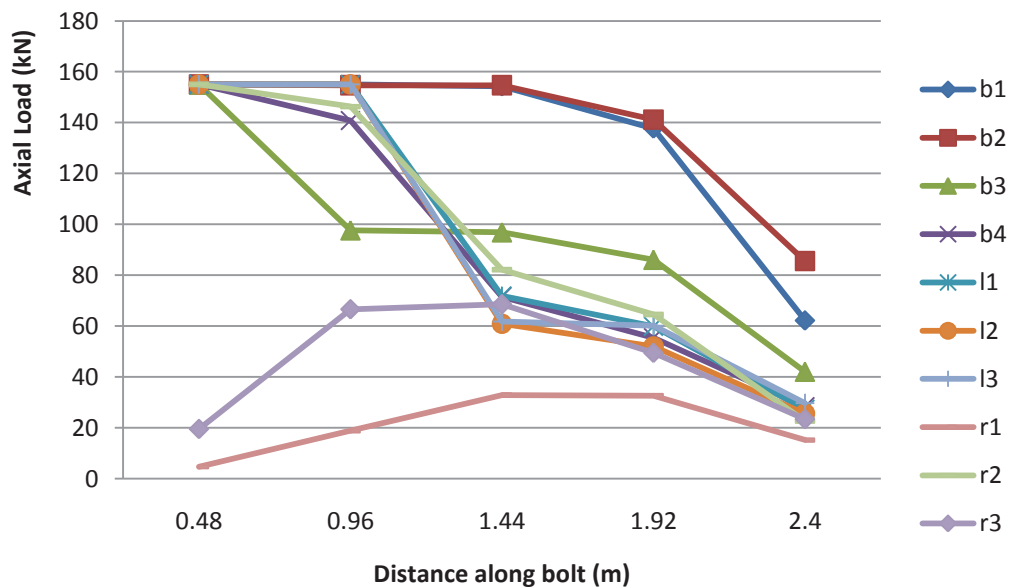


Figure 6-28 Axial loads in MCBs when installed after stope 1 is mined out

## 6.4 Conclusion and discussion

A number of findings can be concluded based on the numerical modeling study of support performance with respect to mining sequence. Primary support alone is not sufficient for haulage drift during the service life of a mine. When the enhanced support system is installed, the total support system is capable of sustaining mining induced loads to the end of the planned mining sequence. The system performance may be further improved if the enhanced support is placed after stope 1 has been mined out and backfilled. Shotcrete

plays an important role in the enhanced support system performance. Verification of normal and shear stresses developed in the shotcrete shows that the spot with highest stress in the shotcrete layer is at the left upper corner of the drift at the end of the mining sequences.

While these results are consistent and interesting, the developed *FLAC* model should be calibrated with field instrumentation data. Three dimensional analyses should be conducted to examine the haulage drift to cross cut junction and how it is affected by the mining sequences. Suggestions from this study, if support system were to be examined using numerical models in the future, would be:

- 1) Choose right element type to represent rock bolt/support system and well define the feature of the reaction between rock mass and support element interface
- 2) Examine the reading of axial loads along rock bolt with theoretical calculation to determine the right track for rock bolt simulation
- 3) Calibrate numerical model with field instrumentation data

## **Chapter 7**

### **Summary and Conclusions**

#### **7.1 Summary**

In sublevel mining systems, the transportation of blasted ore from the draw point to a nearby ore pass, or dumping point is carried out in haulage drifts. During production, haulage drifts are occupied by mine operators and haulage equipment. Therefore, the stability of haulage drifts is important for the safe and uninterrupted production of mining operations. It would be advantageous to know a priori how drift stability is influenced by mining activities in the proximity of the drift. This thesis presents a methodology to examine the stability issues of a haulage drift, based on a case study of the Vale Inco Garson mine in Sudbury, Canada.

The general procedure for studying haulage drift stability issues, is illustrated in Figure 7-1, and can be applied to any other mine; it is described as follows.

- Establishing a geomechanical database for the mine to manage all the geotechnical information
- Using numerical models to examine the influence of distance from orebody contact to haulage drift, taking into account the fact that key factors such as drift convergence, stress concentration and extent of yielding could all be different in different mines

- Evaluation of the characteristics of the selected primary support system, and assessment of the enhanced support system. This latter would involve additional bolting patterns and shotcrete liners.
- Numerical model validation with onsite instrumentation data
- Conclusions and recommendations to assure the stability of the haulage drift during its planned service life.

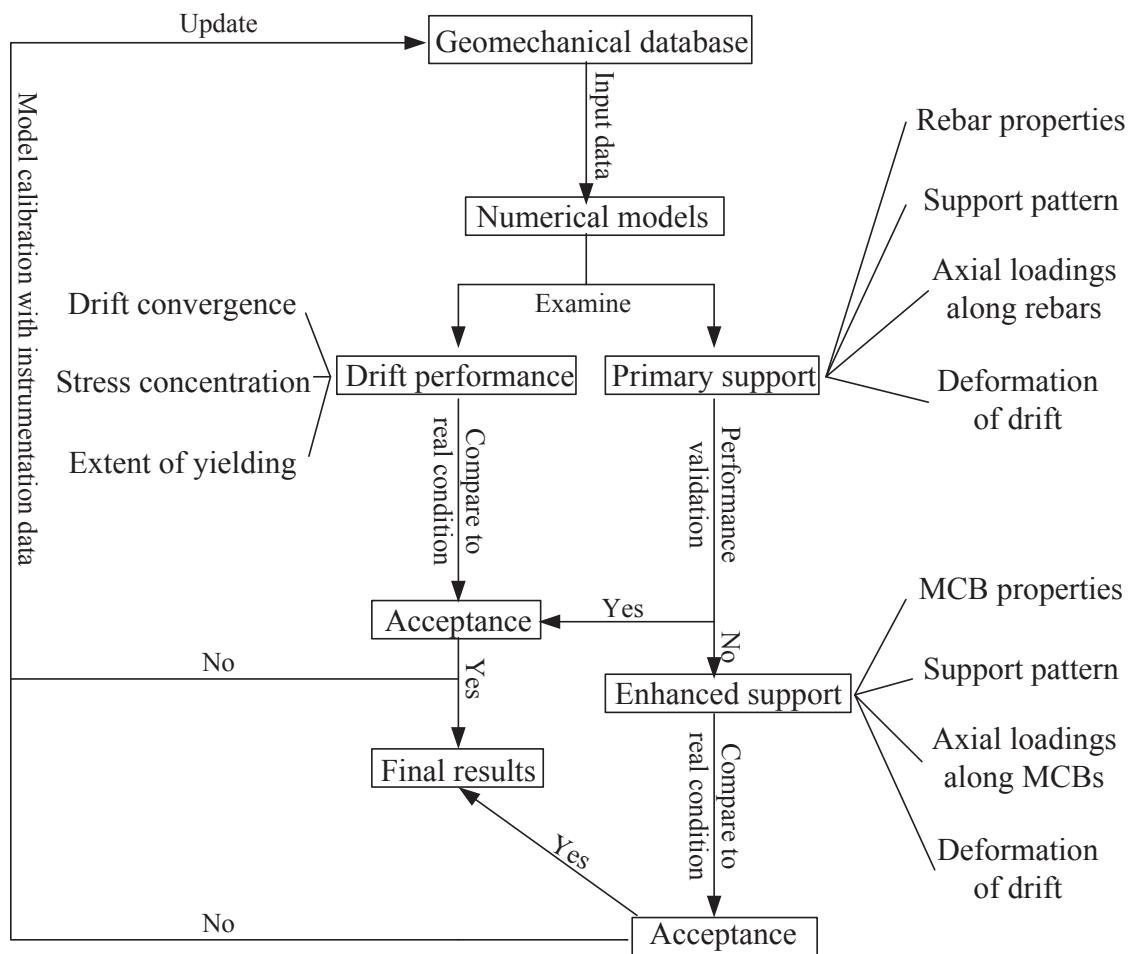


Figure 7-1 Procedure for haulage drift stability assessment

## 7.2 Conclusions

The following are the principal conclusions drawn from this study.

- Parameters like rock mass character, mining plan and stress environment need to be known ahead of time in preparation for setting up the numerical model. Included in each of the three groups of parameters listed above, there are many details, regarding the volume of data, CAD plans, charts, etc. Hence, efficient management and precise utilization of the information is absolutely essential. In the present work, a geomechanical database named “Data Integrator for Mine Analysis and Design (DIMAND)”, has been set up to include the most important features related to mining activities.
- Four numerical simulations have been carried out to examine the influence of drift orientation with respect to principal in situ stress, and drift proximity to orebody contact, while three lower level stopes and three same level stopes were being mined and backfilled. The results are examined in terms of stress and yield zones around the drift, as well as drift wall convergence. Stress results show that there is a dominant trend of low stress regime (postpeak) in the drift back, which results from the stoping activities in both cases of low and high  $k$  ratio. Yield zone results show a gradual spread of yielding with mining activity. However, it was not until the two stopes nearest to the haulage drift were mined and backfilled, that the haulage drift was affected severely, with yielding extending from the drift toward the orebody. Drift deformation results show significantly higher wall convergence ratio of the haulage drift when the stope nearest to the drift was mined.

- Commonly used rock supports, such as mechanical rockbolts, rebars, swellex, cone bolts, cable bolts, etc., as well as rock support design methods, were both reviewed in detail. It facilitates the numerical analysis by presenting further understanding of the interaction between rock mass and rockbolts.
- A number of findings, based on the numerical modeling study of support methods with respect to mining sequence is reported below.
  - Primary support alone is not adequate for supporting the haulage drift during the life of a mine plan.
  - When an enhanced support system is installed, the total support system is capable of sustaining induced mining loads, to the end of the planned mining sequence.
  - The system performance may be further improved if the enhanced support is placed after the first stope situated lower than the haulage drift, has been mined out and backfilled.
  - Shotcrete plays an important role in the enhanced support system performance. An examination of normal and shear stresses developed in the shotcrete shows that the spot with highest stress in the shotcrete layer is at the left upper corner of the drift, and the stress reaches a critical value at the end of the mining sequences.

### **7.3 Future work**

The following are some suggestions for future work:

- The numerical models should be calibrated with field instrumentation data.

- Three dimensional analyses should be conducted to examine the haulage drift to cross cut junction and how it is affected by the mining sequences.



## References

- Barton, N., Lien, R., & Lunde, J. (1974). Engineering Classification of Jointed Rock Masses for the Design of Tunnel Support. *Rock Mechanics: Journal of the International Society for Rock Mechanics*, Vol.6, pp. 189-236.
- B.H.G. Brady, E.T. Brown *Rock mechanics for underground mining*, 4th edition
- B. Stillborg. *Professional users handbook for rock bolting*. 1986
- Bieniawski, Z. T. (1973). Engineering Classification of Jointed Rock Masses. *Transactions of the South African Institution of Civil Engineers*, Vol.15, pp. 335-344.
- Cai, Y., Y. Jiang, et al. (2004). "A study of rock bolting design in soft rock." *International Journal of Rock Mechanics and Mining Sciences* 41(3): 463-463
- Carnavas, P. (2000). *Mining geomechanics I, Post Peak Behaviour of Rock Samples in Uniaxial Compression (Course notes)*: University of Queensland, Australia.
- Chen, W. F., & Han, D. J. (1988). *Plasticity for structural engineers*. New York, Springer-Verlag.
- Chen, J, and H.S. Mitri. (2005). Shear bond characteristics of grouted cable bolts. In *Proceedings of the 24th International Conference on Ground Control in Mining, Morgantown, WV, August 2-4 2005*, eds. Peng, Mark, Finfinger, Tadolini, Khair and Heasley , 342-348. West Virginia University.
- Cividini, A. (1992). Constitutive Behavior and Numerical Modeling. In *Comprehensive Rock Engineering*. Vol.1, pp.395-426.

- Clough, R. W. (1960, Sept.). The Finite Element Method in Plane Strain Analysis. Paper presented at the Proc. 2nd ASCE Conf. Electronic Computation, Pittsburgh, PA.
- Corneau, I. C. (1975). Numerical stability in quasi-static elasto-visoplasticity. *Int J Numer Methods Eng*, 9(1), pp 109-127.
- Coulomb, C. A. (1776). Essai sur une application des règles des maximis et minimis à quelques problêmes de statique relatifs à l'architecture. *Mem. Acad.*, 5(7).
- Creus, G. J. (1986). Viscoelasticity : basic theory and applications to concrete structures. Berlin ; New York :: Springer-Verlag.
- Cundall, P. A. (2006). Constitutive Models: Theory and Background. In *FLAC 6.0 User's Manual*: Itasca Consulting Group, Inc.
- D. D. Tannant, R. K. Brummer & X. Yi "Rockbolt behaviour under dynamic loading: field tests and modelling, *International Journal of Rock Mechanics & Mining Sciences*, 32(6), 1995, pp 537-550." *International Journal of Rock Mechanics and Mining Science & Geomechanics Abstracts* 33(1): A31-A31
- Deere, D. U., Hendron Jr., F. D., Patton, F. D., & Cording, E. J. (1967). Design of Surface and Near Surface Construction in Rock. In C. Fairhurst (Ed.), *Failure and Breakage of Rock* (pp. 237-302): Society of Mining Engineers of AIME.
- Diederichs, M. S. (1999). Instability of Hard Rockmasses: The Role of Tensile Damage and Relaxation. University of Waterloo.
- Drucker, D. C., & Prager, W. (1952). Soil Mechanics and Plastic Analysis or Limit Design. *Quarterly of Applied Mathematics*, 10, pp 157-165.

- Fahimifar, A. and M. Ranjbarnia (2009). "Analytical approach for the design of active grouted rockbolts in tunnel stability based on convergence-confinement method." *Tunnelling and Underground Space Technology* 24(4): 363-375
- Gomez-Hernandez, J., & Kaiser, P. K. (2003). Modeling Rock Mass Bulking around Underground Excavations. Paper presented at the ISRM 2003-Technology Roadmap for Rock Mechanics, South African Institute of Mining and Metallurgy, Vol.1, pp.389-395.
- Griffiths, D. V. (1988). An iterative method for plastic analysis of frames. *Comput Struct*, 30(6), pp 1347-1354.
- Griffiths, D. V., & Willson, S. M. (1986). An explicit form of the plastic matrix for Mohr-Coulomb material. *Commun. Appl. Numer. Methods*, Vol.2, pp. 423-529.
- Hajiabdolmajid, V. R., & Kaiser, P. K. (2003). Brittleness of Rock and Stability Assessment in Hard Rock Tunneling. *Tunneling and Underground Space Technology*, Vol. 18, pp. 35-48.
- Hajiabdolmajid, V. R., Kaiser, P. K., & Martin, C. D. (2002a). Mobilization of Strength in Brittle Failure of Rock-In Laboratory vs. In Situ. Paper presented at the Proceedings of the 5th North American Rock Mechanics Symposium, Toronto, Canada, pp. 227-234.
- Hajiabdolmajid, V. R., Kaiser, P. K., & Martin, C. D. (2002b). Modelling Brittle Failure of Rock. *Int. J. of Rock Mech. Min. Sci.*, Vol.39, pp. 731-741.
- Hallbauer, D. K., Wagner, H., & Cook, N. G. W. (1973). Some Observations Concerning the Microscopic and Mechanical Behaviour of Quartzite Specimens in Stiff, Triaxial Compression Tests. *Int. J. Rock Mech. Min. Sci.*, Vol.10, pp. 713-726.

- Hamrin, H. (2001). Underground Mining Methods and Applications. In Underground Mining Methods: Engineering Fundamentals and International Case Studies. edited by Hustrulid, W. A. and Bullock, R. L. Littleton, CO: Society for Mining, Metallurgy, and Exploration.
- Herget, G. (1987). Stress Assumptions for Underground Excavations in the Canadian Shield. International Journal of Rock Mechanics and Mining Science & Geomechanics Abstracts, 24(1), pp. 95-97.
- Hoek, E. (1983). Strength of Jointed Rock Masses. 23rd Rankie Lecture, Géotechnique, Env., Vol.33(3), pp 187-223.
- Hoek, E. (1994). Strength of Rock and Rock Masses. ISRM News Journal, Vol.2(2), pp. 4-16.
- Hoek, E., & Brown, E. T. (1980a). Empirical Strength Criterion for Rock Masses. J. Geotech. Engng Div., ASCE, Vol.106 ((GT9)), pp. 1013-1035.
- Hoek, E., & Brown, E. T. (1980b). Underground Excavations in Rock. Paper presented at the Instn. Min. Metall., London, England.
- Hoek, E., & Brown, E. T. (1988). The Hoek-Brown Failure Criterion—a 1988 update. Paper presented at the 15th Canadian Rock Mech. Symp, Dept. Civil Engineering, University of Toronto, Toronto, Canada, pp. 31-38.
- Hoek, E., & Brown, E. T. (1997). Practical Estimates of Rock Mass Strength. Intl. J. Rock Mech. & Mining Sci. & Geomechanics Abstracts, Vol.34(8), pp. 1165-1186.
- Hoek, E., Carranza-Torres, C., & Corkum, B. (2002). Hoek-Brown Failure Criterion—2002 Edition. Paper presented at the Proc. 5th North American Rock Mechanics Symposium and the

- 17th Tunnelling Association of Canada Conference—NARMS-TAC, University of Toronto Press, Toronto, Canada, pp. 267-271.
- Hoek, E., Kaiser, P. K., & Bawden, W. F. (1995). *Support of Underground Excavations in Hard Rock*: AA Balkema: Rotterdam.
- Hoek, E., Marinos, P., & Benissi, M. (1998). Applicability of the Geological Strength Index (GSI) Classification for Very Weak and Sheared Rock Masses: The Case of the Athens Schist Formation. *Bull. Engg. Geol. Env.*, Vol.57(2), pp.151-160.
- Hoek, E., Marinos, P., & Marinos, V. (2004). Rock Mass Characterisation for Molasses. *Int. J. Rock Mech. Min. Sci.*
- Hoek, E., Wood, D., & Shah, S. (1992). A Modified Hoek-Brown Criterion for Jointed Rock Masses. Paper presented at the Proc. Rock Characterization, Symp. Int. Soc. Rock. Mech.: Eurock'92, London, Brit. Geotech. Soc., pp. 209-214.
- H.S. Mitri and H. Rajaie (1990). "Stress analysis of rock mass with cable support – A finite element approach." *Proceedings – Stresses in Underground Structures, CANMET*: 110-119
- Irons, B. and Ahmad, S. "Techniques of Finite Elements". 1980. John Wiley & Sons
- Jeng, F. S. and T. H. Huang (1999). "The holding mechanism of under-reamed rockbolts in soft rock." *International Journal of Rock Mechanics and Mining Sciences* 36(6): 761-775
- Kaiser, P. K., Diederichs, M. S., Martin, C. D., Sharp, J., & Steiner, W. (2000). *Underground Works in Hard Rock Tunnelling and Mining*. Paper presented at the Keynote Lecture. GeoEng2000 Conference. Technomic Publishing Co., Melbourne, Australia, pp 841-926.

- Lade, P. V., & Jackobsen, K. P. (2002). Incrementalization of a Single Hardening Constitutive Model for Frictional Materials. *Int. J. Numer. Anal. Meth. Geomech*, Vol.26, pp. 647-659.
- Lorig, L., & Varona, P. (2004). Numerical Analysis. In D. C. Wyllie & C. W. Mah (Eds.), *Rock Slope Engineering: Civil and Mining* (4th ed.), pp. 218-244. London: Spon Press.
- McNiven, H. D. and H. M. Ewoldsen (1969). "Rockbolting of tunnels for structural support part I-- Theoretical analysis." *International Journal of Rock Mechanics and Mining Sciences & Geomechanics Abstracts* 6(5): 465-481
- Martin, C. D. (1997). 17th Canadian Geotechnical Colloquium: The Effect of Cohesion Loss and Stress Path on Brittle Rock Strength. *J. Can Geotech*, Vol.36(1), pp.136-151.
- Martin, C. D., Kaiser, P. K., & Creath, D. R. (1999). Hoek-Brown Parameters for Predicting the Depth of Brittle Failure around Tunnels. *J. Can Geotech*, Vol.36(1), pp.136-151.
- Mitri, H.S. (2009) Course notes. Finite Elements in Rock Mechanics. McGill University.
- Mitri, H.S. & Hassani, F. P. (1988). Nonlinear Finite Element Analysis of Mine Roadway Arch Support Systems. *Computers & Structures*, Vol. 29(No. 3), pp. 335-364.
- Mitri, H. S. & Tang, B. (2003). Stability Analysis of Mine Opening with e-z tools. Paper presented at the 4th Int. Conf. on Comp. Appl. in the Minerals Industry (CAMI), Calgary, Alberta, Canada.
- Mitri, H.S. and H. Rajaie. 1990. Stress analysis of rock mass with cable support – a finite element approach. In *Proceedings of stresses in underground structure*, Ottawa. 110-119.
- Obert, L., Duvall, W. I., & Merril, R. H. (1960). Design of Underground Openings in Competent Rock. *Bulletin: US Bureau of Mines*, 587, pp. 9.

- Owen, D. R. K., & Hinton, E. (1980). *Finite Element in Plasticity: Theory and Practice*. Swansea, U. K.: Pineridge Press Limited.
- Pariseau, W. G. (1980). *Finite Element Method Applied to Cut and Fill Mining*. Proceedings of the Conference on the Application of Rock Mechanics to Cut and Fill Mining.
- Pariseau, W. G. (1992a). Applications of Finite Element Analysis to Mining Engineering. In *Comprehensive Rock Engineering*. Vol. 1, pp. 491-522.
- Pariseau, W. G. (1992b). Rock Mechanics. In *SME Mining Engineering Handbook*, 2nd Edition. Vol. 1, pp. 829-847.
- Potvin, Y. (1988). *Empirical Open Stope Design in Canada*. Unpublished PhD, Dept. of Mining and Mineral Processing, University of British Columbia.
- Ranken, R. E., & Ghaboussi, J. (1975). *Tunnel Design Considerations: Analysis of Stresses and Deformations around Advancing Tunnels*. Report UILU-ENG 75-2016.
- Rao, S. S. (1989). *The Finite Element in Engineering*: Pergamon Press, U. K.
- Reed, M. B., P. Grasso, et al. (1993). "Improvement of rock properties by bolting in the plastic zone around a tunnel: A numerical study." *International Journal of Rock Mechanics and Mining Sciences & Geomechanics Abstracts* 30(5): 567-571
- RocScience Inc. Phase 2 finite element modelling software - 1989
- Smith, I. M., & Griffiths, D. V. (2004). *Programming the finite element method*. Hoboken, NJ :: Wiley.

- Tesarik, D. R., Seymour, J. B., & Yanske, T. R. (2003). Post-Failure Behavior of Two Mine Pillars Confined with Backfill. *International Journal of Rock Mechanics and Mining Sciences*, 40(2), 221.
- Traina, L. A. (1983). Experimental Stress-Strain Behaviour of a Low Strength Concrete under Multiaxial States of Stress, Technical Report AFWL-TR-82-92. Kirtland Air Force Base, New Mexico: Air Force Weapons Laboratory.
- Turner, M. J., Clough, R. W., Martin, H. C., & Topp, L. J. (1956). Stiffness and Deflection Analysis of Complex Structures. *A. Aeron Sci.*, 23(9), pp 805-823.
- Vermeer, P. A. (1998). Non-associated Plasticity for Soils, Concrete and Rock. In H. J. Herrmann (Ed.), *Physics of Dry Granular Media*. Vol. 350, pp. 163-196: Kluwer Academic Publishers.
- Wei et al. 2009. Stability of haulage drift in the dynamic mine environment. In proceedings of 18th International Symposium on Mine Planning and Equipment Selection (MPES 2009), Banff.
- Yi, X. and P. K. Kaiser (1994). "Impact testing for rockbolt design in rockburst conditions." *International Journal of Rock Mechanics and Mining Sciences & Geomechanics Abstracts* 31(6): 671-685
- Zienkiewicz, O. C., & Corneau, I. C. (1974). Viscoplasticity, Plasticity and Creep in Elastic Solids: A Unified Approach. *Int. J. Numer. Methods Eng.*, 8, pp 821-845.
- Zienkiewicz, O. C., & Humpheson, C. (1977). Viscoplasticity: A generalized Model for Description of Soil Behaviour. In Desai C. & Christian J. T. (eds.), *Numerical Methods in Geotechnical Engineering*. London: McGraw-Hill.



Zienkiewicz, O. C., & Taylor, R. L. (1989). The finite element method (4th ed.). London ; New York: McGraw-Hill.

Zienkiewicz, O. C., Valliappan, S., & King, I. P. (1968). Elasto-plastic Solutions of Engineering Problems: Initial Stress Finite Element Approach. Int. J. Num. Meth. Engng., Vol.1, pp. 75-100.

Zhang Y.H and Mitri. H.S Elastoplastic stability analysis of mine haulage drift in the vicinity of mined stopes, International Journal of Rock Mechanics and Mining Sciences, Vol. 45, No. 4, pp 574-593. 2008